

DESIGN AND PIV MEASUREMENTS ON A WIRE-WRAPPED 61-ROD
HEXAGONAL FUEL ASSEMBLY EXPERIMENTAL FACILITY

A Thesis

by

NOLAN EDWARD GOTH

Submitted to the Office of Graduate and Professional Studies of
Texas A&M University
in partial fulfillment of the requirements for the degree of
MASTER OF SCIENCE

Chair of Committee,	Yassin A. Hassan
Committee Members,	Rodolfo Vaghetto
	William H. Marlow
	Maria King
Head of Department,	Yassin A. Hassan

May 2017

Major Subject: Nuclear Engineering

Copyright 2017 Nolan Edward Goth

ABSTRACT

The superior uranium utilization efficiency of fast spectrum reactors relative to thermal spectrum reactors was recognized shortly after commercial reactor development started. The sodium fast reactor design, a type of liquid metal fast breeder reactor, was progressed the furthest during the 1960s and 1970s. However in the late 1970s, 1980s, and early 1990s, the expansion of known uranium reserves, decline in nuclear power demand in the USA, and cancellation of the Integral Fast Reactor program slowed the technology development until recently.

With modern computational tools for fluid dynamics, the understanding of exterior and interior subchannel coolant flow behavior can be improved. This improvement will allow existing conservatisms in thermal-hydraulic fuel assembly analysis to be minimized. This will lead to more profitable and safer fuel designs. In the past, thermal-hydraulic experiments were performed on sodium fast reactor fuel assemblies. Unfortunately, the data collected is not suitable for computational fluid dynamics simulation validation due to measurements performed with intrusive probes or poor spatial and temporal resolution.

Therefore, a need exists for validation reference data for Reynolds-averaged Navier-Stokes and large-eddy simulation turbulence modeling. Completion of this thesis partially met that demand by designing, procuring, constructing, and collecting PIV shakedown data on an experimental flow loop containing a 61 rod hexagonal fuel assembly with helically wrapped wire spacers. The facility was designed for laser-based optical measurement techniques using the matched index of refraction technique. The experimental setup will provide isothermal high spatial and temporal resolution velocity and pressure data for computational fluid dynamics validation.

ACKNOWLEDGEMENTS

I would like to express my sincere appreciation to my supervisors, Dr. Yassin Hassan, Dr. Rodolfo Vaghetto, Dr. Thien Duy Nguyen, and Dr. Saya Lee for their constant guidance, without which this work would not have been possible.

This project represented a unique opportunity for collaboration between computational and experimental work, as both activities were conducted in parallel. The teamwork with Areva (Anthony Chang, Kelly Dugan, Tom Galioto, Brian Mays), ANL (Elia Merzari, Aleksandr Obabko), and Terrapower (Brian Jackson, Daniel Leonard, Nate Salpeter) throughout the iterative design phase improved the quality of the experimental output.

I would also like to thank the army of graduate and undergraduate students that participated in the design, construction, and operation of the Wire-Wrapped Experimental Facility. Special thanks to Mason Childs, Philip Jones, Will Headley, Nicolas Quintanar, Mateusz Marciniak, and Marilyn Delgado.

My final gratitude goes to my wife, Jordan Goth, in-laws, John and Virginia Pratt, and parents, Norman and Nancy Goth, who provided me with an endless supply of support, nourishment, and a decent genome.

CONTRIBUTORS AND FUNDING SOURCES

Contributors

This work was supervised by a thesis committee consisting of Professors Yassin Hassan, William Marlow, and Rodolfo Vaghetto of the Department of Nuclear Engineering and Professor Maria King of the Department of Mechanical Engineering.

All work for the thesis was completed by the student, under the advisement of Professors Yassin Hassan, Rodolfo Vaghetto, and Thien Nguyen of the Department of Nuclear Engineering.

Funding Sources

This material is based upon work supported by the Department of Energy [National Nuclear Security Administration] under Award Number [DE-NE0008321]. This report was prepared as an account of work sponsored by an agency of the United States Government. Neither the United States Government nor any agency thereof, nor any of their employees, makes any warranty, express or implied, or assumes any legal liability or responsibility for the accuracy, completeness, or usefulness of any information, apparatus, product, or process disclosed, or represents that its use would not infringe privately owned rights. Reference herein to any specific commercial product, process, or service by trade name, trademark, manufacturer, or otherwise does not necessarily constitute or imply its endorsement, recommendation, or favoring by the United States Government or any agency thereof. The views and opinions of authors expressed herein do not necessarily state or reflect those of the United States Government or any agency thereof.

NOMENCLATURE

ABS acrylonitrile butadiene styrene

AEC Atomic Energy Commission

ANL Argonne National Laboratory

BWR boiling water reactor

CCD charge-coupled device

CFD computational fluid dynamics

DAS data acquisition system

DI deionized

DOE U.S. Department of Energy

DP differential pressure

DWO Discrete Window Offset

ECA ethyl-2-cyanoacrylate

FEP fluorinated ethylene propylene

FFT fast Fourier transform

FTF flat-to-flat

INL Idaho National Laboratory

LDV laser Doppler velocimetry

LES large-eddy simulation

LMFBR liquid metal fast breeder reactor

LWR light water reactor

MIR matched-index-of-refraction

NaI sodium iodide

OSHA Occupational Safety and Health Administration

P/D pitch-to-diameter ratio

PID piping and instrument diagram

PIV particle image velocimetry

PMMA Poly(methyl methacrylate)

PSA project safety assessment

PTFE Polytetrafluoroethylene

PVC polyvinyl chloride

PWR pressurized water reactor

RAM random access memory

RANS Reynolds-averaged Navier Stokes

Re Reynolds

RFQ request for quote

RMS root-mean-square

ROI region of interest

RPC robust phase correlation

RTD resistance temperature detector

SFR sodium fast reactor

SLA stereolithography

SPIV stereoscopic particle image velocimetry

SLS selective layer sintering

SNR signal-to-noise ratio

SS stainless steel

TAMU Texas A&M University

UHMWPE ultra-high-molecular-weight polyethylene

UOD universal outlier detection

USB University Services Building

VFD variable frequency drive

TABLE OF CONTENTS

	Page
ABSTRACT	ii
ACKNOWLEDGEMENTS	iii
CONTRIBUTORS AND FUNDING SOURCES	iv
NOMENCLATURE	v
TABLE OF CONTENTS	viii
LIST OF FIGURES	x
LIST OF TABLES	xiv
1. INTRODUCTION	1
2. OBJECTIVES, REQUIREMENTS, AND SPECIFICATIONS	4
2.1 Objectives	4
2.2 Requirements and Specifications	4
3. LITERATURE REVIEW	6
3.1 LMFBR Fuel Assembly Flow Characterization	6
3.2 Matched-Index-of-Refraction Facilities	8
3.3 Matched-Index-of-Refraction Materials	9
4. FACILITY DESIGN	11
4.1 Matched-Index-of-Refraction	11
4.2 Materials Testing	12
4.2.1 Optical Testing	13
4.2.2 Chemical Testing	22
4.2.3 Mechanical Testing	26
4.2.4 Final Material Selection	28
4.3 Test Section	30
4.3.1 61-Rod Wire-Wrapped Assembly	31
4.3.2 Hexagonal Duct	38

4.3.3	Plena	40
4.3.4	Guide Plates	41
4.4	Primary Loop	42
4.4.1	Leak Testing	46
4.5	Secondary Loop	47
4.6	Tertiary Loop	50
4.7	Facility Room	51
4.8	Imaging Hardware	53
4.9	Pressure Hardware	56
4.10	Operating Procedures	57
5.	PARTICLE IMAGE VELOCIMETRY METHODOLOGY	59
6.	PIV RESULTS	71
6.1	Ensemble-Averaged Vertical Velocity Component	71
6.2	RMS Vertical Velocity Component	73
6.3	Ensemble-Averaged Horizontal Velocity Component	73
6.4	RMS Horizontal Velocity Component	74
6.5	Reynolds Shear Stress	74
7.	CONCLUSIONS AND LESSONS LEARNED	81
	REFERENCES	84
	APPENDIX A. AS-BUILT GEOMETRY	89
	APPENDIX B. FACILITY OPERATING PROCEDURES	111
	APPENDIX C. PROJECT SAFETY ANALYSIS	123
	APPENDIX D. TEST SECTION DRAWINGS	134
	APPENDIX E. HARDWARE INVENTORY	151

LIST OF FIGURES

FIGURE	Page
1.1 DOE joint project team members	3
1.2 Texas A&M scope of the DOE joint project	3
4.1 Isometric view of a CAD rendering of the experimental facility	12
4.2 The experimental facility with major components highlighted.	13
4.3 VeroClear-RGD810 and Accura 60 samples	15
4.4 P-cymene and PMMA refractive indices as a function of temperature [24]	16
4.5 0.5 inch diameter cylinder of Poly(methyl methacrylate) (PMMA) im- mersed in p-Cymene at 22°C	17
4.6 Unpolished edge of PMMA cylinder immersed in p-Cymene at 22°C .	18
4.7 0.625 inch PMMA cylinder immersed in water (left) and p-Cymene (right) at 22°C	19
4.8 NaI solution (62 W%) after 0 hr, 5 hr, and 92 hr of exposure to air .	19
4.9 PMMA rod and NaI aqueous solution (62 W%) after 1 month of ex- posure to air at 22°C	20
4.10 PMMA rod in p-Cymene showing the gas bubbles formed during the solvent curing process	21
4.11 Elapsed time of 0 days; Top: cast PMMA, Bottom: extruded PMMA	23
4.12 Elapsed time of 6 days; Top: cast PMMA, Bottom: extruded PMMA	23
4.13 Elapsed time of 16 days; Top: cast PMMA, Bottom: extruded PMMA	24
4.14 Elapsed time of 36 days; Top: cast PMMA, Bottom: extruded PMMA	24

4.15	Elapsed time of 36 days; Extruded sample highlighting the physical deformation	25
4.16	LEFT: Discolored p-Cymene after exposure to air, cast PMMA, and extruded PMMA for 36 days; RIGHT: fresh p-Cymene	25
4.17	Lower and upper grid plates	27
4.18	19-rod test assembly	28
4.19	Closeup of the lower plate and test assembly	28
4.20	PMMA rod immersed in three fluids to display the result of matching the index of refraction	30
4.21	Test section filled with water	31
4.22	Test section filled with p-Cymene to demonstrate the MIR condition .	31
4.23	PMMA test section of the experimental facility	32
4.24	Typical LMFBR fuel assembly [31]	33
4.25	61-rod hexagonal fuel assembly primary dimensions	34
4.26	Cast PMMA rods produced by PolyOne with attached wire spacers .	36
4.27	Aluminum guide block to set the bottom of the rod and wire parallel axes	37
4.28	3-D printed guide block to set parallel axes and wire azimuthal position at the top of the rod.	37
4.29	Closeup showing the wire attachment	39
4.30	Closeup showing the top of a rod after the coning process	39
4.31	Before installation	40
4.32	After installation	40
4.33	Plenum before the upper circular flange was attached	41
4.34	Lower plenum	42
4.35	Upper plenum	42

4.36	Lower and upper guide plates	42
4.37	Laminar/turbulent flow transition [32]	44
4.38	UHMWPE flexible hoses anchored to support structure	45
4.39	Seeding particle injection was performed by manipulating two valves and a 50 mL syringe	46
4.40	Initial leak testing configuration	47
4.41	Final leak testing configuration	48
4.42	Secondary loop is copper, while the tertiary loop is PVC	49
4.43	Secondary reservoir is visible and p-Cymene returns to the top of the primary reservoir	50
4.44	Tertiary reservoir, air-cooled chiller, and chilled water lines into the facility room	51
4.45	Aluminum framing of the facility room	52
4.46	Drywall preparation	53
4.47	PIV setup containing test section, laser, camera, and traverse system	54
4.48	600 nm fluorescent particles illuminated through an optical prism in the near-wall region of the 61-rod assembly	55
4.49	Vertical laser sheet and optical prism without MIR conditions	56
4.50	Horizontal laser sheet with MIR conditions	56
4.51	Pressure hardware location	57
5.1	Side view of the PIV setup for the lower and upper windows	62
5.2	Top view of the PIV setup for the lower window, Axial 1	63
5.3	Top view of the PIV setup for the upper window, Axial 2	64
5.4	LaVision calibration plate [34]	65
5.5	Raw PIV image	66

5.6	Mean background of image set	67
5.7	Background subtracted image	68
6.1	Flow regime map for hexagonal fuel assemblies [32]	72
6.2	Ensemble-averaged vertical velocity component for Re = 3200, 6400, and 9600. Axial 1 (left) and Axial 2 (right)	76
6.3	RMS vertical velocity component for Re = 3200, 6400, and 9600. Axial 1 (left) and Axial 2 (right)	77
6.4	Ensemble-averaged horizontal velocity component for Re = 3200, 6400, and 9600. Axial 1 (left) and Axial 2 (right)	78
6.5	RMS horizontal velocity component for Re = 3200, 6400, and 9600. Axial 1 (left) and Axial 2 (right)	79
6.6	Reynolds shear stress, $\overline{u'v'}$, for Re = 3200, 6400, and 9600. Axial 1 (left) and Axial 2 (right)	80

LIST OF TABLES

TABLE	Page
2.1 Requirements and specifications for the isothermal flow loop	5
4.1 Refractive index measurements of NaI aqueous solutions at 22°C	18
4.2 Final materials used in the experimental facility	29
4.3 Dimensions of the rods and wire spacers in the experimental facility .	35
4.4 Pressure hardware used in the experimental test	58
5.1 X-Y coordinate system for both PIV measurement windows	63
5.2 Camera frame rate for 5-15 pixel seeding particle displacement	65
5.3 PIV post-processing parameters	69

1. INTRODUCTION

The superior resource utilization efficiency of fast spectrum reactors relative to thermal spectrum reactors was recognized shortly after the beginning of commercial reactor development. In the 1950s, when known uranium reserves were small and rapid nuclear growth was anticipated, the estimated uranium reserves were expected to last until 2000 to 2020. Therefore, fast spectrum breeder reactors were viewed as the solution to maximize the uranium resource utilization. In 1967, the Atomic Energy Commission (AEC) recommended that research be focused on the liquid metal fast breeder reactor (LMFBR) over other fast and thermal breeding systems. The sodium fast reactor (SFR) design, a type of LMFBR, progressed the furthest during the time period when breeder reactors were in demand. However in the late 1970s, 1980s, and early 1990s, the expansion of known uranium reserves, decline in nuclear power demand in the USA, and cancellation of the Integral Fast Reactor program slowed the SFR technology development until recently.

The typical LMFBR fuel assembly contains fuel rods placed in a triangular lattice. Each fuel rod is helically wrapped with a wire spacer. This complex geometry makes analytical thermal-hydraulic analysis difficult. Therefore, empirical analysis, along with computational fluid dynamics (CFD), need to be utilized to understand the coolant flow behavior in this assembly type. CFD analysts wish to perform Reynolds-averaged Navier Stokes (RANS) and large-eddy simulation (LES) on liquid metal fast reactor fuel assemblies to reduce the existing conservatisms in thermal hydraulic codes. Experiments on the thermal-hydraulic behavior were performed in the past on LMFBR fuel assemblies. Unfortunately, the data collected in the past is not suitable for RANS or LES validation of the flow behavior in the exterior, corner, and edge

subchannels due to existing measurements being performed with intrusive probes or poor spatial and temporal resolution.

Experimental flow loops containing LMFBR fuel assemblies utilizing particle image velocimetry (PIV) and laser Doppler velocimetry (LDV) have been previously built and studied to attempt to quantify the flow behavior. However, these fuel assemblies only contained 7 or 19 rod. Such small assemblies have non-negligible wall effects on the interior subchannels. Therefore, a demand exists for PIV and LDV experimental data on fuel assemblies containing a larger number of rods. The demand exists because larger experimental assemblies are expected to behave more hydraulically similar to the 217-rod fuel assemblies used in practice.

The completion of this thesis met that demand by designing, procuring, constructing, and collecting data on an experimental flow loop containing a 61-rod hexagonal fuel assembly with helically wrapped wire spacers. The facility was designed for PIV and LDV measurements using the matched-index-of-refraction (MIR) technique. The experimental setup provided valuable isothermal velocity and pressure data for RANS and LES simulation validation.

A joint project was funded by the U.S. Department of Energy (DOE) to generate CFD validation reference data with the ultimate objective of extending the lifetime of hexagonal fuel assemblies. Project team members were Areva, Argonne National Laboratory (ANL), TerraPower, and Texas A&M University (TAMU), Figure 1.1. Areva performed temperature and pressure measurements on a 61-rod heated assembly [1, 2]. TAMU performed velocity and pressure measurements on a 61-rod isothermal assembly. The pitch-to-diameter ratio (P/D) of both facilities was very similar but total lengths were different. ANL [3, 4] and TerraPower [5] performed LES and RANS simulations on both experimental bundles.

Figure 1.2 contains the TAMU scope of the project. This thesis covers a partial



Figure 1.1: DOE joint project team members

scope of the DOE joint project. Specifically, it covers the literature review, material testing, facility design, construction, shakedown testing using DI water as the working fluid, and DI water PIV results in the set of exterior subchannels near the hexagonal duct wall. The hydraulic shakedown testing was necessary to confirm the integrity of the experimental flow loop by eliminating leaks and vibrations before switching to the MIR fluid of p-Cymene. The instrument shakedown testing was necessary to debug all imaging, pressure, temperature, and flow rate hardware. It also minimized the immersion time of PMMA in p-Cymene during the debugging process.

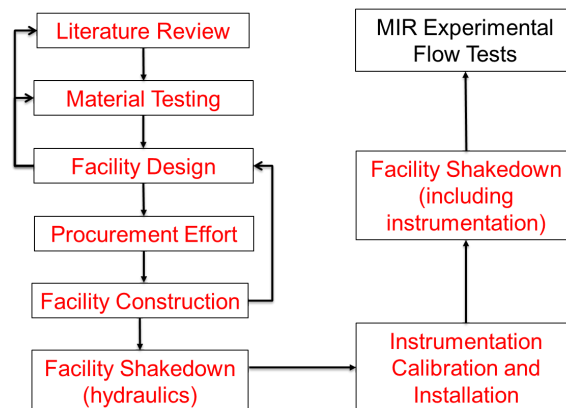


Figure 1.2: Texas A&M scope of the DOE joint project

2. OBJECTIVES, REQUIREMENTS, AND SPECIFICATIONS

Critical project requirements and specifications were initially outlined in a test specification provided by TerraPower. After several iterations, the test specification defined the fuel assembly P/D, turbulent flow regime, and preferred velocity and pressure measurement locations. Objectives, requirements, and specifications are provided below.

2.1 Objectives

The two primary objectives of this research were:

1. Design, procure, and construct an appropriate isothermal experimental facility.
2. Collect velocity and pressure measurements to characterize the flow in a experimental 61-rod fuel assembly in the fully turbulent flow regime.

2.2 Requirements and Specifications

Requirements were defined as what the experimental flow loop must do. Specifications were defined as how the requirements would be met. Table 2.1 provides the primary requirements of the experimental facility.

Table 2.1: Requirements and specifications for the isothermal flow loop

Requirement	Specification
Velocity measurements in edge, corner, and interior sub-channels shall be possible.	Edge, corner, and interior subchannel measurements will be made possible via MIR materials selection.
Pressure measurements must capture both the axial and azimuthal pressure differences in the fuel assembly.	Axial pressures will be measured at various axial positions along the same azimuthal position. Azimuthal pressures will be measured at various azimuthal positions along the same axial position.
All wetted surfaces shall be chemically compatible with the test fluid.	All materials will be submerged in the test fluid and possible chemical interactions investigated.
The Reynolds number shall be at least 20,000.	The selection of long radius elbows, non-restricting valves, large piping, low viscosity, and appropriate pump sizing will ensure a Reynolds number of at least 20,000.
The flow loop shall be volumetrically flow rate controlled and measured.	Flow rate will be controlled and measured via centrifugal pump, variable frequency drive (VFD), and flow meter
The flow loop shall be temperature controlled and measured.	Temperature will be controlled and measured via an resistance temperature detector (RTD) and air-cooled chiller.
Flow-induced vibrations shall be minimized in the fuel assembly and support structure.	Rubber isolation, flexible hosing, and steel framing will be utilized to dampen flow-induced vibrations.
The flow loop shall be protected from over-pressurization to prevent inlet plenum failure.	Overpressure protection will be provided via a pressure relief valve at the location of highest expected pressure.
All temperature, pressure, and flow rate measurements shall be made such repeatability is possible.	A data acquisition system will be used to record simultaneous measurements of temperature, pressure, and flow rate.
Sufficient length shall be provided to ensure that the flow is fully developed in the visualization region.	At least 2.5 pitches will be provided in the inlet plenum and hexagonal duct to allow the flow to fully develop.
Sufficient length shall be provided to minimize the downstream effects on measurement locations.	At least 0.25 pitches will be provided in the hexagonal duct and outlet plenum to minimize downstream effects.

3. LITERATURE REVIEW

A literature review was performed to understand the current state of velocity field and pressure measurements on LMFBR fuel assemblies, along with lessons learned from prior MIR experimental facilities. The review covers prior measurement techniques, the motivation for non-intrusive optical measurements, existing MIR facilities, and conclusions about the feasibility of various solid/fluid pairs to achieve MIR conditions.

3.1 LMFBR Fuel Assembly Flow Characterization

Collingham et al. [6] were first to present coolant mixing experimental results in a full-scale model of a wire wrapped LMFBR assembly with 217 rods. The technique of salt injection and conductivity monitoring with over 400 probes was employed on the assembly. They also proposed two models for turbulent mixing and cross flow. Lorenz and Ginberg [7] recognized that prior work primarily focused on interior subchannel characterization. Therefore, their work focused on the edge subchannels near the hexagonal duct wall. Electrolytic tracers and isokinetic sampling techniques were applied on a 91-rod assembly. These techniques were also used to reduce the uncertainty in the measurements performed by Collingham et al.

With advances in charge-coupled device (CCD) cameras and computational performance, optical techniques of flow visualization have gained popularity due to their non-intrusive nature. LDV came first, which can quantify the velocity vector in a very small volume around a single point in space using photon fringe interference patterns. PIV followed and is capable of producing two and three-dimensional vector fields. Interest in LMFBRs has resurged after the development of these modern visualization techniques.

In 2008, Idaho National Laboratory (INL) [8] designed a 7-rod wire-wrapped hexagonal assembly to place inside their test section. This was the first experiment capable of measuring velocity fields in interior subchannels of a LMFBR fuel assembly. The target Reynolds (Re) number was 22,000, which limited the assembly size to 7 rods, due to lack of sufficient pumping power and heat rejection required to reach such an inlet velocity using mineral oil with a relatively high viscosity. Quartz tubes of 85 mm diameter simulated the fuel rods, while 25 mm diameter quartz rods simulated the helical wire spacer. The inlet end of the tubes were closed. The bundle length was 2.13 m. The helical wire spacers were formed by increasing the quartz temperature until it softened, and then wrapping it around the fuel rod. The wire spacer was attached at the two ends, similar to existing LMFBR fuel fabrication.

Nishimura et al. [9] performed PIV on a 3-rod bundle to quantify interior sub-channel behavior. Sato et al. [10] used both PIV and LDV to investigate the flow in interior subchannels around the central rod of a 7-rod bundle. The study also investigated the impact of a deformed assembly by bowing the central rod.

With a full size LMFBR assembly containing 217 rods, the scalability of assemblies with a smaller number of rods is a concern due to the influence the hexagonal duct wall may have on interior subchannels. Brockmeyer et al. [11] performed a study on the dependency of inter-subchannel exchange on assembly size. They performed CFD simulations using RANS turbulence models on 19-, 37-, 61-, and 91-rod assemblies and concluded that the 91-rod assembly was not yet large enough to isolate the inner subchannels from the impact of the wall effect from the hexagonal duct.

Nevertheless, a 61-rod assembly was selected in this project based on the feasibility of construction, expense, and PIV measurement capability. The experimental results will be used for CFD validation, but larger bundles will need to be investigated

using PIV and LDV.

3.2 Matched-Index-of-Refractive Facilities

A review of prior MIR facilities was important to understand the advantages, disadvantages, and operational complexities associated with different approaches to achieve MIR conditions. Key parameters from several MIR facilities will now be discussed.

INL [12] has the largest MIR facility in the world with test section dimensions of $0.6 \text{ m} \times 0.6 \text{ m} \times 2.5 \text{ m}$. The solid structures are formed from quartz, while the fluid is Drakeol 5 light mineral oil. The facility was designed to accommodate any solid structure capable of fitting inside the test section physical envelope, giving the versatility to support multiple projects without major facility overhaul. This facility contains an auxiliary loop for temperature control via a 20-ton glycol chiller and 8.5 kW heater, which gives the ability to control the inlet fluid temperature to $\pm 0.05 \text{ }^\circ\text{C}$. PIV and LDV imaging hardware is mounted on a three-dimensional traverse system that spans the entire test section. Laser sources are double-pulsed, neodymium-doped yttrium aluminum garnet lasers that produced laser sheets of 1-3 mm thick. Disadvantages of the facility are the price of the quartz solids for complex geometries, large pumping requirements to achieve the target Re number, and minimizing the leakage of the mineral oil.

Dominguez and Hassan [13] constructed an experimental MIR facility to perform PIV and LDV on a prototypical Westinghouse 5×5 pressurized water reactor (PWR) assembly. Water was the working fluid, fuel rods were made of polycarbonate and a visualization region was created by using fluorinated ethylene propylene (FEP) tubing near the inlet and outlet of the spacer grids. FEP has a similar refractive index of water, approximately 1.33 at room temperature [14]. Disadvantages of these

techniques for our application are the complexity of using flexible tubing to fabricate the helical wire spacers, along with the inability to perform optical measurements at any axial location in the assembly because the majority of the measurement locations required feasibility testing in the 61-rod assembly.

3.3 Matched-Index-of-Refraction Materials

After reviewing prior LMFBR flow characterization studies and investigating other MIR experimental facilities, the search began for plausible solid/fluid pairs for the 61-rod assembly and test section of this experimental facility. In an effort to use water as the working fluid, fluorinated resins were of primary interest. Prior work performed in Japan [10] [9] utilized a fluorinated resin, Mexflon-DC™, to cast rods and wires. Unfortunately, this product is no longer commercially available. Flexible FEP tubes were considered, but concerns about vibration, tolerances, and how to fabricate helical wire spacers eliminated the option. Several other fluoropolymers exist, but none existed with sufficient shear moduli to withstand 2 m spans.

A review of several promising solids and fluids was performed by Hassan et al. [15]. The three most promising solids for their pebble bed application were PMMA (1.4873), soda-lime glass (1.504), and FEP (1.33). MIR fluids were p-Cymene (1.49), 60% volume aqueous sodium iodide (1.49), and water (1.33). After optical testing, they selected PMMA and p-Cymene.

For a prior experimental facility at the TAMU Thermal-Hydraulic Research Laboratory, the use of quartz and mineral oil had been considered and request for quote (RFQ)s sent out. Based on those quotes (for simple geometries), it was cost prohibitive to further investigate fabricating a LMFBR assembly from quartz. Also, the MIR fluid, Drakeol 5 light mineral oil, has a higher viscosity than water [16], which would require substantially larger pumping and cooling equipment.

Song et al. [17] studied multiple 3D printed transparent resins and attempted to find refractive index matching fluids. They utilized three fabrication techniques, selective layer sintering (SLS), stereolithography (SLA), and vacuum casting. They found these resins had indices between 1.46 and 1.55. The most promising sample was produced by vacuum casting SLA from a silicon mold of a cylindrical rod and accompanying helical wire spacer. The final refractive index was 1.51 and a suitable working fluid mixture was determined to be anise oil and light mineral oil. Unfortunately, the kinematic viscosity of the oil mixture is roughly 10 times greater than water. If selected for this project, this would have required an axial velocity 10 times greater to achieve the same Re number.

Scholz et al.[18] investigated PIV measurements using 3D printed transparent materials, specifically Somos WaterClear[®] Ultra 10122 and RenShape[®] SL 7870. These materials required a sprayable transparent coating, because the printed products were initially opaque. The disadvantage is the coating reduces the fine detail of the printed parts. They also had trouble finding a fluid with a similar refractive index (1.51 - 1.56) and low viscosity. One option, a zinc iodine aqueous solution could match the refractive index, but only at high zinc iodine concentration. The high concentration yielded a red-colored solution with a lowered optical transparency. Their fluid choice was a 62.5% weight sodium iodide aqueous solution. Discoloration was noted as the fluid yellowed when exposed to air. Their experimental facility kept a nitrogen overpressure blanket to minimize the solution oxidation and were able to extend the solution life to over one year. Ouzo et AL also had success with PMMA and 64% weight sodium iodide aqueous solution. Discoloration/oxidation of sodium iodide was investigated in this thesis, see Section 4.2.1.

4. FACILITY DESIGN

An experimental facility containing a mock 61-rod hexagonal fuel assembly with helically wrapped wire spacers has been designed, procured, and constructed to conduct isothermal flow tests, Figures 4.1 and 4.2. The facility has produced high spatial and temporal resolution data of the flow velocity and pressure at different locations in the experimental fuel assembly. Brief facility descriptions have been provided in [19–23]. This section provides a detailed description of the materials testing and final design configuration.

The experimental facility consists of three loops, which are described in Sections 4.4, 4.5, and 4.6.

4.1 Matched-Index-of-Refracton

To meet the objectives defined in Section 2.1, a facility utilizing the MIR technique was required. The MIR technique involves matching the refractive index of the fluid and solid structures in the experimental facility. The primary objective of utilizing the MIR technique in combination with PIV and LDV laser-based measurement techniques is to measure the fluid velocity without disturbance via intrusive probes. The components of the facility with the MIR requirement were the fuel rods, wire spacers, and hexagonal test section.

The material selection of the test section and 61-rod assembly were primarily driven by Table 2.1, Requirement 1. It states that velocity measurements must be possible in edge, corner, and interior subchannels. The test section is where PIV and LDV measurement techniques were applied and will be discussed later in Section 4.3. Variables under consideration when selecting materials were cost, density, toxicity, flammability, and reactivity, and viscosity. Also, the refractive index is a

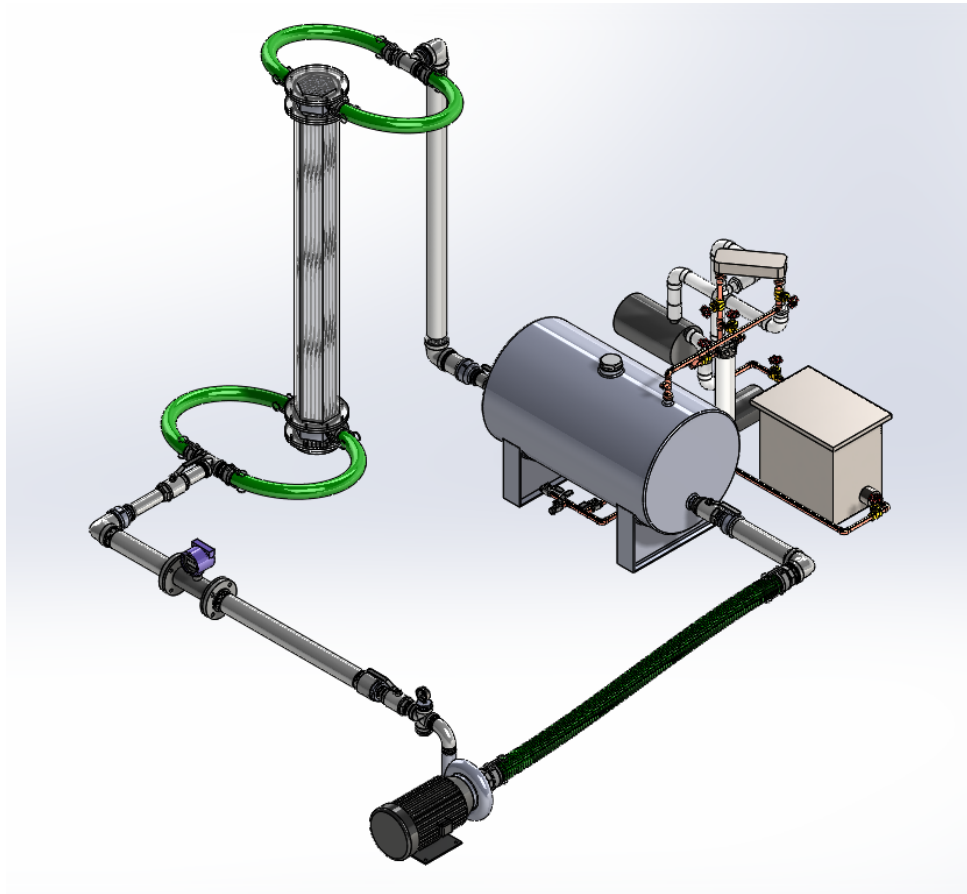


Figure 4.1: Isometric view of a CAD rendering of the experimental facility

function of incident photon wavelength and temperature of the medium. Therefore, the laser source's wavelength must be carefully selected. Temperature control is a design requirement to hold the fluid density and viscosity constant throughout all experimental runs. But with a MIR facility, constant temperature also guarantees that the refractive index of the fluid and solid structures are constant.

4.2 Materials Testing

Extensive material testing for the test section and experimental fuel assembly was required to ensure that all requirements could be met. Materials testing can be segregated into two distinct areas: optical and chemical testing.

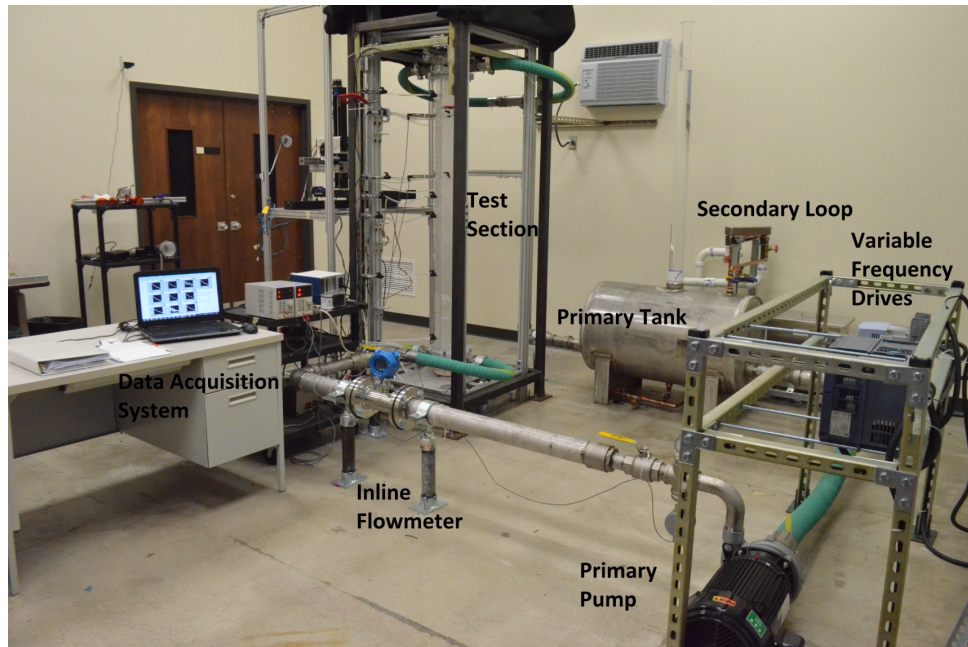


Figure 4.2: The experimental facility with major components highlighted.

4.2.1 *Optical Testing*

Optical testing was required to confirm refractive index matching and sufficient transparency of potential materials. As a result of the literature review, the number of solid/fluid pairs for optical testing was narrowed significantly. Tests that resulted in insufficient refractive index matching eliminated potential pairs of solid materials and fluids. Sufficient transparency was confirmed by illuminating solids and fluids with the 527 nm photon source, which is defined in further detail in Section 4.8. A lack of transparency could result in insufficient illumination of the seeding particles, thus decreasing the quality of the PIV measurements.

Optical tests presented in this thesis include cover two solids and fluids. The solids were PMMA and 3-D printed plastics. The fluids were p-Cymene and sodium iodide (NaI). In January 2015, the most promising 3-D printed transparent materials

were:

- VeroClear-RGD810 by Stratasys
- Accura 60 by 3D Systems

At that time, very little literature existed involving optical measurements on transparent 3-D printed materials. Therefore, samples of VeroClear-RGD810 and Accura 60 were acquired from respective companies, Figure 4.3. 3-D printed transparent materials were not pursued further due to the following reasons:

- TAMU does not have the capability to quantify the refractive index of solids.
- 3-D printers capable of printing lengths over 1 meter were not readily available. A bonding method would be required to fabricate the rods and enclosure.
- Stratasys was not confident that either material had sufficient strength to be used in the desired fuel rod geometry (large axial dimension with small radial dimension).
- Note the build lines that formed during the printing process. The build lines can be removed via sufficient surface polishing and transparent coating. However, The manual labor associated with surface polished was regarded as impractical to meet the time and fabrication tolerances required by the schedule and test specifications.
- RFQs were obtained from Stratasys for individual rods and the hexagonal enclosure. The final cost of the 3-D printed components were not significantly less than other options with lower risk.
- Tolerances of printed components were significantly poorer that achievable by casting or machining fabrication techniques



Figure 4.3: VeroClear-RGD810 and Accura 60 samples

With transparent 3-D printed materials no longer an option, PMMA was investigated. PMMA has been used in previous MIR facilities, as mentioned in Section 3. Qualitative optical tests on PMMA included:

- Confirmation of MIR conditions in p-Cymene and NaI
- Optical degradation of cast and extruded PMMA as a function of immersion time in p-Cymene
- Wire attachment methods and their optical disturbances
- Surface imperfections (cracks and scratches)

It is important to note refractive index is a temperature-dependent property. Bardet et al. [24] has quantified temperature dependence of the refractive index for p-Cymene and PMMA, Figure 4.4.

Refraction of light in PMMA and p-Cymene was investigated for the expected range of facility operating temperatures between 18-24°C. The first qualitative ob-

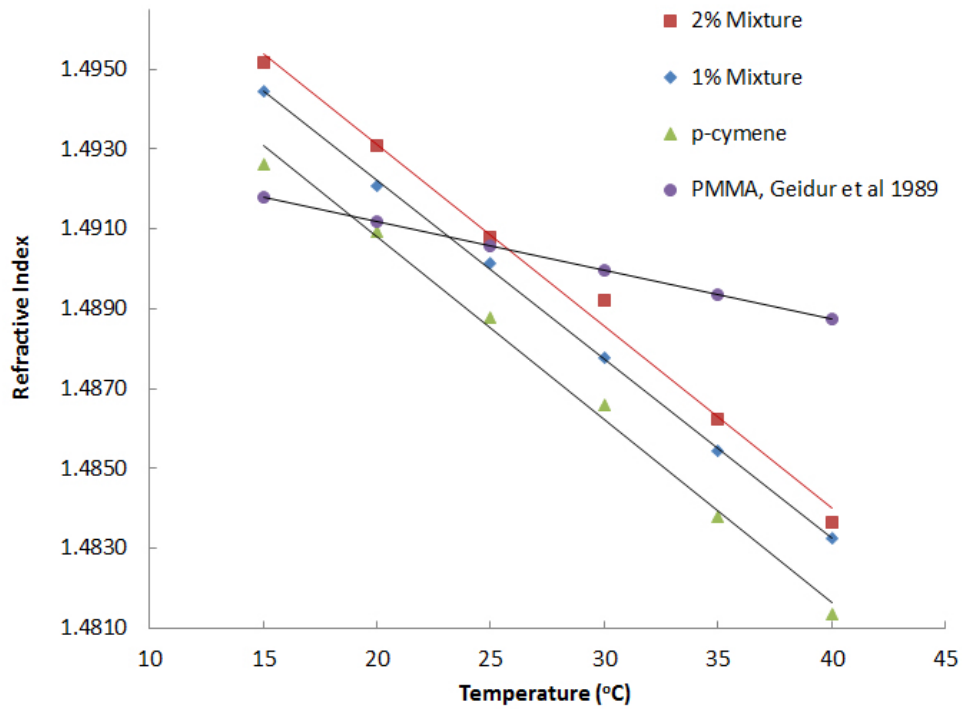


Figure 4.4: P-cymene and PMMA refractive indices as a function of temperature [24]

servation, Figure 4.5, was performed on a 0.5 inch diameter cylinder of PMMA. This was considered to be a successful optical test.

Next, the cut and unpolished edge of a PMMA cylinder was exposed to p-Cymene, Figure 4.6. The cut and unpolished edge did not have the same transparency and refractive index as the polished rod surface. It was later determined that excessive heating due to drilling or cutting PMMA has the ability to modify the refractive index, even after surface polishing. Therefore, this was considered to be an unsuccessful optical test.

Further optical tests involved using a liquid refractometer (to measure the refractive index of samples of p-Cymene) and the test shown in Figure 4.7. A ruler was placed behind the PMMA cylinder to observe the refraction through water and

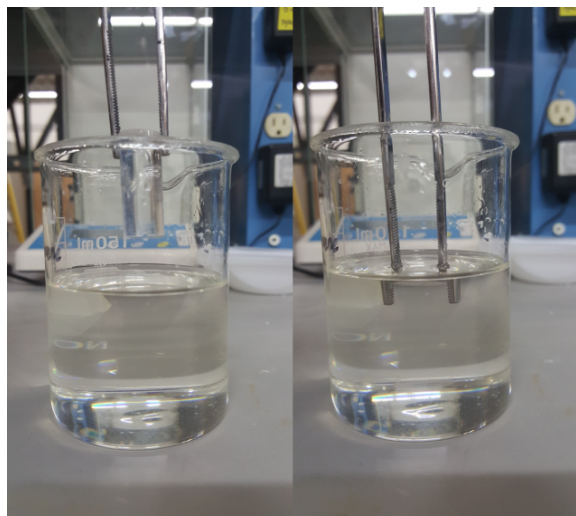


Figure 4.5: 0.5 inch diameter cylinder of PMMA immersed in p-Cymene at 22°C

p-Cymene. Note that the 1 inch lines are not impacted in p-Cymene. Also, the text is nearly unaltered when compared to the text in water.

After confirming that PMMA and p-Cymene passed qualitative optical tests, NaI aqueous solutions were investigated. Because the fluid is a solution of deionized (DI) water and NaI, the concentration of NaI can vary based on the mass added to create the mixture. The refractive index of various concentrations was measured using an in-house liquid refractometer, Table 4.1. The solubility limit at 23°C is approximately 65% [25], so the maximum tested concentration was 62%. The temperature of each solution was kept at 22 ± 1 °C. The measurements taken with the liquid refractometer proved to be nearly identical when compared to the quadratic least squares model and experimental measurements performed by [25], [26], and [27].

The refractive index was monitored for a period of 92 hours to quantify the change in refractive index that occurred during the oxidation period in which NaI aqueous solutions discolor and develop a yellow tint, Figure 4.8. Even though the refractive index remained relatively constant, concerns were raised about the discoloration's

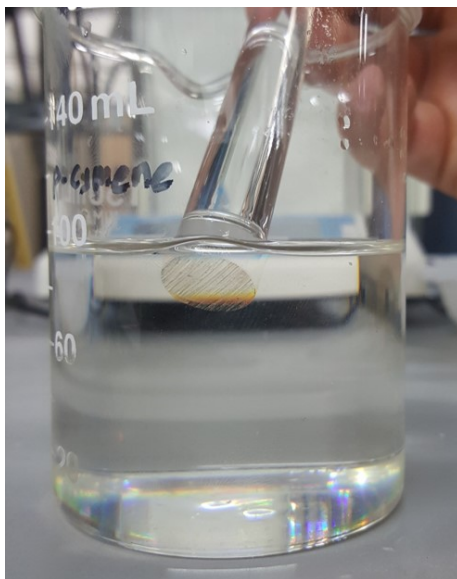


Figure 4.6: Unpolished edge of PMMA cylinder immersed in p-Cymene at 22°C

Table 4.1: Refractive index measurements of NaI aqueous solutions at 22°C

NaI Weight %	NaI (g)	DI Water (g)	RI (t=0)	RI (t=5hr)	RI (t=92hr)
0.5	38	38	1.443	N/A	N/A
0.6	57	38	1.475	N/A	N/A
0.62	62	38	1.484	1.484	1.482

affect on the fluid transparency and potential seeding particle illumination issues.

Figure 4.9 shows a PMMA rod (refractive index of 1.491 [24]) immersed in a NaI aqueous solution left to oxidize for 1 month. The refractive index of the fluid was measured to be 1.475. The perimeter of the PMMA rod is slightly visible. Note that the bubbles on the rod are from a wire attachment method being tested. This will be discussed later. Refraction of the background is clearly visible at the interface between the wood and black background, which is insufficient for laser-based optical measurement techniques.

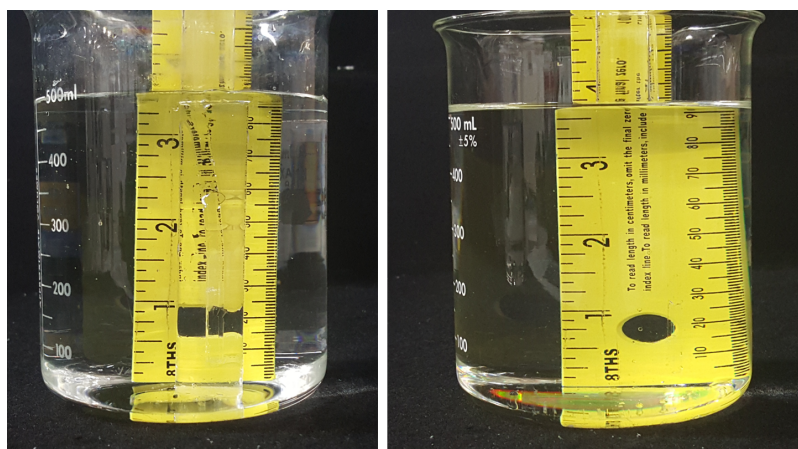


Figure 4.7: 0.625 inch PMMA cylinder immersed in water (left) and p-Cymene (right) at 22°C

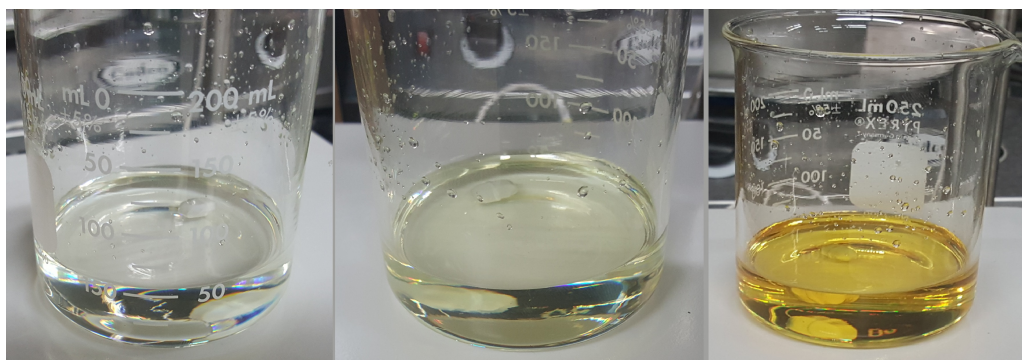


Figure 4.8: NaI solution (62 W%) after 0 hr, 5 hr, and 92 hr of exposure to air

MIR conditions could be achieved by approaching the solubility limit, [25]. However, operational concerns arose about cooling and precipitation when the facility was not in use, along with reheating above the solubility limit, mixing, and ensuring MIR conditions were met before performing an experimental run. Therefore, NaI was not investigated further.

Degradation of cast and extruded PMMA as a function of immersion time in p-Cymene will be discussed in more detail in Section 4.2.2. After 1 month of immersion



Figure 4.9: PMMA rod and NaI aqueous solution (62 W%) after 1 month of exposure to air at 22°C

time, the cast sample had minor surface etching that was only visible when the sample was removed from the fluid and dried. However, the refractive index was not qualitatively affected. The extruded sample experienced significant pitting and began to melt after 1 month. Again, the refractive index was not observed to be affected.

The next open item that involved optical testing was how to attach the helical wire spacer to the rod. Chemical compatibility tests of adhesives will be discussed later. The chemical tests resulted in two plausible adhesives that required optical testing.

The first adhesive, an acrylic solvent-based cement made by SCIPGRIP[®], resulted in the production of gas bubbles during the curing process along the interface between rod and wire. These volumes cannot be filled by p-Cymene, as they are internal to the solid. They did not have the correct refractive index, Figures 4.9 and 4.10. This type of adhesive was considered applicable, so long as the solvent was

not applied to regions where laser-based optical measurement techniques were to be applied.

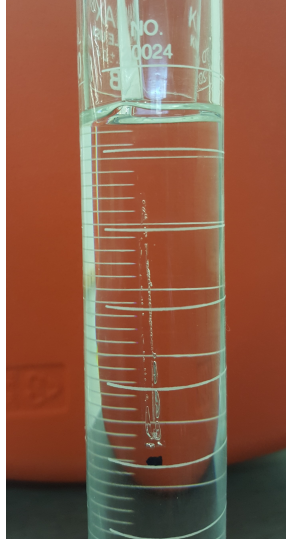


Figure 4.10: PMMA rod in p-Cymene showing the gas bubbles formed during the solvent curing process

The second adhesive, ethyl-2-cyanoacrylate (ECA), did not cause the PMMA to dissolve and re-solidify. This is because it is an adhesive commonly referred to as Super Glue[®]. Ethyl-2-cyanoacrylate was attractive because the adhesive base is an acrylic resin, which implied that MIR conditions could be possible in glued regions. Optical testing proved this to be true. Therefore, ECA could be used in regions where laser-based optical measurement techniques were to be applied.

The important conclusion of these optical tests was ECA could allow for the helical wire spacer to be attached to the rod along the entire length, while the acrylic solvent-based cement was limited to non-measurement regions. At the time of this testing, the measurement regions were not well defined.

One final note as a result of PMMA and p-Cymene optical testing was that any small scratches to the PMMA surface as a result of improper care or handling were not an issue. This is because once the PMMA was immersed in p-Cymene, the fluid would fill the small imperfection and MIR conditions were still achieved.

4.2.2 Chemical Testing

Chemical compatibility testing was required to ensure that wetted materials could survive facility operation while immersed in p-Cymene or water, the fluid used in the initial shakedown tests. Shakedown tests with water were performed to confirm piping integrity and hardware functionality before using p-Cymene. Chemical testing included:

- Surface degradation of cast and extruded PMMA as a function of immersion time in p-Cymene
- Wire attachment methods and adhesive performance in p-Cymene
- Performance of SCIGRIP acrylic solvent-based cement in p-Cymene to determine the feasibility of fabricating the test section hexagonal duct

Surface degradation of cast and extruded PMMA as a function of immersion time in p-Cymene was first tested. Observations took place over 36 days. Half of each sample was immersed in p-Cymene. Fresh samples are presented in Figure 4.11. There was no qualitative optical difference.

Surface degradation was not visible until the elapsed time reached 6 days. At that time, pitting was detected around the cut edges of the extruded sample. The cast sample appeared to be experiencing a slight etching, making it slightly less transparent, Figure 4.12.



Figure 4.11: Elapsed time of 0 days; Top: cast PMMA, Bottom: extruded PMMA

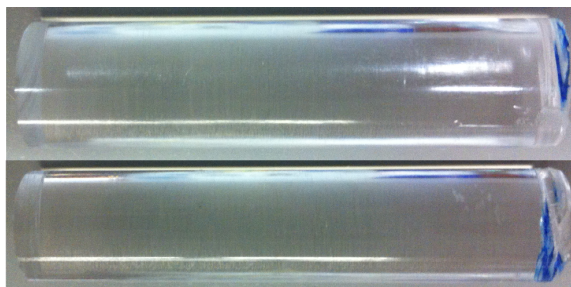


Figure 4.12: Elapsed time of 6 days; Top: cast PMMA, Bottom: extruded PMMA

After 16 days, significant pitting of the cut edges on the extruded sample were occurring. It was also tacky where the sample had been in contact with the glass beaker holding the p-Cymene and samples. There was no further visible pitting or etching of the cast sample, Figure 4.13.

The immersion test concluded after 36 days. The extruded sample was initially stuck to the glass beaker. Also, the wetted surface experienced severe pitting, melting, deformation, and was spongy when squeezed. The cast sample had minor etching with a slightly rougher surface. The loss of transparency is visible on the right side of the sample, where the grid lines of the paper are blurred, Figure 4.14. A closeup of the cut end of the extruded sample is visible in Figure 4.15.

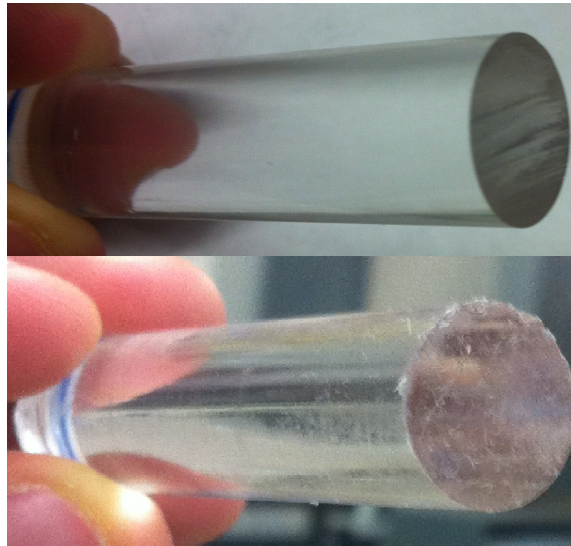


Figure 4.13: Elapsed time of 16 days; Top: cast PMMA, Bottom: extruded PMMA

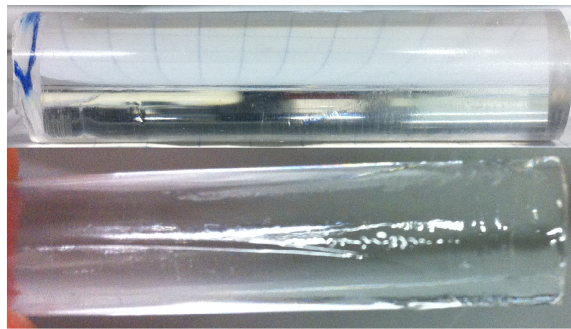


Figure 4.14: Elapsed time of 36 days; Top: cast PMMA, Bottom: extruded PMMA

Conclusions from this testing were:

- Structural integrity of cast PMMA is vastly superior to extruded
- Optical transparency of both cast and extruded PMMA is sufficient after 36 days
- Some interaction between the cast sample, extruded sample, air, and p-Cymene caused the P-Cymene to discolor slightly, Figure 4.16

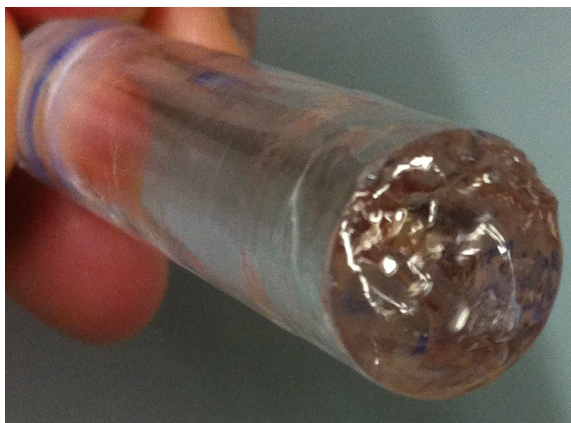


Figure 4.15: Elapsed time of 36 days; Extruded sample highlighting the physical deformation

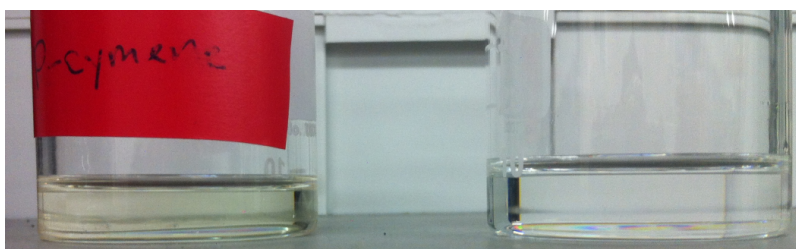


Figure 4.16: LEFT: Discolored p-Cymene after exposure to air, cast PMMA, and extruded PMMA for 36 days; RIGHT: fresh p-Cymene

The second chemical test involved evaluating the performance of different adhesives when used to attach PMMA helical wire spacers to PMMA rods. There are very few materials that are chemically stable in p-Cymene [28], [29]. Therefore, if an adhesive could withstand the mechanical stress of the helical wrap, the rod was immersed in p-Cymene and the impact observed.

The following adhesives were tested:

- SCIGRIP[®] acrylic solvent-based cement
- Ethyl-2-cyanoacrylate (Super Glue[®])

- Silicon caulk for waterproofing
- Polyurethane-based waterproof glue (Gorilla Glue[®])
- UV curable resin
- Waterproofing tape for ductwork

The silicon caulk and waterproofing tape for ductwork were unable to meet the mechanical requirement of maintaining the wire tension. The Gorilla Glue[®] had such a high viscosity that application of a fine bead, such as to not disturb the flow, proved difficult. The UV curable resin had a relatively long set time which made fabrication difficult.

Before immersion in p-Cymene, the acrylic solvent-based cement and ECA were the most promising because they had sufficiently low viscosities and quick set times. However, the acrylic solvent-based cement was only able to maintain integrity for 5 minutes before failing and unraveling the wire. It appears that p-Cymene was able to fill the small surface imperfections caused by the acrylic solvent and dissolve the interface. Ethyl-2-cyanoacrylate maintained integrity for the entire immersion time of two weeks with no observable cracking, pitting, or loss of strength.

4.2.3 Mechanical Testing

Mechanical testing was performed to determine the desired method of establishing the triangular lattice, along with investigating the rigidity of the PMMA rods and flexibility of the PMMA wires. The preferred method of establishing the triangular lattice was by using lower and upper grid plates, Figure 4.17. The grid plates contain the rod triangular lattice, along with a specific clocking angle for the helical wire spacer. The specific clocking angle in the grid plates ensures all fuel rods are

installed similarly. The plates were printing using an in-house MakerBot Replicator 2X.

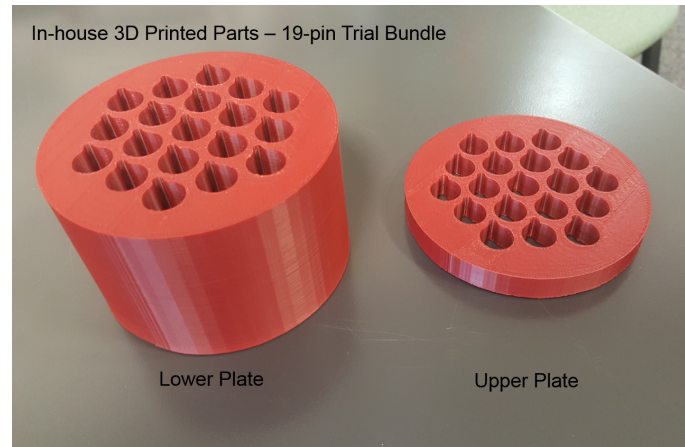


Figure 4.17: Lower and upper grid plates

A 19-rod test assembly of one wire pitch was installed in the 3D printed grid plates. Installation confirmed the feasibility of constructing the 61-rod assembly. The flexibility of various wire sizes was confirmed during the test rod fabrication process.

In order to allow the flow to fully develop, rod lengths were required to be greater than 72 inches. Samples of 0.5 inch and 0.625 inch diameter cast PMMA rods of various lengths were investigated for their rigidity after concerns of flow-induced vibrations arose from handling the 24 inch rods with 0.5 inch diameter used in the 19-rod test assembly. Rigidity testing concluded with the selection of 0.625 inch diameter rods.



Figure 4.18: 19-rod test assembly

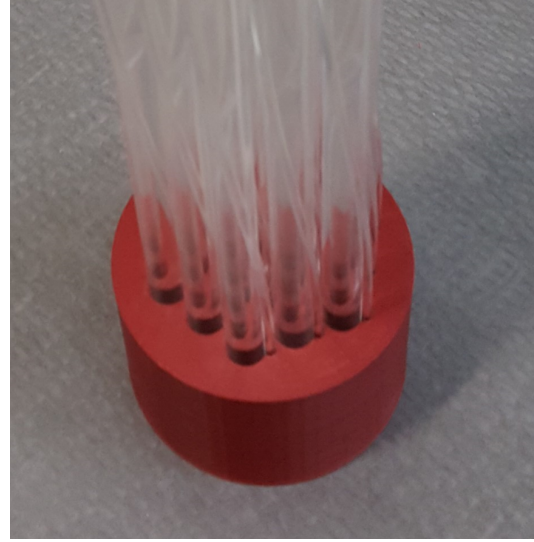


Figure 4.19: Closeup of the lower plate and test assembly

4.2.4 Final Material Selection

With the completion of optical and chemical testing, along with a thorough literature review of chemical compatibility, the set of final materials were selected, Table 4.2. After selecting p-Cymene as the fluid, the chemical compatibility of all wetted surfaces needed to be checked, including pump shaft seals, flange gaskets, and flexible hosing. p-Cymene has a density of 857 kg m^{-3} and a dynamic viscosity of $8.33\text{E}-4$ Pa sec.

Figure 4.20 displays the results of a sufficiently matched refractive index for PMMA at room temperature. The exterior surface of the PMMA rod is clearly visible in the lower and upper regions, while very difficult to see in the middle region. Three fluids are inside the beaker. The lower region is water with a refractive index of 1.330 [14]. The middle region is p-Cymene with a refractive index of 1.491 [30]. The upper region is air with a refractive index of 1.000277 [14].

Table 4.2: Final materials used in the experimental facility

	PMMA	ECA	SS316	Viton	UHMWPE	p-Cymene
Test Fluid						X
Rod	X					
Wire	X					
Wire Attachment		X				
Test Section	X					
Flexible Hosing					X	
Piping			X			
Pumps			X	X		
Gaskets				X		

The components that comprise the experimental facility will be discussed in the following sections. Figure 4.21 displays the test section filled with water for shakedown testing. After completing the shakedown testing, Figure 4.22 displays the MIR condition inside the test section when the facility was first filled with p-Cymene. The PMMA rods are visible above the fluid level, and the background of the room is visible below. Small amounts of florescent particles remain embedded from the water shakedown tests.

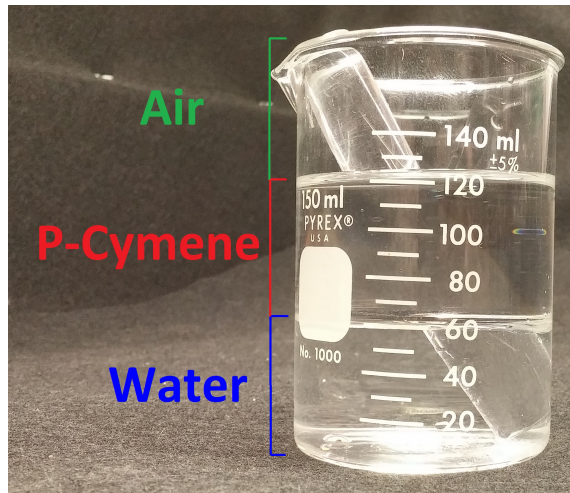


Figure 4.20: PMMA rod immersed in three fluids to display the result of matching the index of refraction

4.3 Test Section

The test section includes the following components:

- 61-rod wire-wrapped assembly
- Lower guide plate
- Inlet plenum
- Hexagonal duct
- Outlet plenum
- Upper guide plate
- Top cap

All components of the test section are made from PMMA to achieve MIR conditions in the test section, fuel assembly, and test fluid. This allows for velocity field

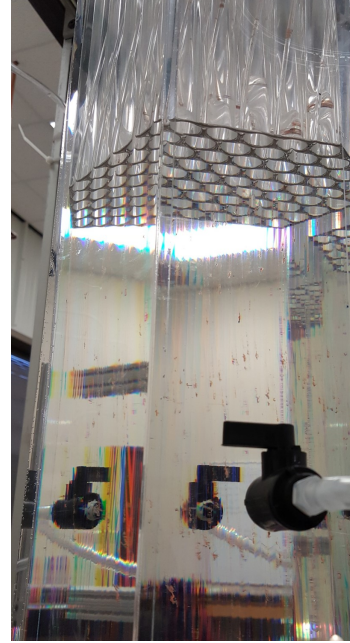
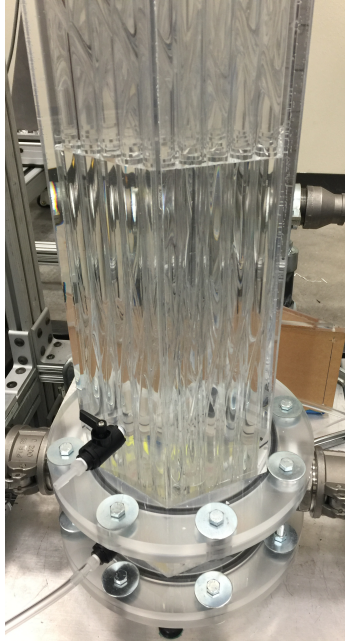


Figure 4.21: Test section filled with water Figure 4.22: Test section filled with p-Cymene to demonstrate the MIR condition

measurements to be performed in both the developing and fully-developed regions of the assembly.

Figure 4.23 contains the 61-rod wire-wrapped assembly, hexagonal duct, inlet and outlet plena, and guide plates

4.3.1 61-Rod Wire-Wrapped Assembly

LMFBR fuel assemblies typically utilize a triangular lattice of fuel rods, helically wrapped wire spacers, and a hexagonal duct, Figure 4.24. Similar to modern light water reactor (LWR) fuel rods, LMFBR fuel rods are cylindrical in shape but typically 66% of the LWR fuel rod diameter [31]. Both LWR and LMFBR fuel rods utilize a cladding tube. The cladding encases the fuel and serves as the first barrier to the release of fission products by containing fission gases and mitigating against

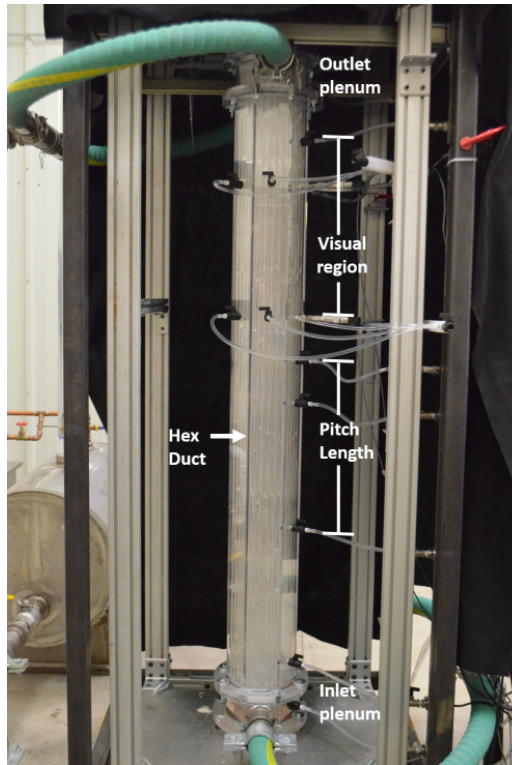


Figure 4.23: PMMA test section of the experimental facility

chemical interactions with the coolant. In this experimental case, the solid PMMA rods simulate the exterior surface of the fuel cladding.

The primary function of the helically wrapped wire spacers is to ensure sufficient lateral spacing between adjacent fuel rods. This spacing creates subchannels for coolant flow. Other functions are to enhance subchannel mixing to increase convective heat transfer and mitigate vortex-induced vibration.

The hexagonal duct of an LMFBR assembly has a similar function as the boiling water reactor (BWR) channel. It provides structural strength and a well-defined coolant flow path through the assembly.

The experimental fuel assembly consisted of 61 wire-wrapped rods arranged in a tightly packed triangular lattice. The tightly packed lattice indicates the wire spacer

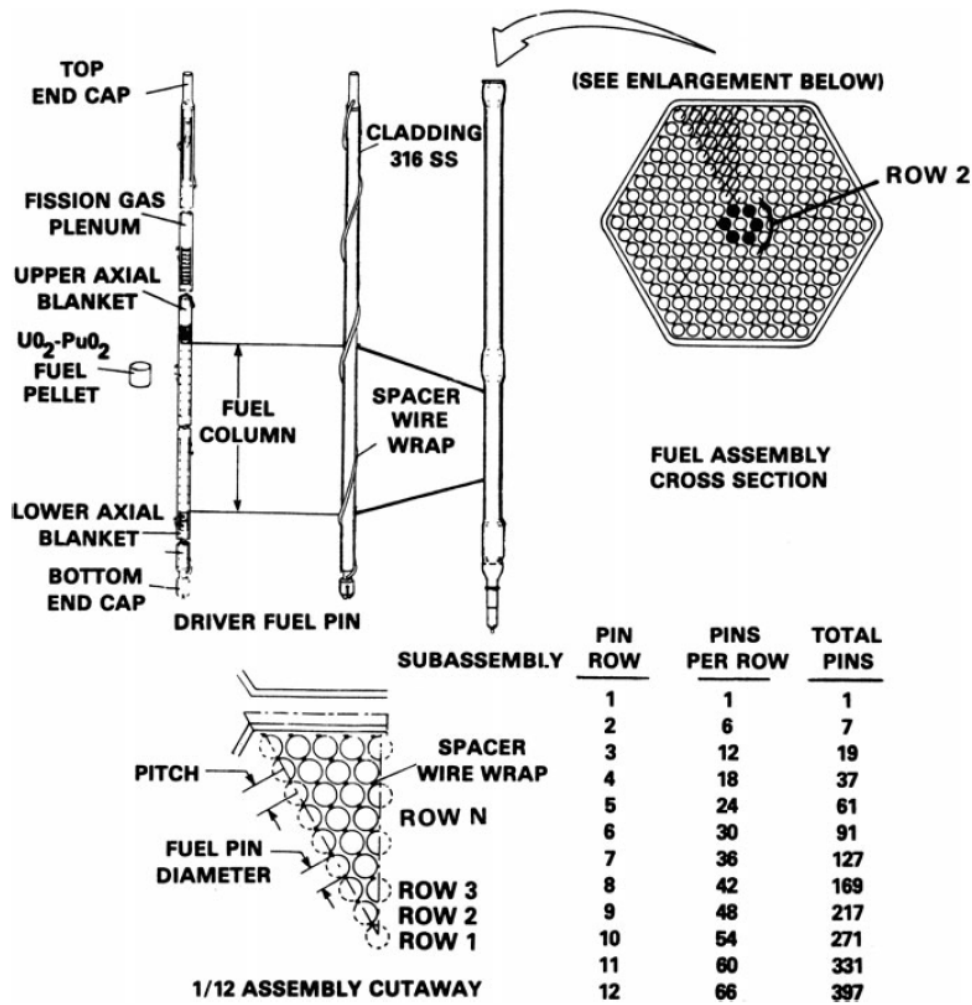


Figure 4.24: Typical LMFBR fuel assembly [31]

diameter is equal to the distance between adjacent rods with no additional gap. Dimensions of the experimental fuel assembly and hexagonal duct are identified in Figure 4.25.

The final dimensions of the experimental 61-rod fuel assembly are defined in Table 4.3. The P/D was chosen to be the constant scaling variable of the experimental design. The SFR fuel rod P/D typically ranges from 1.06 to 1.29 [31]. The target P/D was 1.18. After several iterations between off-the-shelf commercial availability

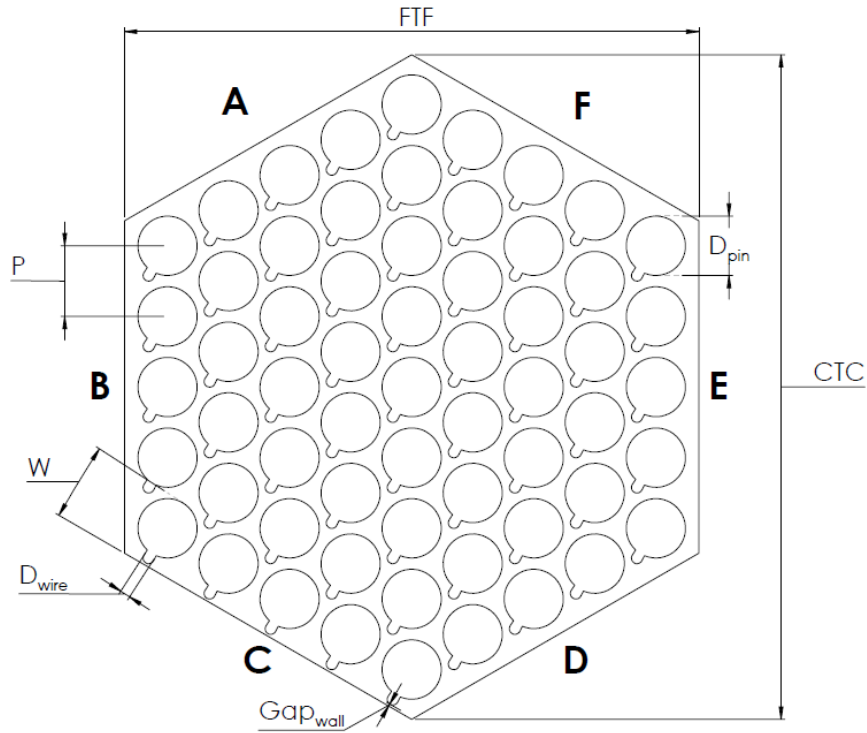


Figure 4.25: 61-rod hexagonal fuel assembly primary dimensions

and engineering specification, the final P/D for the experimental fuel assembly was converged to 1.189. Based on typical SFR fuel rod dimensions, the experimental assembly is scaled up approximately by a factor of 2.5.

4.3.1.1 Rod Fabrication Process

The rod fabrication process involved characterizing the diameter of the rods and wires, along with attaching the wires to the rods. Cast PMMA rods produced by PolyOne were selected for the experimental fuel rods, Figure 4.26. The specified cast diameter and fabrication tolerance were $0.0159 \text{ m} \pm 0.000254 \text{ m}$, respectively. Extruded PMMA rods were procured from Wuxi YanYang International Trading Co. Ltd for the wire spacers. The specified extruded diameter and fabrication tolerance were $0.003 \text{ m} \pm 0.00015 \text{ m}$, respectively.

Table 4.3: Dimensions of the rods and wire spacers in the experimental facility

Symbol	Parameter	Value (m)
D_{rod}	Rod Diameter	0.0159
P	Rod Pitch	0.0189
D_{wire}	Wire Diameter	0.0030
H	Wire Pitch	0.4763
W	Edge Pitch	0.0195
Gap_{wall}	Wall Gap Size	6.71E-4
FTF	Flat-to-Flat	6.0560
CTC	Corner-to-Corner	0.1778
P/D	Rod Pitch to Rod Diameter	1.1890
H/D	Wire Pitch to Rod Diameter	30.000
L	Assembly Total Length	1.8570
L_{ts}	Assembly Length in Test Section	1.6670

The diameter of each rod and wire was quantified at three different axial locations (bottom, middle, and top). Rods and wires with the smallest standard deviation about the nominal value were selected. 100 rods and 100 wires were characterized to generate the final set of 61 rod/wire pairs. The rod mean diameter and standard deviation were 15.918E-3m and 1.524E-5 m, respectively. The wire mean diameter and standard deviation were 2.97E-3 m and 3.00E-5 m, respectively. A more detailed characterization process is summarized in Appendix A.

LMFBR fuel assemblies typically only attach the helical wire spacers via tacking to the bottom and top of the rods. This technique was mirrored for the first experimental assembly. Consideration was made to fully adhere the wire along the length of the rod. However, the risk of disturbing the flow, along with the extra labor expense, was deemed greater than the reward.

As discussed in Section 4.2.1, the adhesive used in the fabrication of the rods and wires was ECA with a water-thin viscosity. Two guide blocks were used to assist in the rod fabrication. An aluminum guide was fabricated from a rectangular prism of



Figure 4.26: Cast PMMA rods produced by PolyOne with attached wire spacers

aluminum by milling a pair of rod and wire holes with the appropriate offset, Figure 4.27. This aluminum guide simulated a single rod position found on the lower plate. This avoided using the lower plate during the fabrication process, where cracking, scratching, or inadvertent gluing could occur. The aluminum guide ensured the rod and wire axes were parallel before the helical wrap. This was required for the rods to fit into the lower plate. Another guide was created using a Makerbot Replicator 2X 3-D printer, Figure 4.28. This 3D printed guide also ensured the rod and wire axes were parallel, so the upper plate could be installed on the 61-rod assembly. It also provided the desired azimuthal wire position at the top to achieved the desired helical pitch length.

The fabrication process required two people and took approximately one hour

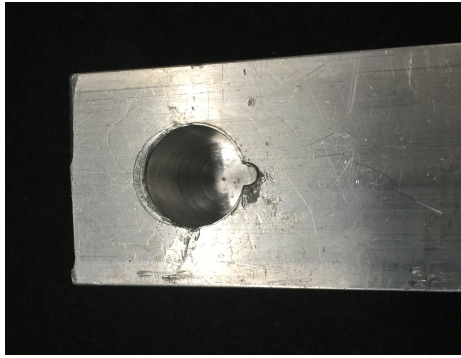


Figure 4.27: Aluminum guide block to set the bottom of the rod and wire parallel axes

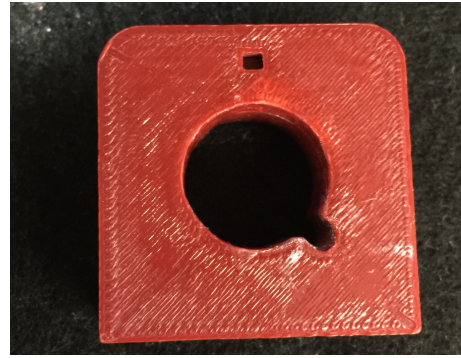


Figure 4.28: 3-D printed guide block to set parallel axes and wire azimuthal position at the top of the rod.

per rod. A closeup of a single completed rod is shown in Figure 4.29. The process will now be described:

1. The wires were attached to the bottom of the rods with the assistance of an aluminum guide block, Figure 4.27.
2. While laying horizontally on the fabrication table, the bottoms of the rod and wire were inserted into the aluminum guide.
3. The tops of the rod and wire were secured with a rubber band.
4. The slack in the wire was then removed.
5. The rod and wire were then stood vertical, with the aluminum guide forming the base.
6. A single drop of adhesive was placed on both sides of the joint formed by the adjacent faces of the rod and wire. The drops were applied approximately 38 mm above the bottom of the rod.

7. After allowing 10 seconds to cure, the rod was laid horizontally and remained in the aluminum guide.
8. The rubber band was then removed from the top and a 3-D printed guide block was slid into place, Figure 4.28.
9. The 3D printed guide block was revolved four times (in a clockwise manner when viewed from the bottom of the rod) to create the desired wire wrap.
10. Tension was applied to the wire to remove slack.
11. A single drop of adhesive was placed on both sides of the joint formed by the adjacent faces of the rod and wire. The drops were applied approximately 15 mm below the top of the rod.
12. The aluminum and 3-D printed guides were removed.
13. A quality check was performed to verify the wire clocking position at each pitch along the rod. The check involved a visual inspection that the wire was at the 12 o'clock position for 0.514 m, 0.991 m, and 1.467 m distances from the bottom of the rod.
14. The top of each rod was ground into a cone to assist in placing the upper guide plate simultaneously over the 61-rod assembly during the final stage of construction, Figure 4.30.

4.3.2 Hexagonal Duct

The hexagonal duct was fabricated by Moore Fabrication, a custom PMMA fabrication shop that specializes in solving unique CNC machining and fabrication challenges. The hexagonal duct was formed by gluing six cast PMMA sheets together.

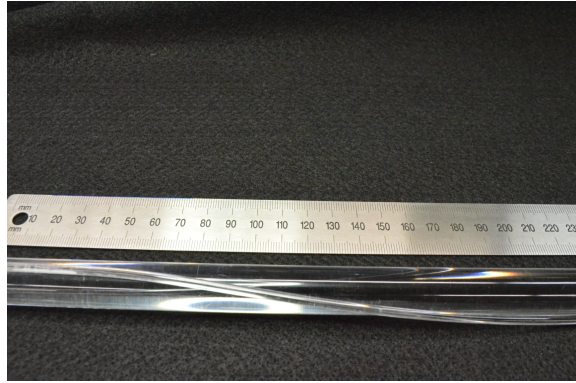


Figure 4.29: Closeup showing the wire attachment

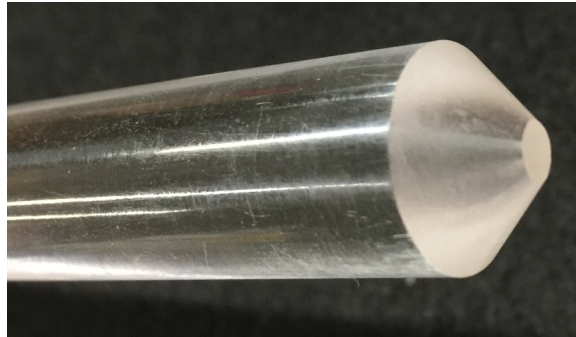


Figure 4.30: Closeup showing the top of a rod after the coning process

The desired wall thickness was 0.5 inches. Moore Fabrication characterized sheets from PolyOne and found the sheets to vary in thickness by an unacceptable amount. Therefore, each sheet was milled to 0.5 ± 0.001 inches and polished to avoid the MIR issues associated with unpolished surfaces, Figure 4.6. The hexagonal duct flat-to-flat (FTF) was set by forming the walls around three hexagonal guides at the top, middle, and bottom of the duct. After gluing the walls, the guides were removed and the duct was formed. 0.125 inch holes were drilled and tapped to create pressure taps at various axial and azimuthal locations. Circular flanges, with 0.5 inch thickness, were attached after the duct was formed. Engineering drawings and as-built dimen-

sions can be found in Appendix D and A, respectively. The length of the hexagonal duct was chosen so that the total length was 3.5 wire pitches. This created for a development region of 2.25 wire pitches to allow flow development, a visualization section of 1 wire pitch where the velocity field measurements were performed, and an exit section of 0.25 wire pitches to minimize exit effects.

Figures 4.31 and 4.32 show the hexagonal duct before and after installation in the experimental facility.



Figure 4.31: Before installation



Figure 4.32: After installation

4.3.3 Plena

The inlet and outlet plena were also fabricated by Moore Fabrication. The hexagonal shape of two plena were cut from the single piece formed by the process for the hexagonal duct. 2 inch diameter holes were cut in opposite faces of the hexagon to

form the inlet and outlet passages. Threaded circular blocks were then glued to the faces to create a connection for piping. 0.125 inch holes were drilled and tapped to create pressure taps and a drain port in the plenum. Circular flanges, with 0.5 inch thickness, were attached after the plenum were formed. Figure 4.33 shows the lower plenum with one circular flange attached. Engineering drawings and as-built dimensions are can be found in Appendix D and A, respectively.

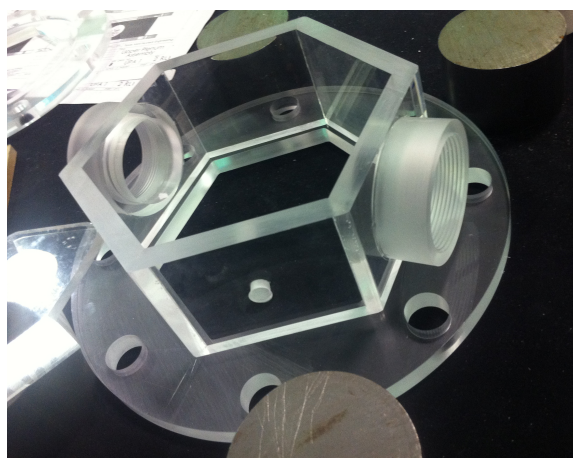


Figure 4.33: Plenum before the upper circular flange was attached

Figures 4.34 and 4.35 show the lower and upper plenum installed in the experimental facility.

4.3.4 *Guide Plates*

Lower and upper guide plates were utilized to establish the triangular lattice with the desired P/D of 1.189. Both plates contain holes for the rods and wires to guarantee the helical wire spacer azimuthal position of each rod is identical at a given axial location. The depth of the holes in the lower plate are 1.5 and 1.25 inch for the rod and wire, respectively. The holes in the upper plate are through holes.

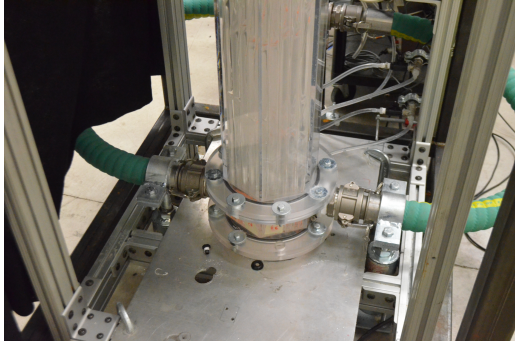


Figure 4.34: Lower plenum

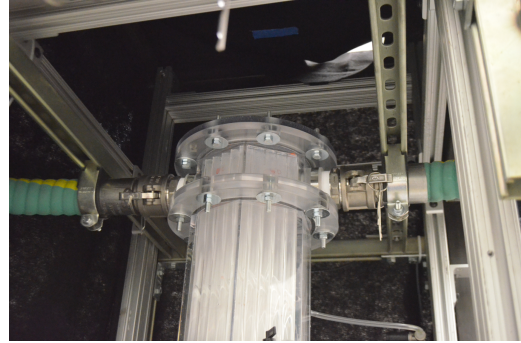


Figure 4.35: Upper plenum

Engineering drawings can be found in Appendix D.

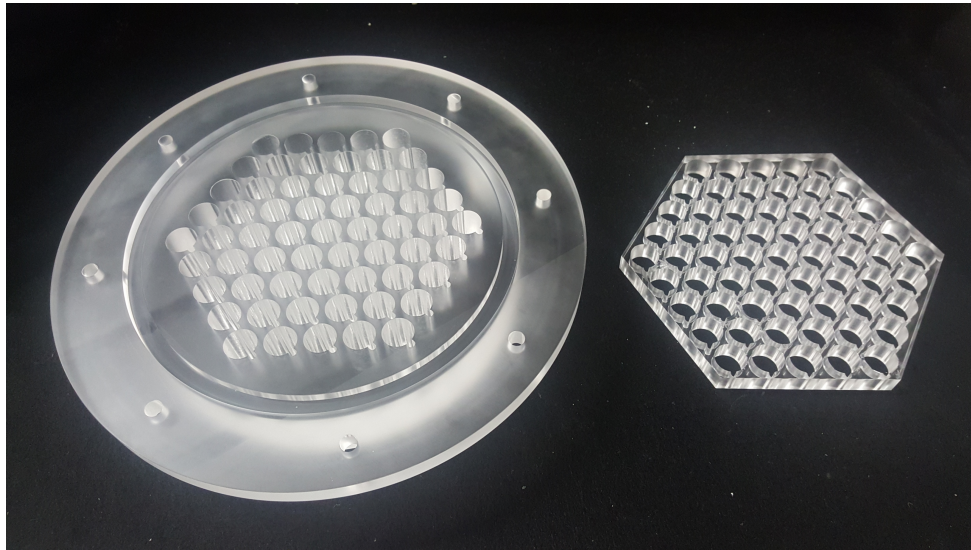


Figure 4.36: Lower and upper guide plates

4.4 Primary Loop

The primary loop circulates p-Cymene to the test section, where velocity field and pressure measurements are performed. Calculations of the pressure drop through

the flow loop were made and used to select the appropriate size of the piping, primary pump, and primary reservoir to hit the target Re of 20,000. The piping and instrument diagram (PID) in Appendix B displays the layout of the primary loop. Appendix E contains the manufacturer, model number, and serial number of the main components. A list of components is provided below:

- Primary pump
- Primary VFD
- Primary reservoir with 80 gallon capacity
- Test section
- Nine axial pressure transducers
- Two sets of 4 azimuthal differential pressure transducers
- Seeding particle injection port
- RTD
- Inline turbine flow meter
- 2 and 3 inch stainless steel (SS) diameter piping and valving
- 2 inch flexible hosing for vibrational dampening
- Framing for test section isolate and imaging hardware mounting points

Figure 4.37 displays a flow regime map proposed by Cheng and Todreas [32]. With an experimental assembly P/D of 1.189, the minimum Re number for fully turbulent flow is approximately 14,000. The target Re number was 20,000 to increase the certainty that measurements would be performed in the turbulent regime.

Measurements in the turbulent regime are required for RANS turbulence model validation.

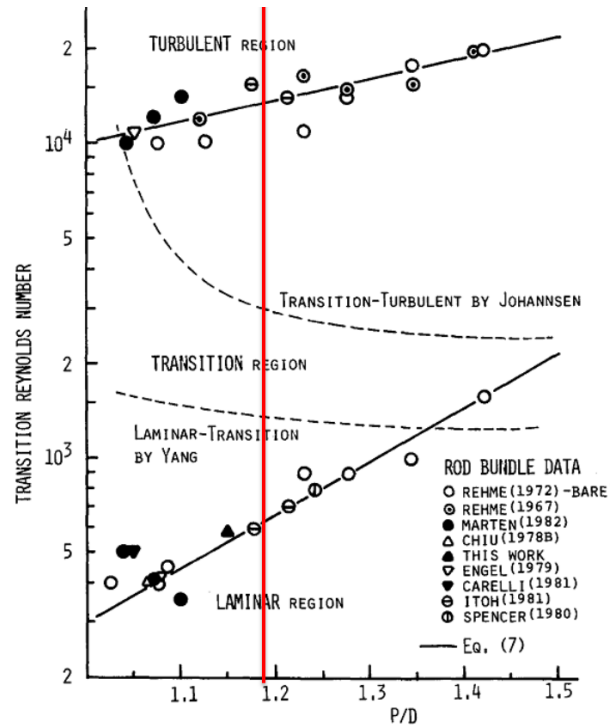


Figure 4.37: Laminar/turbulent flow transition [32]

This requirement was significant, because it required a robust flow loop with sufficient vibrational dampening of the test section to avoid movement of the test section or rod assembly during the PIV image capture process. Vibration was mitigated by utilizing support structures, pipe stands, and flexible hoses. Also, the PIV imaging hardware was mounted to the support structure which stabilized the test section. By doing this, the test section and PIV imaging hardware became coupled so that vibrations of the test section and imaging hardware would be approximately equal. Two support structures were built. The former structure was from iron tubing, which

was used to dampen the vibration in the piping and flexible hosing. Strut rails were also welded to this structure to provide mounting points. The later structure was from aluminum t-slotted framing, which is the common interface for lasers, cameras, and traversing systems. The structures were designed to minimize the interference with various PIV hardware setups, by minimizing support thicknesses and ensuring adequate spacing for even stereoscopic and tomographic PIV.

To secure the primary piping, pipe stands were anchored to the concrete floor. Neoprene inserts were also added between the piping and pipe stands. Chemical resistant ultra-high-molecular-weight polyethylene (UHMWPE) flexible hoses with quick disconnecting cam and groove fittings were utilized to connect the piping to the test section. The hoses were anchored to the iron frame to offload the tension caused by bending the hoses from the PMMA outlet plenum, Figure 4.38.



Figure 4.38: UHMWPE flexible hoses anchored to support structure

Seeding particles were initially prepared and mixed into the primary reservoir. However at low Re number, settling and accumulation was apparent by the decreasing particle density in the PIV images over a span of 10-30 minutes. Therefore, particle

injection was moved immediately downstream the primary pump. By using two valves and a syringe, Figure 4.39, injection could be performed while the facility was full and also running at any given flowrate. Also, the primary reservoir was recirculated by the secondary loop through the heat exchanger.



Figure 4.39: Seeding particle injection was performed by manipulating two valves and a 50 mL syringe

4.4.1 Leak Testing

The primary loop was leak tested multiple times with water before using p-Cymene. Figure 4.40 shows the configuration for the first leak test of the primary piping structure, with a flexible hose to close the loop. The primary pump was increased until a flowrate of $68 \text{ m}^3 \text{ hr}^{-1}$ (300 GPM) was achieved. The test proved that Polytetrafluoroethylene (PTFE), commonly known as Teflon[™], would be insufficient at several of the threaded connections.

To avoid welding the piping, a chemically resistant thread sealant, Loctite[®] 554, was employed. Figure 4.41 shows the final leak test configuration before installation

of the PMMA test section. A PVC pipe with similar inlet and outlet configuration to the test section was fabricated to close the loop to test the remaining piping structure, along with the quick disconnecting cam and groove fittings. It was realized here that supports would be needed to offload the flexible hose tension from the PMMA inlet connections.



Figure 4.40: Initial leak testing configuration

4.5 Secondary Loop

The secondary loop provides temperature and inventory control, along with particulate filtration. The PID in Appendix B displays the layout of the secondary loop. Appendix E contains the manufacturer, model number, and serial number of the main components. A list of components is provided below:

- Secondary pump
- Secondary VFD
- Secondary reservoir with 20 gallon capacity



Figure 4.41: Final leak testing configuration

- Brazed-plate heat exchanger
- Particulate filter, 1 micron removal capability
- Copper piping and gate valves, 0.75 inch diameter

Temperature control is important for MIR experiments, because the refractive index is a temperature dependent property. Temperature control is achieved by constantly circulating the primary fluid to and from the primary reservoir by the secondary pump into the heat exchanger. Chilled water is fed to the other side of the heat exchanger by the tertiary loop, Section 4.6. Pressure drop and heat rejection

calculations were performed to size the secondary pump and heat exchanger such that a constant temperature could be maintained in the primary loop. p-Cymene has a specific heat approximately 10 times less than water, so even short experimental runs could result in a relatively quick increase in fluid temperature without adequate cooling.

Minimizing the time duration of p-Cymene in the test section was important to extend the life of the hexagonal duct and experimental fuel assembly. Therefore when the facility was not in use, the test section was isolated from the primary loop and the p-Cymene inventory in the test section was transferred to the secondary reservoir.

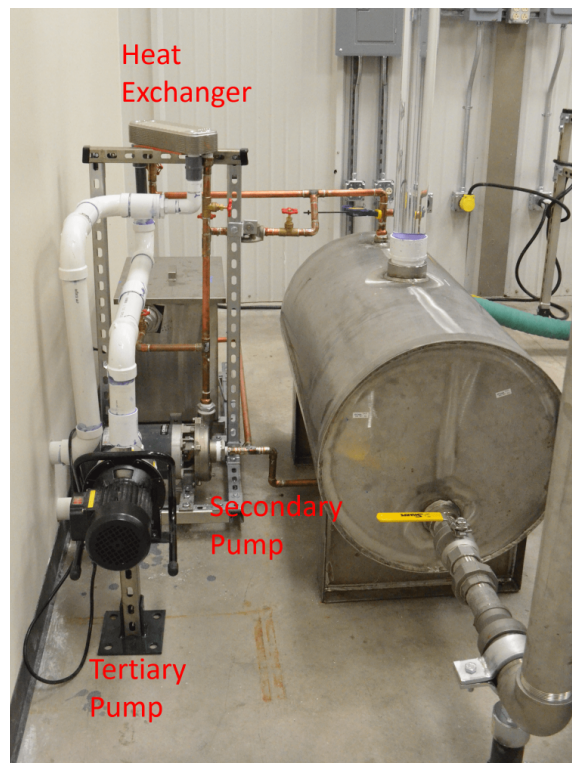


Figure 4.42: Secondary loop is copper, while the tertiary loop is PVC

Filtration is achieved by circulating p-Cymene to and from the primary reservoir by the secondary pump into the particulate filter. This operation was necessary to minimize dust and remove the seeding particles used in the PIV imaging technique, Section 4.8. Also, the filter can be bypassed, allowing for the recirculation of the primary reservoir. This was necessary to minimize settling of the seeding particles when operating the facility at low flow rates.

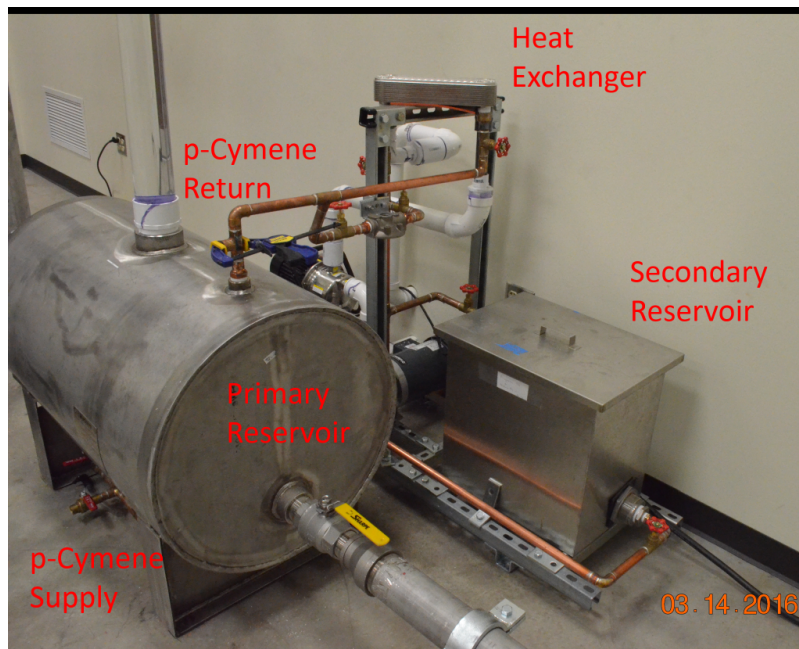


Figure 4.43: Secondary reservoir is visible and p-Cymene returns to the top of the primary reservoir

4.6 Tertiary Loop

The tertiary loop provides chilled water to the experimental facility so that the primary loop temperature can be maintained, Figure 4.44. It interfaces with the secondary loop at the heat exchanger. The loop consists of the following components:

- Tertiary pump, 1 HP, constant speed
- Insulated tertiary reservoir with 500 gallon capacity and level indication
- Air-cooled portable chiller to cool the tertiary reservoir
- 2 inch polyvinyl chloride (PVC) piping and valving
- Quick disconnect hose fitting for easy draining



Figure 4.44: Tertiary reservoir, air-cooled chiller, and chilled water lines into the facility room

4.7 Facility Room

Before construction began on the experimental facility, a project safety assessment (PSA) was performed by Texas A&M University to determine the occupational risks and requirements. The PSA is located in Appendix C. A portion (22 ft x 28 ft)

of the Texas A&M Nuclear Engineering Department's Thermal-Hydraulic Research Laboratory was enclosure to meet these requirements. The primary functions of the room include:

- Personnel control for laser safety
- Dedicated exhaust system
- Dedicated air conditioning system



Figure 4.45: Aluminum framing of the facility room

Personnel control was achieved by a set of locked doors and "LASER ON" warning indicators outside of the facility room. Personnel control was necessary to adhere to Class IV laser safety protocol. Direct and indirect light from these lasers can cause severe and permanent damage to the eye of individuals without personal protective equipment.

The dedicated exhaust system was necessary to meet respiratory requirements inside the facility room. Air inlet is achieved through a set of louvers. Exhaust is

directed out the ceiling of the facility room and driven out of the University Services Building (USB) with a blower and ductwork.

The dedicated air conditioning system helped maintain a constant temperature in the facility room. This assisted in achieving MIR conditions, as well as meeting personnel habitability requirements in an enclosed space with multiple heat generating components.



Figure 4.46: Drywall preparation

4.8 Imaging Hardware

The PIV system consisted of a 10 W continuous laser at a wavelength of 527 nm and one digital CMOS high-speed Memrecam GX-3 camera. See Figures 5.2 and 5.3 in Section 5 for a top-down view of the PIV hardware configuration used for the results presented in this thesis. The laser beam was adjusted by beam combination optics to form a 1.5 mm thick laser sheet. The laser and camera position was adjusted with three motorized linear translation stages. Laser alignment for the vertical plane discussed in this thesis is provided in Section 5. The high-speed Memrecam GX-3 camera has a full resolution of 1280 x 1024 pixels, maximum frames per second (at

full resolution) of 2,068, and 12-bit image depth. Figure 4.47 displays the imaging hardware setup for a typical PIV measurement.

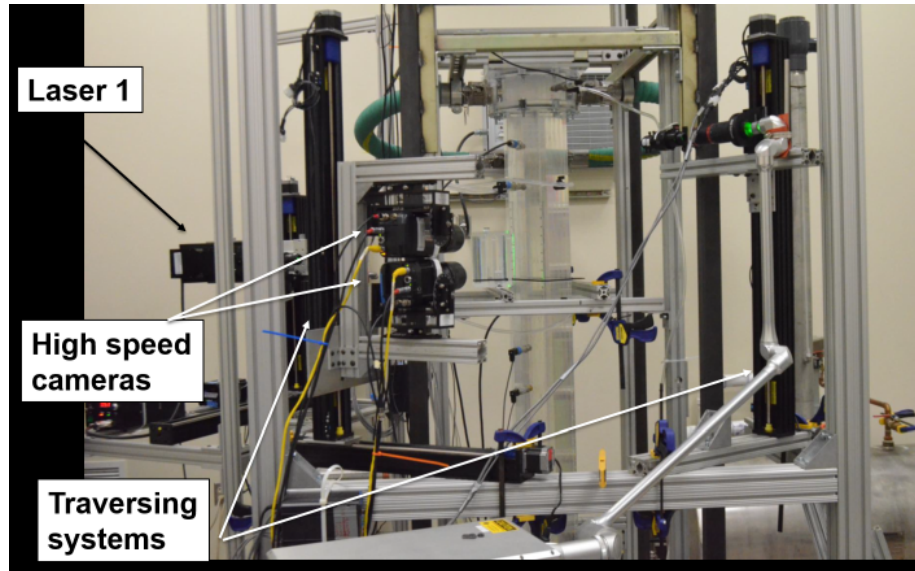


Figure 4.47: PIV setup containing test section, laser, camera, and traverse system

Seeding particles were fluorescent particles (UVPMS-BO Cospheric) with a mean diameter of $50 \mu\text{m}$, a density of 1.0 g cm^{-3} , and an emission wavelength of 600 nm . Figure 4.48 displays the fluorescent particles as viewed through laser safety goggles that attenuate the majority of the 527 nm light. The seeding particles were selected based on a parametric optimization of the reflectivity, diameter, and density. The density of the particle must approximately equal the fluid density under investigation to best match the movement of a fluid element. Reflectivity and diameter are inversely proportional, so testing must be done with the laser source to determine if sufficient particle illumination can be achieved with the smallest diameter particle. Also, the particle-image should be approximately 3-5 pixels on the PIV images.

A Quantum Composers digital delay pulse generator with 1 ns resolution was

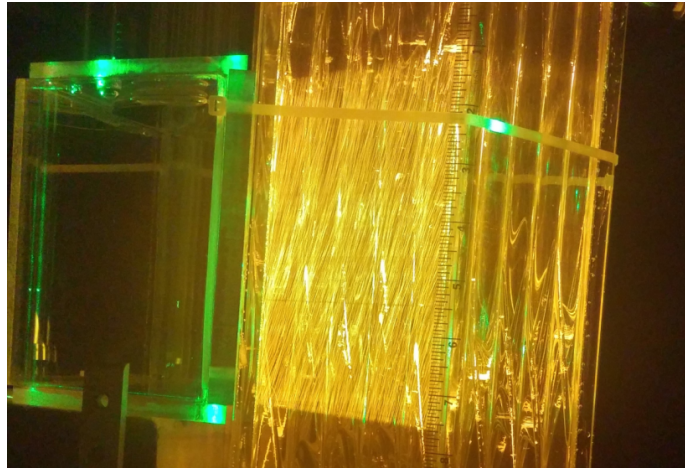


Figure 4.48: 600 nm fluorescent particles illuminated through an optical prism in the near-wall region of the 61-rod assembly

utilized to synchronize the recording start time of the PIV and pressure hardware. When possible, sampling frequency of both systems was set to be equal. By doing this, time-synchronized data was collected.

Hollow, 30-60-90 triangular prisms were constructed from PMMA sheets of 0.25 inch thickness. The optical prisms were mated to the exterior wall of the hexagonal duct in the visualization region to achieve a perpendicular orientation between camera and laser. The prisms were filled with p-Cymene to minimize refraction of the laser sheet as it passed through various media before reaching the near-wall region of the 61-rod assembly. Figures 4.49, 5.2, and 5.3 show an optical prism mounted adjacent to the hexagonal duct. Figures 4.49 and 4.50 display the test section illuminated by the laser source. Figure 4.50 displays a horizontal laser sheet across the 61-rod assembly. The triangular lattice of the rods is clearly visible inside the hexagonal duct.

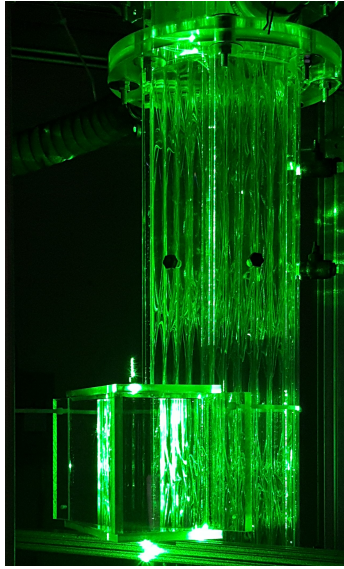


Figure 4.49: Vertical laser sheet and optical prism without MIR conditions

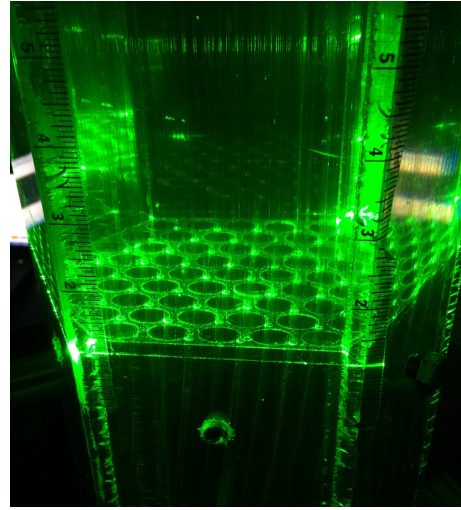


Figure 4.50: Horizontal laser sheet with MIR conditions

4.9 Pressure Hardware

High accuracy pressure transducers were procured from Omega[®]. The transducers have stainless steel wetted parts to be chemically compatible with p-Cymene. Initial testing showed no signs of hysteresis. Pressure taps were drilled and tapped in the inlet plenum, hexagonal duct, and outlet plenum so that pressure transducers could be installed. The inlet plenum transducer measures the maximum gauge pressure in the test section at the lowest axial location. The outlet plenum transducer measures the minimum gauge pressure in the test section at the highest axial location. The difference between these measurements is pressure drop across the entire bundle. The outlet plenum tap is also used to degas the facility during the filling process. The location of all pressure taps was carefully considered to not obstruct potential PIV viewing windows.

The hexagonal duct contains 7 axial pressure transducers and 2 sets of azimuthal

pressure transducers. The axial transducers measure the gauge pressure at various axial locations, while the azimuthal taps allow for the differential pressure (DP) to be measured between 2 different faces at the same axial locations. Figure 4.51 shows the experimental facility with the installed pressure hardware. Appendix A contains the axial and azimuthal pressure tap locations. Table 4.4 contains the hardware used in the experimental facility.

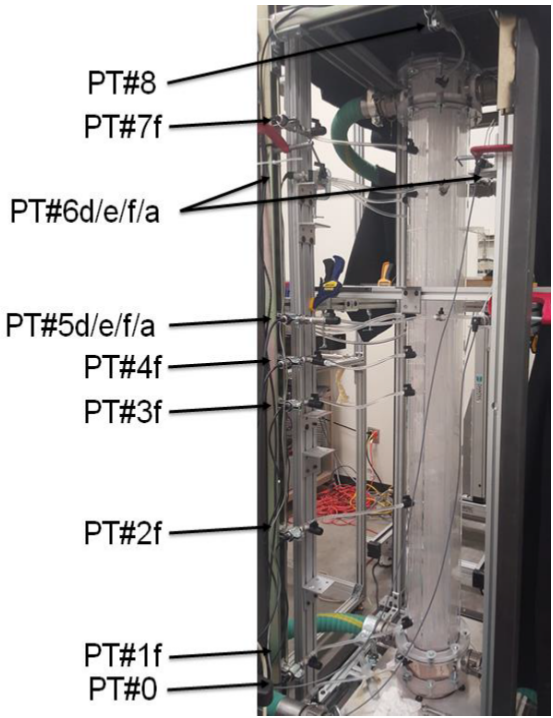


Figure 4.51: Pressure hardware location

4.10 Operating Procedures

A set of operating procedures were developed as part of the quality assurance plan. The procedures ensured that the experimental facility was returned to the same initial state so measurements could be repeated with confidence. Operating procedures for

Table 4.4: Pressure hardware used in the experimental test

Position	Model Number	Description	Accuracy
0F	PX309-030G5V	30 psi Gauge	< 4.0% FS
1F	PX309-030G5V	30 psi Gauge	< 4.0% FS
2F	PX419-030G5V	30 psi Gauge	< 0.1% FS
3F	PX419-030G5V	30 psi Gauge	< 0.1% FS
4F	PX419-030G5V	30 psi Gauge	< 0.1% FS
5F	MMG015V5P1D0T4A6CEPS	15 psi Gauge	< 0.1% FS
6F	PX419-030G5V	30 psi Gauge	< 0.1% FS
7F	MMG015V5P1D0T4A6CEPS	15 psi Gauge	< 0.1% FS
8A	PX309-015G5V	15 psi Gauge	< 1.0% FS
5 D/E/F/A	P55D-4-N-20-S-5-A	5 inch H_2O DP	< 4.3% FS
6 D/E/F/A	MMDWB10WBIV5P2D0T2A2CE	10 inch H_2O DP	< 0.1% FS

p-Cymene as the working fluid are located in Appendix B The operating procedures include:

- Filling the facility by transferring p-Cymene from the secondary reservoir into the test section
- Degasification of the primary loop
- Instrument startup testing
- Draining the facility by transferring p-Cymene from the test section into the secondary reservoir

5. PARTICLE IMAGE VELOCIMETRY METHODOLOGY

PIV is a non-intrusive, laser-based, optical measurement technique to quantify velocity vector fields of a fluid. The velocity of a fluid element is defined as its displacement over a given time interval. To capture the displacement of fluid elements, highly reflective micro seeding particles of a similar density can be added to the fluid without impacting the flow characteristics. A laser sheet is used to illuminate the particles. The reflected light from the particles is captured by a CCD digital camera to create an image. A series of images is then collected at a suitable frequency. The suitable sampling rate is based on the requirement to capture an individual particle multiple times before it leaves the viewing window, along with the particle-image displacement equaling approximately 5-15 pixels. Other assumptions regarding the seeding particles include:

- Homogeneous distribution
- Perfectly match the behavior of a fluid element

Various camera and laser sheet configurations are possible to measure either 2D or 3D velocity fields/volumes. The simplest PIV setup involves a single camera viewing normal to a laser sheet. This configuration produces 2D2C vector fields (2 dimension, 2 component). Figures 5.2 and 5.3 displays the 2D2C setup, which was used to quantify the velocity vector fields presented in this thesis. Additional cameras may be added to increase the viewing window. Stereoscopic PIV utilizes 2 cameras with an off-normal viewing angle from the laser sheet and produces 2D3C vector fields. Tomographic PIV requires 4 cameras but is able to produce 3D3C vector fields.

The statistical cross-correlation between consecutive images is the method used to estimate particle-image displacement. This is necessary because it is computationally expensive, or sometimes impossible, to uniquely identify the same particle in consecutive images. Consecutive images are defined as image pairs. For a given image pair, the first image is discretized into multiple interrogation windows. The maximum particle displacement should be 25% of this interrogation window. The search window in the second image of the pair is larger than the interrogation window. The movement of the interrogation window is defined by the specified grid. A finer grid will produce a vector field with a larger number of vectors. The number and shape of the particle-images inside the interrogation window for an image is unique to that image. Therefore, to determine the particle-image displacement, the most similar interrogation window in the second image must be located by comparing the interrogation window to areas within the search space and calculating the correlation value at each position. This is performed after converting the image pairs into the spectral domain using fast Fourier transform (FFT). The average intensity of a given interrogation window is calculated by Equation 5.1. The figure of merit for the cross-correlation is determined by Equation 5.2.

$$\bar{I}_a = \frac{1}{B_x B_y} \sum_{k=1}^{B_x} \sum_{l=1}^{B_y} I_a(k, l) \quad (5.1)$$

$$R(i, j) = \frac{\sum_{k=1}^{B_x} \sum_{l=1}^{B_y} (I_a(k, l) - \bar{I}_a)(I_b(k + i, l + j) - \bar{I}_b)}{\left[\sum_{k=1}^{B_x} \sum_{l=1}^{B_y} (I_a(k, l) - \bar{I}_a)^2 \sum_{k=1}^{B_x} \sum_{l=1}^{B_y} (I_b(k + i, l + j) - \bar{I}_b)^2 \right]^{\frac{1}{2}}} \quad (5.2)$$

The assumption that shear between nearby fluid elements can be ignored requires the interrogation window to be small. The assumption is necessary because the resulting displacement from the cross-correlation is an average of the group of

particle-images inside the interrogation window.

Three types of subchannels (corner, edge, and interior) are formed by the hexagonal duct and 61-rod assembly. These unique flow areas are the primary locations of interest for PIV measurements. Both vertical and horizontal laser sheets can be projected into these flow areas. This thesis contains PIV results from velocity measurements on the set of exterior subchannels near the hexagonal duct wall of Face E. Measurements were performed at two axial locations, Figure 5.1. The technical motivation behind the location of the shakedown measurement windows was to determine the lowest and highest feasible measurements that could be performed in the visualization region of 1 wire pitch. The challenge existed due to the pressure hardware mounted at various locations on the hexagonal duct. The bottom of the lower window, Axial 1, is approximately 80 mm above pressure tap 5 and spans 71 mm, which corresponds to measurements between 2.418 and 2.565 wire pitches downstream the zero wire pitch location defined in Appendix A. The bottom of the upper window, Axial 2, is approximately 370 mm above pressure tap 5 and spans 71 mm, which corresponds to measurements between 3.027 and 3.174 wire pitches downstream the zero wire pitch location, which is formed by the interface between the lower plenum and hexagonal duct.

Horizontal cross-sections of the PIV setups for each measurement location are provided in Figures 5.2 and 5.3. The vertical laser sheet used to illuminate particles for the PIV measurements is represented by the green line. The PIV measurement windows are represented by the green rectangles. An X-Y coordinate system was assigned to represent horizontal and vertical directions in the laser sheet. The origin of the X-Y coordinate system is shown. The origin is selected as follow:

- $X = 0$ at the inner corner made by faces D and E

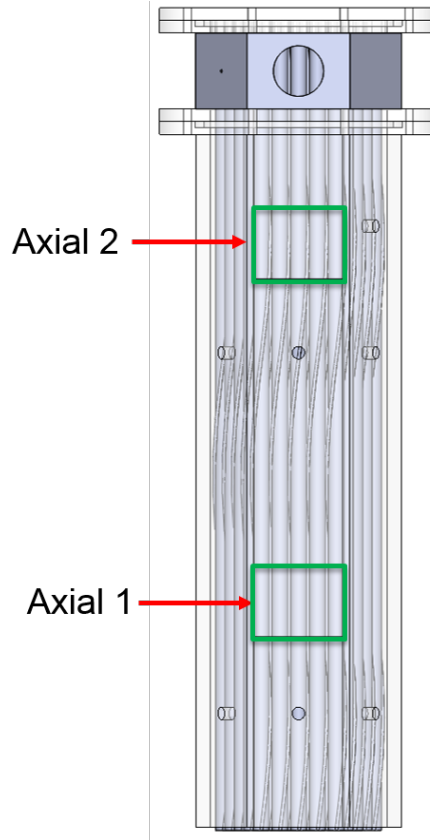


Figure 5.1: Side view of the PIV setup for the lower and upper windows

- $Y = 0$ at centerline of PT5 (corresponding to the axial location of 2.25 pitches, as defined in A)
- $Z = 0$ at the inner side of face E

The minimum and maximum X-Y coordinates of each measurement region are provided in Table 5.1.

A three-dimensional traversing system was utilized to perform fine spatial adjustments of the laser sheet within the edge subchannels. The laser alignment process started by adjusting the base of the laser until the laser sheet was parallel with the inner surface of the wall forming Face E. A parallel orientation was confirmed by

Table 5.1: X-Y coordinate system for both PIV measurement windows

Location	X_{min} (mm)	X_{max} (mm)	Y_{min} (mm)	Y_{max} (mm)
Axial 1	0.6	89.5	79.9	150.8
Axial 2	0.6	89.5	368.7	439.6

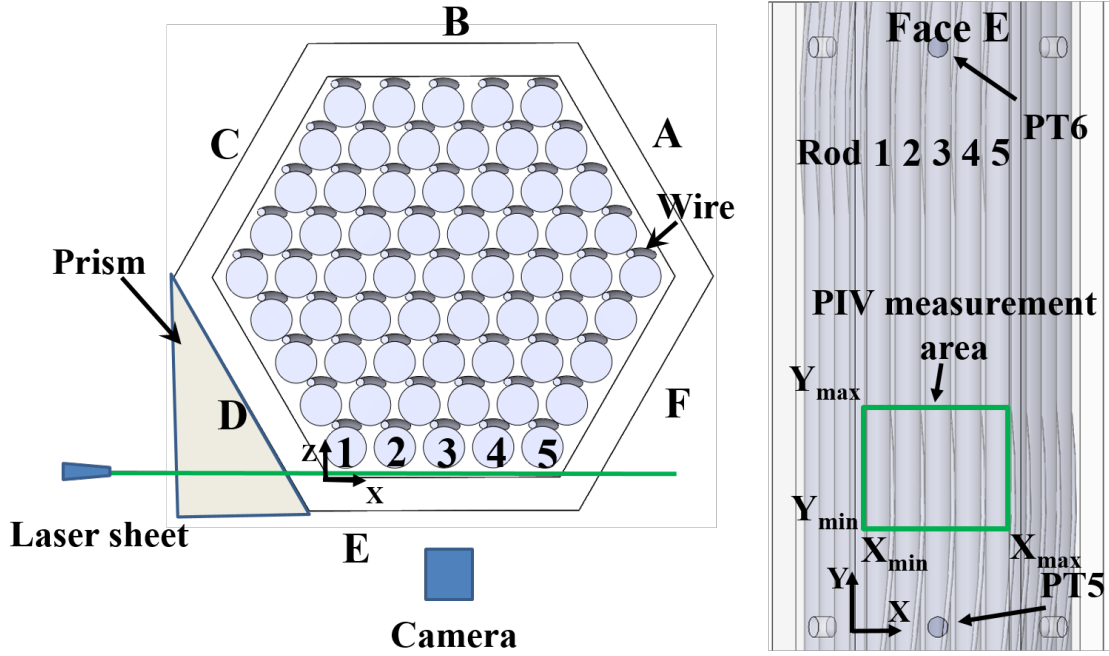


Figure 5.2: Top view of the PIV setup for the lower window, Axial 1

visual inspection. The relative intensity of the laser sheet in the two corners of Face E was monitored until equal. Next, the laser sheet was laterally traversed until it intersected the exterior row of rods. Again, by visual inspection, the laser sheet was confirmed to simultaneously intersect rods 1-5 in the plane parallel to face E. The laser sheet had a thickness of $1.5 \text{ mm} \pm 0.5 \text{ mm}$. The distance of the laser sheet from the tangent plane along the exterior rods was $1.88 \text{ mm} \pm 0.5 \text{ mm}$.

A calibration process was necessary to establish a map between the image pixel

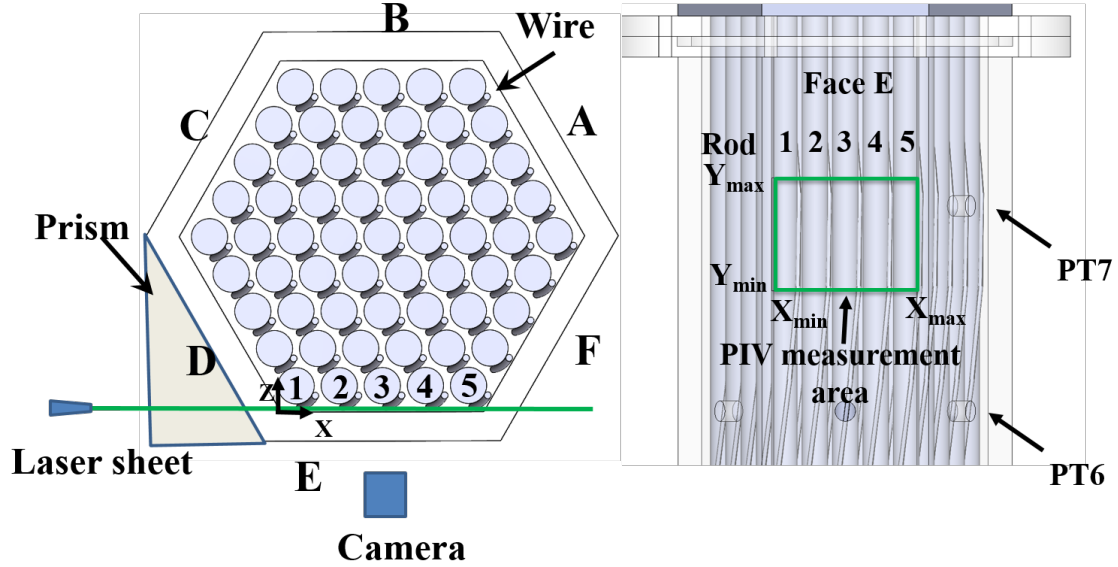


Figure 5.3: Top view of the PIV setup for the upper window, Axial 2

spacing and physical dimensions in the PIV measurement window. A calibration plate manufactured by LaVision assisted in this process, Figure 5.4. The plate contains an array of dots with a high precision pattern on two levels. Tolerances of the plate include [33]:

- plate thickness of ± 0.02 mm
- dot spacing of ± 0.02 mm
- level separation of ± 0.01 mm

For statistical sampling, four sets of images were recorded at various volumetric flow rates for each location. The number of images in each set was limited by the internal random access memory (RAM) of the digital camera. Sequences of 3087 images were taken per set for a total of 12348 images per flow rate per location. The images have a resolution of 1280×1024 pixels. The desired camera frame rate to

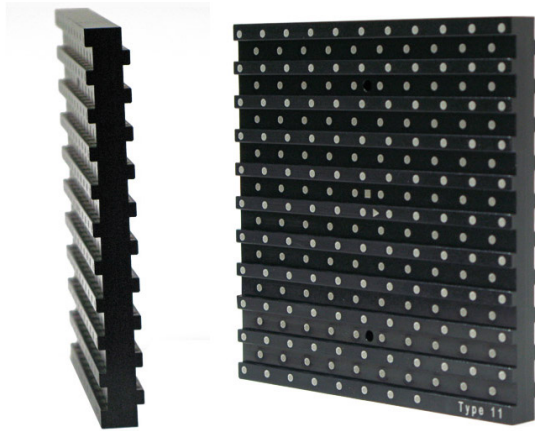


Figure 5.4: LaVision calibration plate [34]

achieve the 5-15 pixel displacement was estimated using the mean axial velocity (\bar{v}) derived from dividing the volumetric flow rate (Q) by the cross-sectional flow area (A_{flow}). Then the camera frame rate was set to the values in Table 5.2 based on the Δt required for the 5-15 pixel displacement. The bulk Re number was also calculated using Equation 5.3 using the hydraulic diameter (D_h) and kinematic viscosity (ν) of water at 22°C. Table 5.2 contains information for three different Re number, because PIV results at those values are discussed in this thesis.

$$Re = \frac{\bar{v}D_h}{\nu} \quad (5.3)$$

Table 5.2: Camera frame rate for 5-15 pixel seeding particle displacement

Q (m^3hr^{-1})	A_{flow} (m^2)	\bar{v} (m sec^{-1})	ν ($\text{m}^2 \text{sec}^{-1}$)	D_h (m)	Re	Δt (sec)	Frame rate (sec^{-1})
11.4	8.03E-3	0.39	9.56E-7	7.73E-3	3200	2.5E-3	400
22.7	8.03E-3	0.78	9.56E-7	7.73E-3	6400	1.1E-3	900
34.1	8.03E-3	1.17	9.56E-7	7.73E-3	9600	0.7E-3	1400

After collecting sets of images, post-processing began by first calculating the mean background intensity from all images of a given set. Next, the mean background intensity was subtracted from each image. This step increases the contrast between the particle-images and extraneous scattered laser light. Cross-correlation PIV algorithms from PRANA were utilized. PRANA is an open-source, GUI-based, MATLAB program for calculating 2D velocity fields developed by Virginia Tech [35].

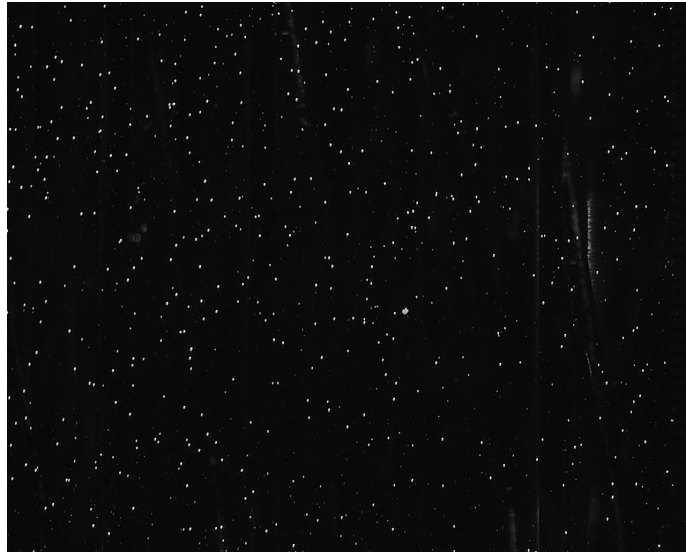


Figure 5.5: Raw PIV image

A static mask was utilized to define a region of interest (ROI) for the post-processing. This is very useful to decrease the computational expense of interior subchannel post-processing, where the majority of the PIV window is not relevant. For the exterior subchannels, the mask simply removed the left and right borders of the PIV window, where hexagonal duct corners were in view.

Post-processing involved two passes of decreasing grid size using the Multigrid - Discrete Window Offset (DWO) and robust phase correlation (RPC) algorithms.

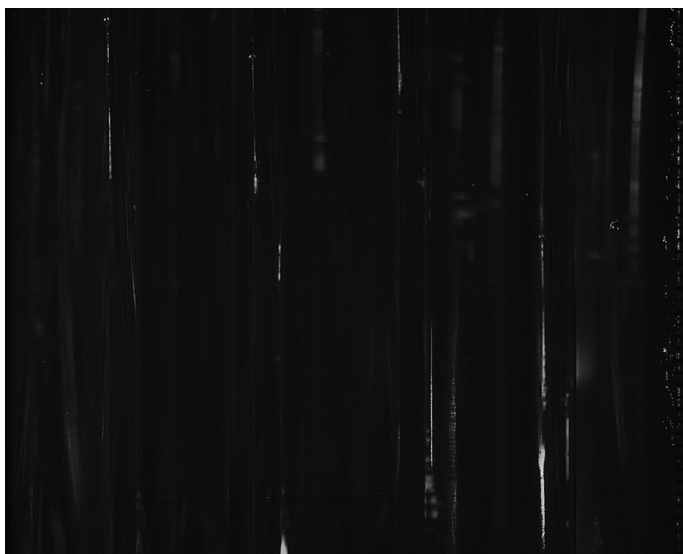


Figure 5.6: Mean background of image set

Two passes were deemed sufficient for the preliminary analysis using water as the working fluid. More passes will be used when MIR conditions are achieved and p-Cymene is used as the working fluid. DWO can increase the cross-correlation accuracy by offsetting the interrogating window between subsequent passes by an amount equal to the integer-pixel-displacement [36]. The increased accuracy allows for the initial pass to be quite coarse relative to the final pass, which greatly reduces the computational cost. The interrogation window size for the final pass was determined to achieve a particle-image density of 5-10 per window.

Pass 1 resulted in a coarse vector field and Pass 2 refined the initial field. The coarse vector field produced by Pass 1 was operated on by a velocity interpolation function to form the initial guess of the Pass 2 refined vector field. The selected function was bi-cubic interpolation. This function requires a uniform grid, uses three points per polynomial, and produces the smoothest result of all built-in velocity interpolation functions. A smooth interpolation is important to establish for the



Figure 5.7: Background subtracted image

Multigrid - DWO method.

The RPC algorithm is summarized below [37]:

1. Each image is spatially discretized into multiple interrogation windows
2. A FFT is applied to each interrogation window to transform to the spectral domain
3. Image pairs are cross-correlated
4. A phase transform filter is applied to increase the amplitude of the correlation peak
5. The product is operated on by a weighted signal-to-noise ratio (SNR) term to reduce the amplitude of the noise
6. An inverse FFT is applied to each interrogation window

7. The correlation peak is operated on by a 3 Pt. Gaussian estimator to increase the probability of peak identification [38]

Once the correlation peak has been identified, the displacement is known only to the integer pixel value. The subpixel displacement can be estimated by several methods. The method chosen in this analysis is the most commonly used Three-Point Gaussian Estimator. The correlation peak maximum is determined by passing a Gaussian curve through three points in both the X and Y directions.

Table 5.3 contains the primary parameters of the post-processing analysis.

Table 5.3: PIV post-processing parameters

Parameter	Pass 1	Pass 2
Multigrid method	Bi-cubic	Bi-cubic
Searching window size (pixel)	256×256	128×128
Interrogation window size (pixel)	64×64 pixels	32×32
Interrogation window overlap	50%	50%
Grid buffer	8×8	8×8
Correlation type	RPC	RPC
Subpixel correlation peak location	3 Pt. Gaussian	3 Pt. Gaussian
Particle diameter (pixel)	2.8×2.8	2.8×2.8

After each pass, a validation check was performed to eliminate spurious vectors. Spurious vectors can be caused by in-plane and out-of-plane loss of particle-image pairs, along with steep velocity gradients. The validation check is called universal outlier detection, where the magnitude of neighboring vectors of a selected vector are compared to the magnitude of said selected vector. The number of neighbor vectors was a 3×3 grid around the selected vector. The location parameter used in the comparison is the median value of neighboring vectors. This process is repeated for

each vector in the grid.

6. PIV RESULTS

Before filling the experimental facility with p-Cymene, shakedown testing with DI water was performed to minimize the immersion time of PMMA in p-Cymene during the initial setup and debug process of the imaging, pressure, flowrate, and temperature hardware. Specifically, shakedown testing was performed by sequentially increasing the bulk Re number by 600 between 3200 and 9600. Figure 6.1 displays three Re numbers of 3200, 6400, and 9600. These are the Re numbers for which post-processing and data analysis have been performed on the shakedown measurements. These are the results presented in this thesis. The variables presented in this section include the ensemble-averaged vertical and horizontal velocity components, v_{mean} and u_{mean} , the root-mean-square (RMS) vertical and horizontal velocity components, v_{RMS} and u_{RMS} , and the Re shear stress, $\overline{u'v'}$.

6.1 Ensemble-Averaged Vertical Velocity Component

The ensemble-averaged vertical velocity component vector field for Re number of 3200, 6400, and 9600 are presented in Figure 6.2 in ascending order by Re number. In each row, Axial 1 is the left column, while Axial 2 is the right column. The fields have been normalized by the bulk velocity for each Re number as defined in Table 5.2.

First, the effect of the Re number will be discussed. As the Re number increases, the observed trend for both locations results in a decrease in the magnitude of the normalized vertical component. This implies that as turbulence inside the assembly increases, the amount of bypass flow in the exterior subchannels decreases which could increase interior subchannel mixing where convective heat transfer limits are typically reached first. Also, the velocity profile may be flattening out, similar to

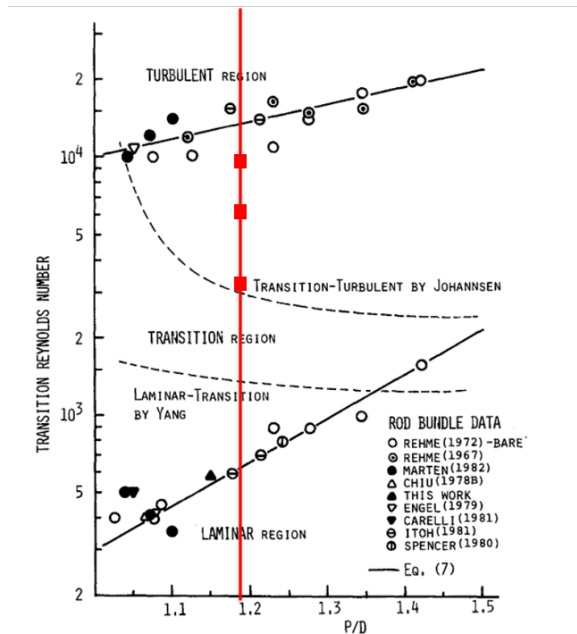


Figure 6.1: Flow regime map for hexagonal fuel assemblies [32]

turbulent pipe flow. However, interior subchannel measurements utilizing MIR conditions are required to further investigate this phenomena. For a given Re number, the normalized vertical velocity component is always greater than the bulk velocity. This is expected due to the larger flow area and smaller expected pressure drop in the exterior subchannel.

Second, a comparison between the different measurement locations will be made. In Axial 1, the wire clocking position is such that the wire is not intersecting the set of exterior subchannels. In fact, this measurement location contains the region least impacted by the wire spacer due to the wire being approximately 180° from the bisecting the set of exterior subchannels. Therefore, the velocity field is similar to an arrangement with no wire spacers, where velocity maxima occur where the flow area decreases and velocity minima occur where the flow area is largest and the flow has the ability to enter the interior subchannels. However in Axial 2, the wire

clocking position is such that the wire is intersecting the set of exterior subchannels. The well-defined minima and maxima observed at Axial 1 is no longer visible at Axial 2. Over the measurement region, the vertical velocity component magnitude is larger for Axial 2 than Axial 1 at lower Re number. This difference reverses as the Re number increases, where the vertical velocity component magnitude is larger for Axial 1 than Axial 2. This implies that bypass flow velocity is minimized in regions where the wire spacer is intersecting the set of exterior subchannels near the wall.

6.2 RMS Vertical Velocity Component

The RMS vertical velocity component vector field for Re number of 3200, 6400, and 9600 are presented in Figure 6.3 in ascending order by Re number. Again, Axial 1 is the left column, while Axial 2 is the right column. The fields have been normalized by the bulk velocity for each Re number as defined in Table 5.2.

First, the effect of the Re number will be discussed. For both measurement locations, the RMS vertical velocity component decreases in magnitude as Re number increases. Specifically, the decrease in fluctuation is most prominent when the rods and wall are close. Also, a left-to-right gradient of the RMS vertical component becomes more apparent as Re number increases, implying that the swirl induced by the helical wire spacer becomes greater as Re number increases.

Second, a comparison between the different measurement locations will be made. At lower Re numbers, the RMS component is larger for Axial 1. However, the difference becomes much smaller as the Re number increases.

6.3 Ensemble-Averaged Horizontal Velocity Component

The ensemble-averaged horizontal velocity component vector field for Re number of 3200, 6400, and 9600 are presented in Figure 6.4 in ascending order by Re number. In each row, Axial 1 is the left column, while Axial 2 is the right column. The fields

have been normalized by the bulk velocity for each Re number as defined in Table 5.2. The effect of increasing Re number on the vector field is not visually apparent for either measurement location, indicating the magnitude of swirling phenomena in the horizontal direction in exterior subchannels does not increase after Re reaches 3200. When comparing Axial 1 and 2, substantial differences exist. Although the swirling phenomena is apparent in both measurement locations, the beginning or bottom of the phenomena is apparent in Axial 1, while the end or top of the phenomena is apparent in Axial 2.

6.4 RMS Horizontal Velocity Component

The RMS horizontal velocity component vector field for Re number of 3200, 6400, and 9600 are presented in Figure 6.5 in ascending order by Re number. In each row, Axial 1 is the left column, while Axial 2 is the right column. The fields have been normalized by the bulk velocity for each Re number as defined in Table 5.2.

The effect of increasing the Re number is very similar to the effect for the RMS vertical velocity component, where the fluctuations decrease in magnitude and the vector field becomes more uniform. The left-to-right gradient is not visible. When comparing the different measurement locations, the RMS horizontal velocity magnitude is less when the wire intersects the set of exterior subchannels in Axial 2 relative to Axial 1.

6.5 Reynolds Shear Stress

The Reynolds shear stress, $\overline{u'v'}$, for Re number of 3200, 6400, and 9600 are presented in Figure 6.6 in ascending order by Re number. In each row, Axial 1 is the left column, while Axial 2 is the right column. The fields have been normalized by the square of the bulk velocity for each Re number as defined in Table 5.2. For both locations, the momentum transfer is primarily in the positive direction and

approximately doubles between a Re number of 3200 and 9600.

Similar to the swirl phenomena noted in Figure 6.4, the beginning or bottom of the phenomena is apparent in Axial 1, while the end or top of the phenomena is apparent in Axial 2. However, the Reynolds shear stress is larger near the middle of Face E and approximately zero close to the corners.

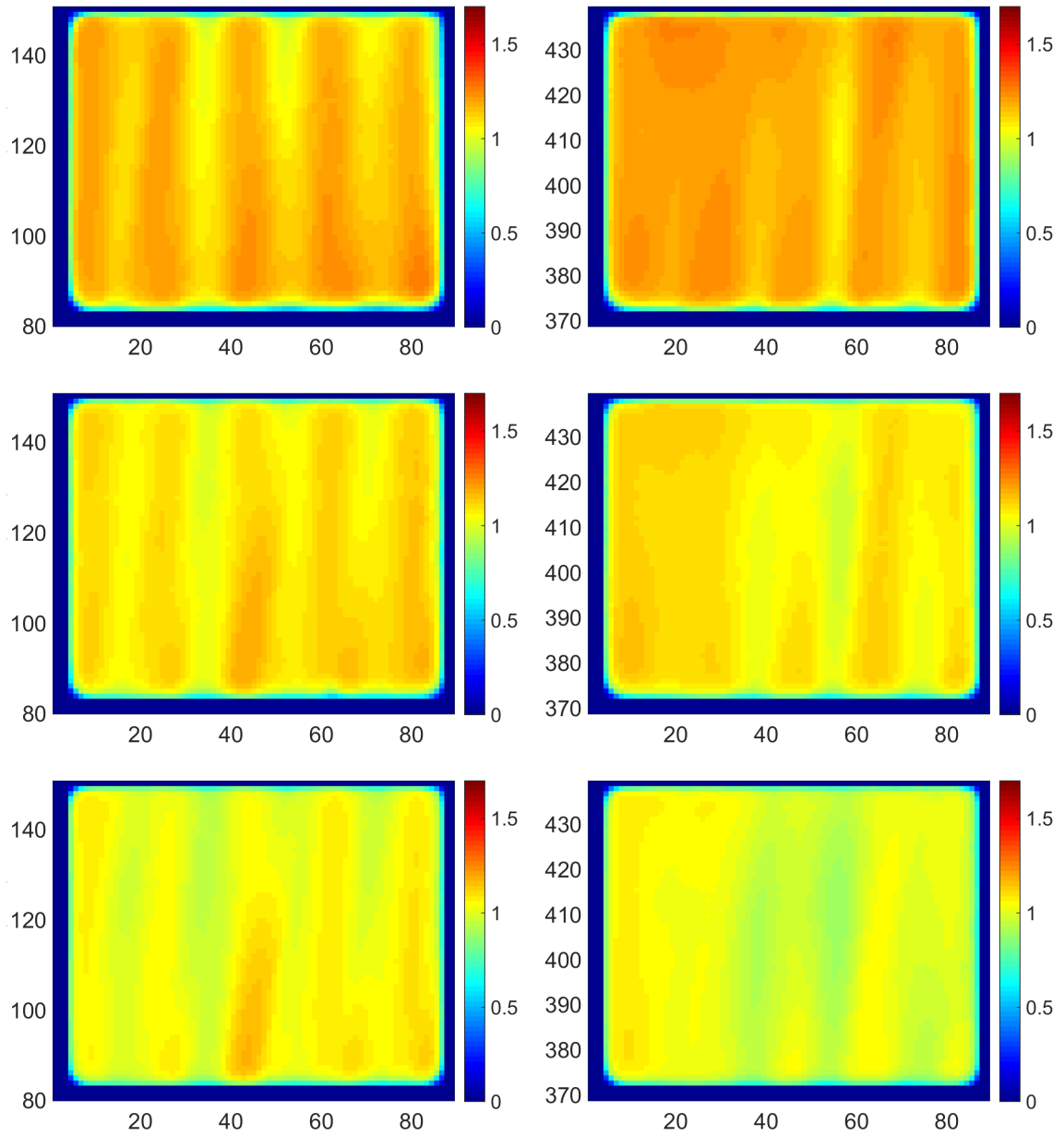


Figure 6.2: Ensemble-averaged vertical velocity component for $Re = 3200, 6400,$ and 9600 . Axial 1 (left) and Axial 2 (right)

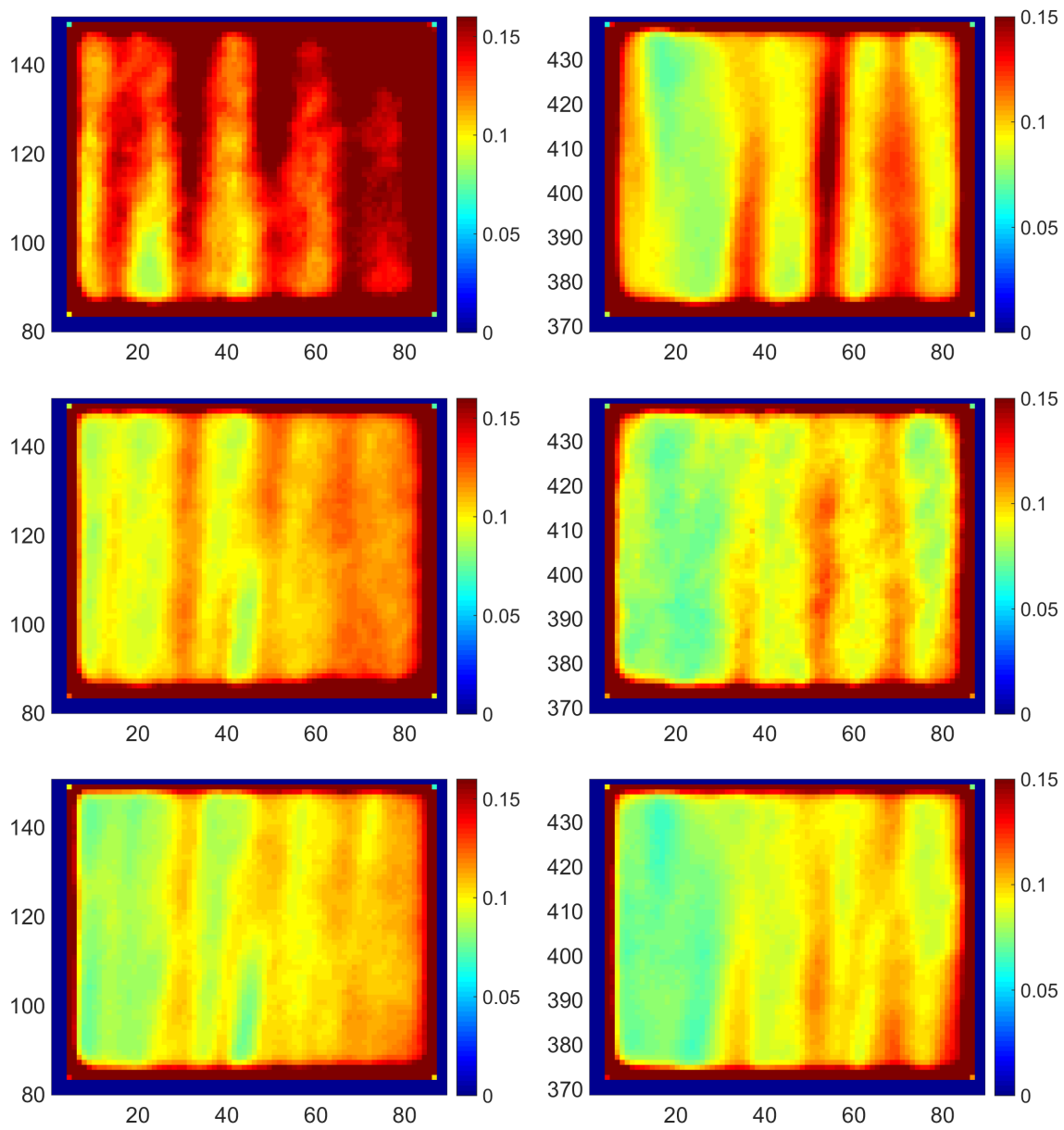


Figure 6.3: RMS vertical velocity component for $Re = 3200, 6400, \text{ and } 9600$. Axial 1 (left) and Axial 2 (right)

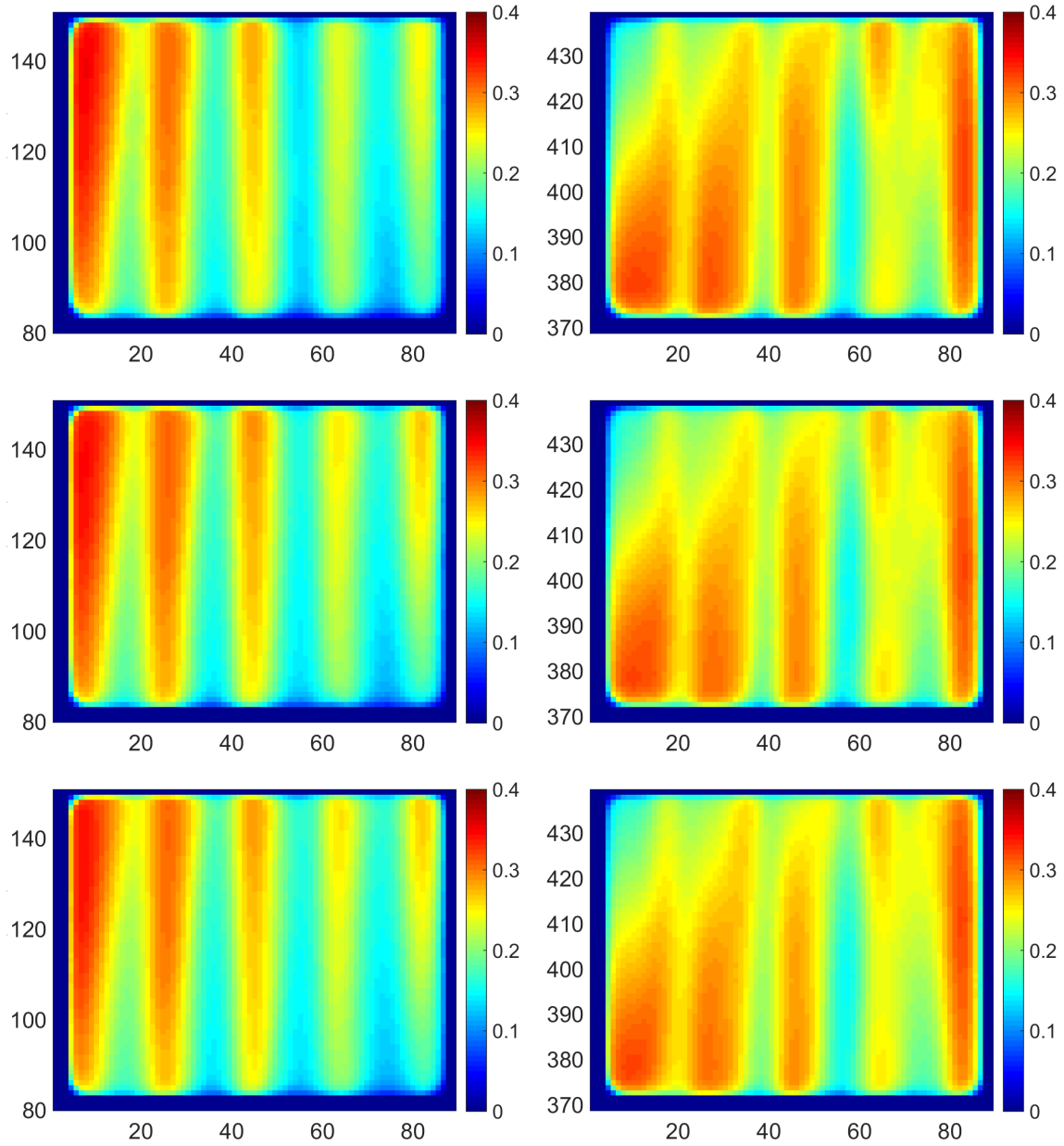


Figure 6.4: Ensemble-averaged horizontal velocity component for $Re = 3200$, 6400 , and 9600 . Axial 1 (left) and Axial 2 (right)

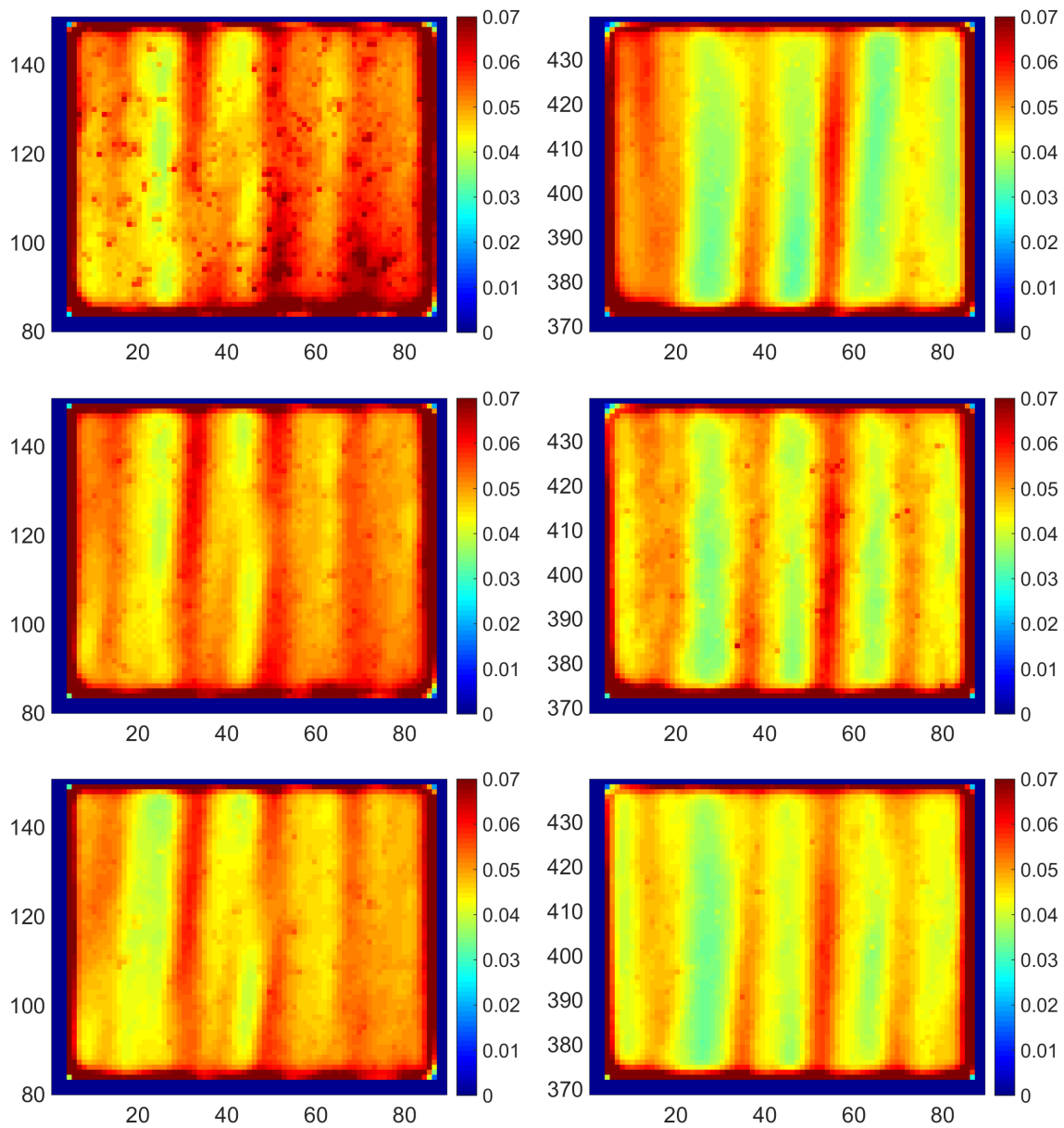


Figure 6.5: RMS horizontal velocity component for $Re = 3200, 6400,$ and 9600 . Axial 1 (left) and Axial 2 (right)

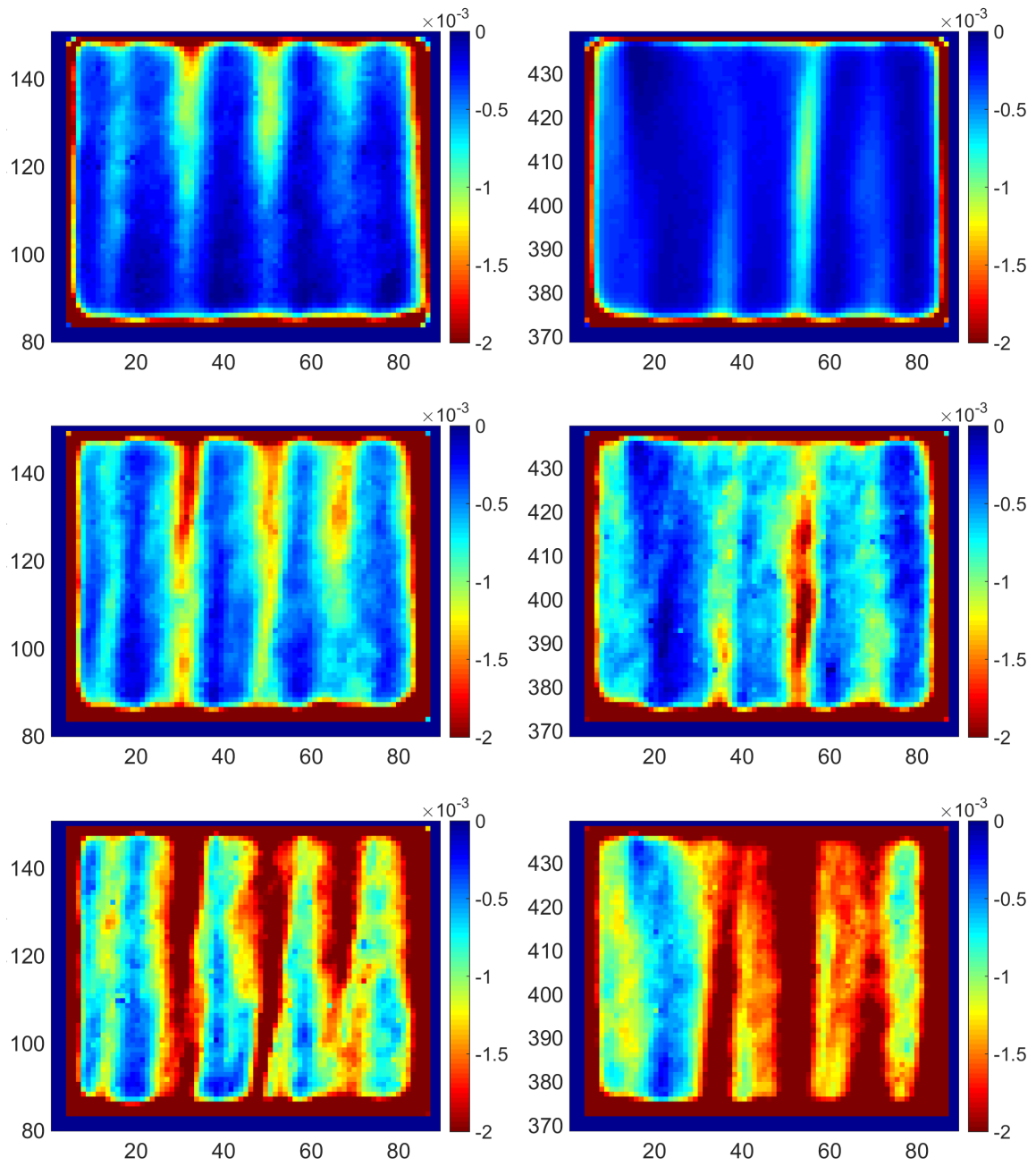


Figure 6.6: Reynolds shear stress, $\overline{u'v'}$, for $Re = 3200, 6400, \text{ and } 9600$. Axial 1 (left) and Axial 2 (right)

7. CONCLUSIONS AND LESSONS LEARNED

A literature review, materials testing, facility design, and PIV methodology were presented, along with results of 2D2C PIV shakedown measurements at two axial locations in the test section. This work is beneficial because the validation of CFD turbulence models on beginning-of-life hexagonal fuel assemblies is necessary to minimize thermal-hydraulic design uncertainties, which lead to increased reactor safety and profitability.

The design of the experimental facility has been described in detail. The selection of cast PMMA and p-Cymene achieved room temperature MIR conditions and will enable measurements of exterior and interior subchannel velocity fields.

All requirements defined in Section 2.2 were met with one exception. The exception being the target Re number of 20000. Utilizing the rod fabrication method described in Section 4.3.1.1, the maximum achievable bulk Re number was approximately 9600. However, an improved fabrication method was later developed, utilized, and the target Re number of 20000 was eventually reached for the MIR flow experiments not described in this thesis. Other lessons learned include:

- A 3D printed assembly was not yet cost-effective and did not possess the mechanical rigidity of an assembly built using cast PMMA.
- The failure rate of PMMA helically wrapped wires depended highly on the mechanical stress added during the fabrication process. Insufficient tension resulted in a wire that did not adhere to the rod, while too much tension resulted in cracking and failure when paired with flow-induced vibration.
- The adhesive, ECA, proved key in the rod fabrication process by possessing a

quick curing time and high chemical resistance to p-Cymene.

- Flexible hosing and isolating the piping support structure from the imaging hardware support structure resulted in sufficient vibrational dampening.
- Although no failures occurred, inlet and outlet plena should be made from stainless steel instead of PMMA to increase the durability of these components where frequent connections and disconnections were made during the facility operation.
- Particle agitation was required in the primary reservoir by means of circulation from the secondary loop to minimize particle accumulation during low Re number experimental tests.
- Thread sealant, specifically *Loctite554* and *LoctitePrimer7649*, was required to stop all leaks of the threaded stainless steel piping.

PIV shakedown measurements using DI water were performed and post-processed utilizing the open-source PRANA algorithms. The presented variables included the ensemble-averaged vertical and horizontal velocity components, v_{mean} and u_{mean} , the RMS vertical and horizontal velocity components, v_{RMS} and u_{RMS} , and the Re shear stress, $\overline{u'v'}$. The ensemble-averaged vertical components were roughly 1.0 to 1.4 times the bulk velocity, while the ensemble-averaged horizontal components were roughly 0.15 to 0.4 times the bulk velocity. For both measurement locations, the RMS components, normalized by the bulk velocity, decreased as the Re number increased. The Re shear stress contour plots exhibited an increasing momentum transfer as the Re increased. Also, the regions of maximum momentum transfer occurred in the larger flow area region of the exterior subchannels, where the fluid is able to traverse into the interior of the assembly.

With this thesis defining the results of the shakedown testing, further experimental work will generate a database of CFD reference data suitable for RANS and LES validation of the flow behavior in the exterior, corner, and edge subchannels of undeformed (beginning-of-life) and deformed (end-of-life) hexagonal fuel assemblies with helical wire spacers.

REFERENCES

- [1] M. Mathieu, K. Duggan, and T. Galioto, “Heated bundle test in areva nps fuel cooling test facility,” in *ANS Winter 2016 Conference*, American Nuclear Society, 2016.
- [2] B. Mays, “Experimental data sets for cfd calculations of flow and heat transfer in deformed fuel assemblies,” in *ANS Winter 2016 Conference*, American Nuclear Society, 2016.
- [3] A. Obabko, E. Merzari, and P. Fischer, “Nek5000 large-eddy simulations for thermal-hydraulics of deformed wire-wrap fuel assemblies,” *Trans. Am. Nucl. Soc.*, vol. 115, 2016.
- [4] E. Merzari, “High fidelity cfd simulation of wire-wrapped 61-pin bundle with nek5000,” *ANS Winter Meeting*, 2016.
- [5] D. Leonard, “Cfd verification and validation of wire-wrapped pin assemblies,” *Trans. Am. Nucl. Soc.*, vol. 115, 2016.
- [6] R. Collingham, W. Thorne, and J. McCormack, “Coolant mixing in a fuel pin assembly utilizing helical wire wrap spacers,” *Nuclear Engineering and Design*, vol. 24, no. 3, pp. 393–409, 1973.
- [7] J. Lorenz and T. Ginberg, “Coolant mixing and subchannel velocities in an lmfbr fuel assembly,” *Nuclear Engineering and Design*, vol. 40, no. 2, pp. 315–326, 1977.
- [8] G. E. McCreery, H. M. McIlroy, K. D. Hamman, and H. Zhang, “Design of wire-wrapped rod bundle matched index-of-refraction experiments,” in *16th International Conference on Nuclear Engineering*, pp. 595–605, American Society of Mechanical Engineers, 2008.

- [9] M. Nishimura, H. Sato, H. Kamide, H. Ohshima, K. Nagasawa, and Y. Imai, “Investigation on velocity distribution around the wrapping wire in an inner sub-channel of fuel pin bundle,” in *2012 20th International Conference on Nuclear Engineering and the ASME 2012 Power Conference*, pp. 299–308, American Society of Mechanical Engineers, 2012.
- [10] H. Sato, J. Kobayashi, H. Miyakoshi, and H. Kamide, “Study on velocity field in a deformed fuel pin bundle: Influence of pin deformation and wrapping wire on velocity distribution,” in *16th International Conference on Nuclear Engineering*, pp. 831–839, American Society of Mechanical Engineers, 2008.
- [11] L. Brockmeyer, L. Carasik, E. Merzari, and Y. Hassan, “Cfd investigation of wire-wrapped fuel rod bundle inner subchannel behavior and dependency on bundle size,” in *24th International Conference on Nuclear Engineering*, American Society of Mechanical Engineers, 2016.
- [12] P. Sabharwall, D. McEligot, and C. Stoots, “Matched-index-of-refraction flow facility at idaho national laboratory,” Tech. Rep. INL MIS-15-36171, Idaho National Laboratory.
- [13] E. E. Dominguez-Ontiveros and Y. A. Hassan, “Non-intrusive experimental investigation of flow behavior inside a 5×5 rod bundle with spacer grids using piv and mir,” *Nuclear Engineering and Design*, vol. 239, no. 5, pp. 888–898, 2009.
- [14] E. Hecht and A. Zajac, “Optics addison-wesley,” *Reading, Mass*, vol. 19872, pp. 350–351, 1974.
- [15] Y. A. Hassan and E. Dominguez-Ontiveros, “Flow visualization in a pebble bed reactor experiment using piv and refractive index matching techniques,” *Nuclear Engineering and Design*, vol. 238, no. 11, pp. 3080–3085, 2008.
- [16] C. Penreco, “White mineral oil product specifications,” *Calumet Specialty Products Partners, L.P.*, p. 1, 2016.

- [17] M. S. Song, H. Y. Choi, J. H. Seong, and E. S. Kim, “Matching-index-of-refraction of transparent 3d printing models for flow visualization,” *Nuclear Engineering and Design*, vol. 284, pp. 185–191, 2015.
- [18] P. Scholz, I. Reuter, and D. Heitmann, “Piv measurements of the flow through an intake port using refractive index matching,” Tech. Rep. a, 16th International Symposium on Applications of Laser Techniques to Fluid Mechanics, a 2012.
- [19] T. Nguyen, N. Goth, P. Jones, S. Lee, R. Vaghetto, and Y. Hassan, “Piv measurements of turbulent flows in a 61-pin wire-wrapped hexagonal fuel bundle,” *International Journal of Heat and Fluid Flow*, vol. 65, pp. 47–59, 2017.
- [20] N. Goth, P. Jones, S. Lee, D. Nguyen, R. Vaghetto, and Y. Hassan, “Velocity and pressure measurements in a wire-wrapped 61-pin hexagonal fuel bundle,” *Engineering Turbulence Modeling and Measurements 11*, 2016.
- [21] N. Goth, M. Childs, P. Jones, S. Lee, D. Nguyen, R. Vaghetto, and Y. Hassan, “Particle image velocimetry measurements in a wire-wrapped 61-pin hexagonal fuel bundle,” *American Nuclear Society Winter Meeting*, 2016.
- [22] R. Vaghetto, N. Goth, M. Childs, P. Jones, S. Lee, D. Nguyen, and Y. Hassan, “Pressure measurements in a wire-wrapped 61-pin hexagonal fuel bundle,” *American Nuclear Society Winter Meeting*, 2016.
- [23] N. Goth, P. Jones, S. Lee, D. Nguyen, R. Vaghetto, and Y. Hassan, “Time-resolved piv/ptv measurements on interior subchannels of a wire-wrapped 61-pin hexagonal fuel bundle,” *American Nuclear Society Annual Meeting*, 2017.
- [24] P. M. Bardet, C. D. Fu, C. E. Sickel, and N. A. Weichselbaum, “Refractive index and solubility control of para-cymene solutions,” Tech. Rep. 17th International Symposium on Applications of Laser Techniques to Fluid Mechanics, George Washington Mechanical Engineering Department, July 2014.
- [25] B. Kunlun and J. Katz, “On the refractive index of sodium iodide solutions for

- index matching in piv,” Tech. Rep. 1, Experimental Fluids, March 2014.
- [26] R. Chen, “Experimental and numerical studies of solidliquid multiphase flow in pipes,” Tech. Rep. PhD Dissertation, Case Western Reserve University, a 1991.
- [27] T. Narrow, M. Yoda, and S. Abdel-Khalik, “A simple model for the refractive index of sodium iodide aqueous solutions,” Tech. Rep. a, Experimental Fluids, a 2000.
- [28] I. Kuriyama, “Chemical resistance chart,” *Alfagomma Chemical Guide*, pp. 58–66.
- [29] K. P. Parts, “Dupont chemical resistance and fluid compatibility,” *DuPont-Kalrez Oring Material Corrosion*, p. 8, 2011.
- [30] W. M. Haynes, *Handbook of Chemistry and Physics*, vol. 93. CRC Press, 2012.
- [31] A. Waltar, D. Todd, and P. Tsvetkov, *Fast Spectrum Reactors*, vol. 1. Springer, 2011.
- [32] S. Cheng and N. Todreas, “Hydrodynamic models and correlations for bare and wire-wrapped hexagonal rod bundles bundle friction factors, subchannel friction factors and mixing parameters,” *Nuclear Engineering Design*, vol. 92, pp. 227–251, 1986.
- [33] LaVision, “3d calibration plates for strainmaster systems,” p. 1, 2016.
- [34] A. Borgoltz, T. Meyers, and W. Georges, “Particle image velocimetry experiments,” 2017.
- [35] A. Eckstein and P. Vlachos, “Assessment of advanced windowing techniques for digital particle image velocimetry (dpiv),” *Meas. Sci. Technol.*, vol. 20, 2009.
- [36] J. Westerweel, D. Dabiri, and M. Gharib, “The effect of a discrete window offset on the accuracy of cross-correlation analysis of digital piv recordings,” *Experiments in fluids*, vol. 23, no. 1, pp. 20–28, 1997.
- [37] A. Eckstein and P. Vlachos, “A robust phase correlation dpiv processing algo-

rithm for time resolved measurements,” in *Proceedings of the Seventh International PIV Symposium*, 2007.

- [38] C. E. Willert and M. Gharib, “Digital particle image velocimetry,” *Experiments in fluids*, vol. 10, no. 4, pp. 181–193, 1991.

APPENDIX A

AS-BUILT GEOMETRY

This appendix includes the As-Built Geometry report developed in partial fulfillment of the quality assurance program plan for this project. It includes rod and wire characterization, along with pressure tap locations on the test section.



TECHNICAL DOCUMENT COVER PAGE

Document No:	TAMU-WW-AS	Revision: 2	Page 1 of 21
Doc Title: TAMU Wire-Wrapped As-Built Geometry (Non-Deformed Bundle)			
Projects No:	DE-NE000832I		
Project Name: Toward a Longer Life Core: Thermal-Hydraulic CFD Simulations and Experimental Investigation of Deformed Fuel Assemblies			
Document Purpose/Summary: This document describes the “as-built” dimensions of the critical geometrical parameters of the test section of the isothermal non-deformed experimental bundle. Total Page Count: 21 pages.			



TECHNICAL DOCUMENT COVER PAGE

Document No:	TAMU-WW-AS	Revision: 2	Page 2 of 21
--------------	------------	-------------	--------------

TAMU	Nolan Goth		
Prepared By:	Printed/Typed Name	Signature	Date
TAMU	Rodolfo Vaghetto		
Reviewed By:	Printed/Typed Name	Signature	Date
Approved By:	Printed/Typed Name	Signature	Date

REVISION HISTORY LOG

Page: 3 of 21

Document Number: TAMU-WW-AS Revision: 2

Document Title: TAMU Wire-Wrapped As-Built Geometry (Non-Deformed Bundle)

REVISION	DATE	DESCRIPTION
Draft	11/04/2015	Initial draft for review.
Draft 2	12/11/2015	Comments from TerraPower Incorporated
Rev.0	01/25/2016	Rev.0 released
Rev.1	10/21/2016	Updated rod and wire characterization for second non-deformed bundle. Added sections for wire-clocking angle, wire-clocking direction, flow inlet/outlet axial locations, and total rod length.
Rev.2	11/02/2016	Included additional geometrical information based on TerraPower request



	TAMU Wire-Wrapped As-Built Geometry (Non-Deformed Bundle)		
	Document No: TAMU-WW-AS	Rev: 2	Page 4 of 21


Table of Contents

1.0	Introduction and Scope.....	6
2.0	Test Section As-Built Geometry	6
2.1	Axial Coordinate System	6
2.2	Test Section Enclosure.....	8
2.3	Total Rod Length	9
2.4	Wire-Clocking Angle	9
2.5	Wire-Wrap Direction	11
2.6	Flow Inlet and Outlet Ports.....	11
2.7	First Non-Deformed Bundle.....	11
	2.7.1 Rods	11
	2.7.2 Wire Spacers.....	13
	2.7.3 Fabrication Process.....	15
2.8	Second Non-Deformed Bundle.....	16
	2.8.1 Rods	16
	2.8.2 Wire Spacer	17
	2.8.3 Fabrication Process.....	19
3.0	Pressure transducer Final Location.....	20
4.0	References.....	21

	TAMU Wire-Wrapped As-Built Geometry (Non-Deformed Bundle)		
	Document No: TAMU-WW-AS	Rev: 2	Page 5 of 21

Acronyms and Definitions

Acronym	Definition
TAMU	The Texas A&M University
CFD	computational fluid dynamics
FTF	flat-to-flat

	TAMU Wire-Wrapped As-Built Geometry (Non-Deformed Bundle)		
	Document No: TAMU-WW-AS	Rev: 2	Page 6 of 21

1.0 INTRODUCTION AND SCOPE

To support the validation of computation fluid dynamics (CFD) calculations, high quality characterization of flow in the same flow regime as those encountered in wire wrapped fuel assemblies prototypic of liquid metal fast reactors is needed. TAMU performs experimental tests focusing on investigating and measuring flow and pressure drop behavior of two geometries (non-deformed and deformed) of a mock 61-rod hexagonal fuel assembly for purposes of generating CFD validation grade data.

This document defines the as-built geometry of the experimental non-deformed test section that will be used gather data from the experimental tests. The dimensions and manufacturing tolerances are provided in this document. Engineering drawings of the test section are also attached to this document.


2.0 TEST SECTION AS-BUILT GEOMETRY

The dimensions reported in this section represent the as-built configuration of the non-deformed geometry. The components of the test section included are:

- The acrylic test section enclosure (Section 2.0)
- The first non-deformed bundle (Section 2.7)
- The second non-deformed bundle (Section 2.8)

2.1 Axial Coordinate System

This section defines the relationship between the two notations used to denote various axial positions. The first notation is described in TWRP-31-TSPEC-00100 Rev. 1 [1], where various axial positions are denoted by the pitch number (I.E. visualization region between $P = 2.25$ and $P = 3.25$). The second notation is the z-axis, which measures the vertical height in inches. The origin of the z-axis ($z = 0$) is equivalent to a pitch number of zero ($P = 0$). This origin is at the interface between the upper flange of the lower plenum and lower flange of the test section. Figure 1 displays a side view of the test section denoting major axial positions using the second notation method.

	TAMU Wire-Wrapped As-Built Geometry (Non-Deformed Bundle)		
	Document No: TAMU-WW-AS	Rev: 2	Page 7 of 21

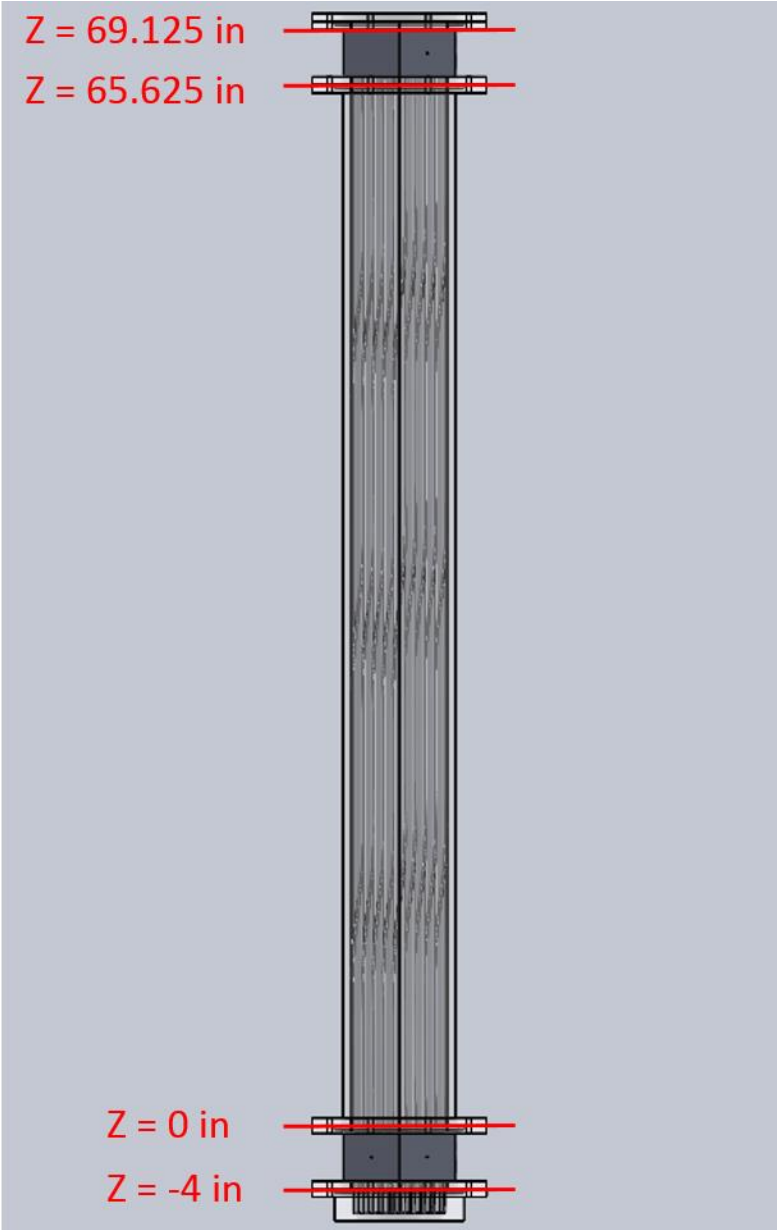



Figure 1. Side-view of the test section with major axial positions

	TAMU Wire-Wrapped As-Built Geometry (Non-Deformed Bundle)		
	Document No: TAMU-WW-AS	Rev: 2	Page 8 of 21

2.2 Test Section Enclosure

The hexagonal test section enclosure was designed following the specifications provided in TWRP-31-TSPEC-0010 Rev. 1 [1]. Table 2.2.1 displays the inner flat-to-flat (FTF) distance of the sides of the enclosure for the test specification and design values.

Table 2.2.1 – Specified and designed inner FTF of the test section enclosure (units of inches)

Test Spec FTF (in)	Design FTF (in)
6.070	6.056

The FTF measurements below are of (1) the outer FTF of the hexagonal guide plate used to manually fabricate the enclosure, and of (2) the inner FTF of the entrance and exit of the test section enclosure. Table 2.2.2 displays the three outer FTF distances of the hexagonal guide plate.¹ These measurements were taken at the midpoint between corners.

Table 2.2.2 - As-built inner FTF distances of the hexagonal guide plate (units of inches)


Measurement #	FTF 1 (in)	FTF 2 (in)	FTF 3 (in)	FTF Average (in)
1	6.065	6.061	6.063	-
2	6.063	6.063	6.063	-
3	6.064	6.062	6.065	-
Average	6.064	6.062	6.064	6.063
Std. Dev.	0.000816	0.000816	0.000943	0.000859

Using the same caliper, the inner FTF of the entrance and exit of the test section enclosure were also measured. Measurements were repeated at different locations along each face. Due to the higher difficulty in performing these measurements on the inner FTF of the enclosure, the standard deviation of the measurement was significantly higher than the standard deviation of the measurements taken on the guide plate.

Average FTF (Test Section Entrance) = 6.082 in with a standard deviation of 0.03175 in

Average FTF (Test Section Exit) = 6.088 in with a standard deviation of 0.02758 in

¹ Three measurements of the FTF distance were taken for each of the three two-side sets. The measurements were performed using a caliper (Starrett No. 180, accuracy 0.001")

	TAMU Wire-Wrapped As-Built Geometry (Non-Deformed Bundle)		
	Document No: TAMU-WW-AS	Rev: 2	Page 9 of 21

2.3 Total Rod Length

The total rod length exposed to the working fluid is 73.125 inches. This accounts for the following sections:

- Lower plenum rod length = 4 inches
- Test section rod length = 65.625 inches
- Upper plenum rod length = 3.5 inches

The length of the section within the upper plenum is less than the one within lower plenum by 0.5 inches due to the presence of the upper guide plate (thickness = 0.5 inches) utilized to maintain the triangular lattice.

2.4 Wire-Clocking Angle

The wire-clocking angle at the bottom of the rod was chosen such that the wire would be positioned in the corner of the hexagonal enclosure formed by Face F and A. The following images are top-view cross-sections of the fuel bundle. The wire-clocking angles are relative to the corner of the hexagonal enclosure Faces C and D. The starting wire-clocking angle was chosen such that the angle would be 180° at an axial location of $z = 42.1875$ inches ($P=2.25$), as defined in [1]. Figure 2 displays the hexagonal enclosure face labeling scheme.

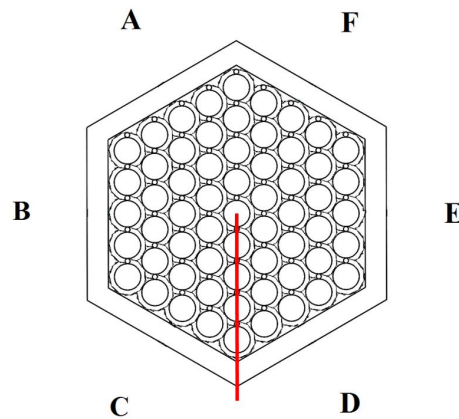



Figure 2. Face labeling scheme showing a wire-clocking angle of 180°

Figure 3 displays the starting wire-clocking angle when it emerges from the lower plate and begins its helical sweep. The axial location is $z = -4$ inches ($P = -0.213$). The angle is 13.19° from a line that passes through the corners formed by Faces C and D.

	TAMU Wire-Wrapped As-Built Geometry (Non-Deformed Bundle)		
	Document No: TAMU-WW-AS	Rev: 2	Page 10 of 21

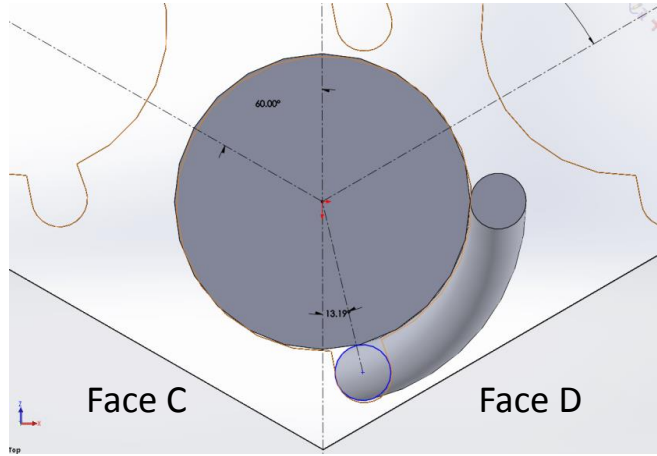


Figure 3. Wire-clocking angle at $z = -4$ inches ($P = -0.213$)

Figure 4 displays the wire-clocking angle at an axial location of $z = 0$ inches ($P = 0$). The angle is 89.83° from a line that passes through the corners formed by Faces C and D.

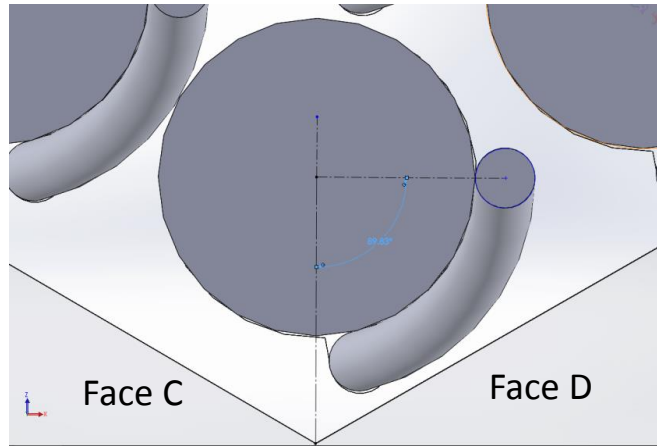



Figure 4. Wire-clocking angle at $z = 0$ inches ($P = 0$)

	TAMU Wire-Wrapped As-Built Geometry (Non-Deformed Bundle)		
	Document No: TAMU-WW-AS	Rev: 2	Page 11 of 21

2.5 Wire-Wrap Direction

The direction of the wire wrap follows the requirement reported in the test specs [1]. The wire is wrapped clockwise around the rod in the direction of the flow (looking from the bottom of the assembly).

2.6 Flow Inlet and Outlet Ports

The flow inlet/outlet ports were located on Faces B and E. The ports were circular in shape with a inner diameter of 2 inches. The inlet ports had a centerline axial location of $z = -2$ inches. The outlet ports had a centerline axial location of $z = 67.625$ inches.

2.7 First Non-Deformed Bundle


2.7.1 Rods

Cast acrylic rods were produced by PolyOne. The target rod diameter was specified in the TWRP-31-TSPEC-0010 Rev. 1 [1]. The selected diameter and casting tolerance was $0.625 \text{ in} \pm 0.010 \text{ in}$. In-house characterization consisted of measuring each rod diameter in three different axial locations. This was performed using a Mitutoyo digital caliper with an accuracy of $\pm 0.001 \text{ in}$. Axial locations 1, 2, and 3 were defined to be distances from the bottom of the rod. These distances were approximately 4 in, 37 in, and 70 in. A total of 94 rods were characterized using this process. The average of the three axial location measurements was calculated for all 94 rods. The final 61 rods that were closest to the mean value were then selected. Table 2.7.1.1 shows the dimensions of the final 61 rods selected with the method described. The average rod diameter was 0.6267 inches with a standard deviation of 0.0006 inches.


Table 2.7.1.1 – First Bundle Fuel Rod Characterization (diameter in inches)²

Rod #	Location 1	Location 2	Location 3	Average	Std. Dev.
1	0.6255	0.6260	0.6285	0.6267	0.0013
2	0.6265	0.6250	0.6265	0.6260	0.0007
4	0.6260	0.6260	0.6280	0.6267	0.0009
7	0.6260	0.6270	0.6270	0.6267	0.0005
9	0.6275	0.6270	0.6275	0.6273	0.0002
10	0.6270	0.6265	0.6270	0.6268	0.0002
11	0.6270	0.6270	0.6280	0.6273	0.0005

² The rod # label is with respect to the total number of rods investigated and may not be sequential

	TAMU Wire-Wrapped As-Built Geometry (Non-Deformed Bundle)		
	Document No: TAMU-WW-AS	Rev: 2	Page 12 of 21

12	0.6265	0.6260	0.6280	0.6268	0.0008
13	0.6275	0.6275	0.6270	0.6273	0.0002
16	0.6260	0.6265	0.6275	0.6267	0.0006
18	0.6255	0.6260	0.6275	0.6263	0.0008
19	0.6265	0.6270	0.6260	0.6265	0.0004
20	0.6275	0.6275	0.6270	0.6273	0.0002
21	0.6270	0.6270	0.6275	0.6272	0.0002
22	0.6255	0.6260	0.6260	0.6258	0.0002
23	0.6275	0.6280	0.6275	0.6277	0.0002
24	0.6250	0.6255	0.6265	0.6257	0.0006
26	0.6270	0.6280	0.6290	0.6280	0.0008
28	0.6270	0.6260	0.6270	0.6267	0.0005
31	0.6260	0.6255	0.6275	0.6263	0.0008
32	0.6255	0.6260	0.6275	0.6263	0.0008
33	0.6265	0.6265	0.6270	0.6267	0.0002
34	0.6270	0.6265	0.6275	0.6270	0.0004
35	0.6255	0.6260	0.6270	0.6262	0.0006
36	0.6270	0.6270	0.6265	0.6268	0.0002
37	0.6275	0.6280	0.6275	0.6277	0.0002
38	0.6270	0.6270	0.6270	0.6270	0.0000
39	0.6250	0.6250	0.6265	0.6255	0.0007
41	0.6250	0.6255	0.6260	0.6255	0.0004
42	0.6255	0.6250	0.6265	0.6257	0.0006
44	0.6255	0.6265	0.6255	0.6258	0.0005
46	0.6260	0.6260	0.6270	0.6263	0.0005
47	0.6270	0.6265	0.6265	0.6267	0.0002
48	0.6260	0.6255	0.6255	0.6257	0.0002
49	0.6260	0.6280	0.6275	0.6272	0.0008
50	0.6270	0.6265	0.6285	0.6273	0.0008
53	0.6265	0.6265	0.6280	0.6270	0.0007
54	0.6280	0.6265	0.6270	0.6272	0.0006
55	0.6270	0.6265	0.6270	0.6268	0.0002
56	0.6255	0.6265	0.6275	0.6265	0.0008
57	0.6270	0.6270	0.6270	0.6270	0.0000
58	0.6255	0.6250	0.6285	0.6263	0.0015
59	0.6265	0.6255	0.6255	0.6258	0.0005
60	0.6260	0.6265	0.6265	0.6263	0.0002
61	0.6285	0.6275	0.6285	0.6282	0.0005

	TAMU Wire-Wrapped As-Built Geometry (Non-Deformed Bundle)		
	Document No: TAMU-WW-AS	Rev: 2	Page 13 of 21

62	0.6265	0.6265	0.6275	0.6268	0.0005
63	0.6275	0.6275	0.6280	0.6277	0.0002
65	0.6270	0.6265	0.6265	0.6267	0.0002
66	0.6265	0.6260	0.6260	0.6262	0.0002
67	0.6255	0.6250	0.6250	0.6252	0.0002
69	0.6255	0.6255	0.6260	0.6257	0.0002
70	0.6270	0.6270	0.6270	0.6270	0.0000
71	0.6260	0.6265	0.6270	0.6265	0.0004
72	0.6270	0.6255	0.6275	0.6267	0.0008
75	0.6265	0.6275	0.6270	0.6270	0.0004
76	0.6270	0.6265	0.6255	0.6263	0.0006
81	0.6270	0.6265	0.6275	0.6270	0.0004
40	0.6260	0.6255	0.6265	0.6260	0.0004
84	0.6275	0.6265	0.6285	0.6275	0.0008
89	0.6255	0.6260	0.6275	0.6263	0.0008
92	0.6265	0.6260	0.6280	0.6268	0.0008

2.7.2 Wire Spacers

Extruded acrylic wire spacers were procured from Wuxi YanYang International Trading Co., Ltd. The target wire spacer diameter was specified in the TWRP-31-TSPEC-0010 Rev. 1 [1]. The selected diameter and extrusion tolerance was $0.003 \text{ m} \pm 0.00015 \text{ m}$. In-house characterization consisted of measuring each wire spacer diameter in three different axial locations. This was performed using the same Mitutoyo caliper used for the rod characterization. Axial locations 1, 2, and 3 were defined to be distances from the bottom of the wire spacer. These distances were 4 in, 37 in, and 70 in. A total of 73 wire spacers were characterized using this process. The average of the three axial location measurements was calculated for all 73 wire spacers. The final 61 wire spacers that were closest to the mean value were then selected. Table 2.7.2.1 shows the dimensions of the final 61 wire spacers selected with the method described. The average wire diameter was 0.00297 m with a standard deviation of 0.00003 m.

Table 2.7.2.1 - Wire Spacer Characterization (diameter in m)³

Wire #	Location 1	Location 2	Location 3	Average	Std. Dev.
1	0.00298	0.00296	0.00302	0.00299	0.00002

³ The wire # label is with respect to the total number of wires investigated and may not be sequential




TAMU Wire-Wrapped As-Built Geometry (Non-Deformed Bundle)

Document No: TAMU-WW-AS

Rev: 2

Page 14 of 21


2	0.00301	0.00296	0.00295	0.00297	0.00003
4	0.00294	0.00291	0.00297	0.00294	0.00002
5	0.00299	0.00298	0.00295	0.00297	0.00002
8	0.00293	0.00296	0.00295	0.00295	0.00001
9	0.00299	0.00297	0.00298	0.00298	0.00001
10	0.00303	0.00304	0.00301	0.00303	0.00001
11	0.00298	0.00298	0.00301	0.00299	0.00001
12	0.00302	0.00297	0.00296	0.00298	0.00003
14	0.00303	0.00294	0.00300	0.00299	0.00004
15	0.00298	0.00295	0.00303	0.00299	0.00003
18	0.00304	0.00302	0.00299	0.00302	0.00002
19	0.00301	0.00300	0.00303	0.00301	0.00001
21	0.00297	0.00302	0.00296	0.00298	0.00003
22	0.00295	0.00300	0.00298	0.00298	0.00002
23	0.00303	0.00302	0.00296	0.00300	0.00003
24	0.00301	0.00299	0.00298	0.00299	0.00001
25	0.00297	0.00301	0.00303	0.00300	0.00002
26	0.00294	0.00299	0.00298	0.00297	0.00002
27	0.00298	0.00301	0.00299	0.00299	0.00001
28	0.00294	0.00294	0.00293	0.00294	0.00000
29	0.00295	0.00296	0.00297	0.00296	0.00001
30	0.00300	0.00295	0.00303	0.00299	0.00003
31	0.00297	0.00292	0.00295	0.00295	0.00002
33	0.00295	0.00297	0.00303	0.00298	0.00003
34	0.00298	0.00298	0.00300	0.00299	0.00001
35	0.00300	0.00299	0.00296	0.00298	0.00002
36	0.00300	0.00296	0.00294	0.00297	0.00002
37	0.00294	0.00297	0.00296	0.00296	0.00001
38	0.00296	0.00301	0.00303	0.00300	0.00003
39	0.00295	0.00296	0.00298	0.00296	0.00001
41	0.00296	0.00293	0.00297	0.00295	0.00002
42	0.00297	0.00295	0.00294	0.00295	0.00001
43	0.00302	0.00297	0.00298	0.00299	0.00002
44	0.00298	0.00305	0.00299	0.00301	0.00003
45	0.00297	0.00296	0.00300	0.00298	0.00002
46	0.00293	0.00294	0.00295	0.00294	0.00001
47	0.00298	0.00296	0.00291	0.00295	0.00003
48	0.00302	0.00299	0.00303	0.00301	0.00002

	TAMU Wire-Wrapped As-Built Geometry (Non-Deformed Bundle)		
	Document No: TAMU-WW-AS	Rev: 2	Page 15 of 21

49	0.00300	0.00297	0.00299	0.00299	0.00001
50	0.00294	0.00300	0.00294	0.00296	0.00003
51	0.00297	0.00296	0.00294	0.00296	0.00001
52	0.00297	0.00294	0.00296	0.00296	0.00001
53	0.00298	0.00293	0.00295	0.00295	0.00002
54	0.00296	0.00294	0.00293	0.00294	0.00001
55	0.00292	0.00295	0.00300	0.00296	0.00003
56	0.00296	0.00296	0.00290	0.00294	0.00003
57	0.00298	0.00300	0.00300	0.00299	0.00001
58	0.00298	0.00291	0.00292	0.00294	0.00003
59	0.00296	0.00296	0.00295	0.00296	0.00000
60	0.00294	0.00293	0.00294	0.00294	0.00000
62	0.00298	0.00296	0.00295	0.00296	0.00001
63	0.00297	0.00294	0.00293	0.00295	0.00002
64	0.00302	0.00298	0.00296	0.00299	0.00002
65	0.00299	0.00301	0.00298	0.00299	0.00001
66	0.00290	0.00298	0.00293	0.00294	0.00003
68	0.00297	0.00294	0.00299	0.00297	0.00002
69	0.00295	0.00296	0.00297	0.00296	0.00001
71	0.00297	0.00295	0.00296	0.00296	0.00001
72	0.00296	0.00300	0.00296	0.00297	0.00002
73	0.00297	0.00299	0.00296	0.00297	0.00001

2.7.3 Fabrication Process

A low viscosity version of ethyl-2-cyanoacrylate was the adhesive used in the fabrication process. The wire was first adhered to the lower 1.5 inches of the rod. For this lower attachment section, the axis of the rod and wire were set parallel with assistance from an aluminum guide block containing milled rod/wire holes. The wire was then helically wrapped around the rod and adhered to the upper 0.5 inches of the rod. Before attaching the wire to the top, tension was applied to the wire to remove slack and mate the rod and wire surfaces. A 3D printed guide block was utilized to set the appropriate wire-clocking angle at the top of the rod.

	TAMU Wire-Wrapped As-Built Geometry (Non-Deformed Bundle)		
	Document No: TAMU-WW-AS	Rev: 2	Page 16 of 21


2.8 Second Non-Deformed Bundle

2.8.1 Rods

Cast acrylic rods were procured from Boedeker. The target rod diameter was identical to the first bundle, as defined in Section 2.7.1. The same In-house characterization process was repeated for 58 new rods. Table 2.8.1.1 shows the dimensions of the 58 new rods. A portion of the 58 new rods, along with several salvaged rods from the first non-deformed bundle, were selected to be used in the second non-deformed bundle. The average rod diameter was 0.6251 inches with a standard deviation of 0.0014 inches.

Table 2.8.1.1 – Second Bundle Fuel Rod Characterization (diameter in inches)


Rod #	Location 1	Location 2	Location 3	Average	Std. Dev.
1	0.6245	0.6265	0.6250	0.6253	0.0008
2	0.6255	0.6250	0.6245	0.6250	0.0004
3	0.6260	0.6260	0.6260	0.6260	0.0000
4	0.6255	0.6255	0.6255	0.6255	0.0000
5	0.6250	0.6250	0.6275	0.6258	0.0012
6	0.6255	0.6255	0.6255	0.6255	0.0000
7	0.6255	0.6255	0.6255	0.6255	0.0000
8	0.6255	0.6255	0.6255	0.6255	0.0000
9	0.6280	0.6240	0.6220	0.6247	0.0025
10	0.6260	0.6260	0.6245	0.6255	0.0007
11	0.6225	0.6240	0.6220	0.6228	0.0008
12	0.6240	0.6265	0.6230	0.6245	0.0015
13	0.6260	0.6450	0.6300	0.6337	0.0082
14	0.6290	0.6255	0.6255	0.6267	0.0016
15	0.6260	0.6250	0.6250	0.6253	0.0005
16	0.6235	0.6235	0.6210	0.6227	0.0012
17	0.6225	0.6260	0.6235	0.6240	0.0015
18	0.6230	0.6235	0.6235	0.6233	0.0002
19	0.6250	0.6230	0.6270	0.6250	0.0016
20	0.6300	0.6270	0.6270	0.6280	0.0014
21	0.6350	0.6230	0.6250	0.6277	0.0052
22	0.6280	0.6300	0.6260	0.6280	0.0016
23	0.6245	0.6245	0.6305	0.6265	0.0028
24	0.6245	0.6250	0.6245	0.6247	0.0002
25	0.6245	0.6240	0.6270	0.6252	0.0013
26	0.6240	0.6255	0.6230	0.6242	0.0010

	TAMU Wire-Wrapped As-Built Geometry (Non-Deformed Bundle)		
	Document No: TAMU-WW-AS	Rev: 2	Page 17 of 21

27	0.6270	0.6235	0.6235	0.6247	0.0016
28	0.6295	0.6250	0.6250	0.6265	0.0021
29	0.6280	0.6260	0.6240	0.6260	0.0016
30	0.6250	0.6240	0.6240	0.6243	0.0005
31	0.6240	0.6240	0.6245	0.6242	0.0002
32	0.6315	0.6250	0.6270	0.6278	0.0027
33	0.6245	0.6245	0.6210	0.6233	0.0016
34	0.6245	0.6225	0.6230	0.6233	0.0008
35	0.6235	0.6225	0.6220	0.6227	0.0006
36	0.6245	0.6265	0.6250	0.6253	0.0008
37	0.6275	0.6240	0.6250	0.6255	0.0015
38	0.6225	0.6235	0.6200	0.6220	0.0015
39	0.6260	0.6235	0.6230	0.6242	0.0013
40	0.6340	0.6240	0.6245	0.6275	0.0046
41	0.6250	0.6230	0.6235	0.6238	0.0008
42	0.6230	0.6250	0.6250	0.6243	0.0009
43	0.6255	0.6245	0.6225	0.6242	0.0012
44	0.6250	0.6230	0.6250	0.6243	0.0009
45	0.6245	0.6245	0.6230	0.6240	0.0007
46	0.6255	0.6220	0.6250	0.6242	0.0015
47	0.6250	0.6245	0.6245	0.6247	0.0002
48	0.6230	0.6250	0.6250	0.6243	0.0009
49	0.6260	0.6245	0.6230	0.6245	0.0012
50	0.6250	0.6200	0.6250	0.6233	0.0024
51	0.6240	0.6240	0.6220	0.6233	0.0009
52	0.6240	0.6250	0.6250	0.6247	0.0005
53	0.6250	0.6250	0.6250	0.6250	0.0000
54	0.6250	0.6255	0.6250	0.6252	0.0002
55	0.6245	0.6250	0.6250	0.6248	0.0002
56	0.6250	0.6240	0.6245	0.6245	0.0004
57	0.6245	0.6250	0.6260	0.6252	0.0006
58	0.6250	0.6250	0.6250	0.6250	0.0000

2.8.2 Wire Spacer

Extruded acrylic wire spacers were procured from Wuxi YanYang International Trading Co., Ltd. The target wire spacer diameter was identical to the first bundle, as defined in Section 2.7.2. The same In-house characterization process was repeated for 200 new wire spacers. The final 61 wire spacers that were closest to the mean value were then selected. Table 2.8.2.1 shows the dimensions of the selected


	TAMU Wire-Wrapped As-Built Geometry (Non-Deformed Bundle)		
	Document No: TAMU-WW-AS	Rev: 2	Page 18 of 21

61 wire spacers used in the second non-deformed bundle. The average wire spacer diameter was 0.00300 m with a standard deviation of 0.00003 m.

Table 2.8.2.1 – Second Bundle Wire Spacer Characterization (diameter in m)⁴

Wire #	Location 1	Location 2	Location 3	Average	Std. Dev.
6	0.00297	0.00299	0.00290	0.00295	0.00004
7	0.00300	0.00301	0.00300	0.00300	0.00000
8	0.00294	0.00293	0.00291	0.00293	0.00001
9	0.00300	0.00300	0.00300	0.00300	0.00000
13	0.00299	0.00298	0.00297	0.00298	0.00001
14	0.00299	0.00295	0.00302	0.00299	0.00003
15	0.00290	0.00295	0.00300	0.00295	0.00004
16	0.00300	0.00300	0.00300	0.00300	0.00000
17	0.00303	0.00300	0.00300	0.00301	0.00001
18	0.00297	0.00300	0.00295	0.00297	0.00002
19	0.00300	0.00302	0.00290	0.00297	0.00005
20	0.00296	0.00290	0.00296	0.00294	0.00003
21	0.00290	0.00293	0.00300	0.00294	0.00004
23	0.00300	0.00305	0.00301	0.00302	0.00002
24	0.00302	0.00303	0.00305	0.00303	0.00001
25	0.00301	0.00301	0.00301	0.00301	0.00000
26	0.00304	0.00301	0.00300	0.00302	0.00002
27	0.00295	0.00300	0.00300	0.00298	0.00002
28	0.00304	0.00302	0.00301	0.00302	0.00001
29	0.00301	0.00301	0.00301	0.00301	0.00000
30	0.00300	0.00300	0.00301	0.00300	0.00000
31	0.00300	0.00309	0.00305	0.00305	0.00004
32	0.00297	0.00302	0.00302	0.00300	0.00002
33	0.00295	0.00300	0.00303	0.00299	0.00003
34	0.00300	0.00301	0.00300	0.00300	0.00000
35	0.00301	0.00304	0.00300	0.00302	0.00002
36	0.00301	0.00300	0.00300	0.00300	0.00000
37	0.00306	0.00300	0.00305	0.00304	0.00003
38	0.00300	0.00301	0.00300	0.00300	0.00000


⁴ The wire # label is with respect to the total number of wires investigated and may not be sequential

	TAMU Wire-Wrapped As-Built Geometry (Non-Deformed Bundle)		
	Document No: TAMU-WW-AS	Rev: 2	Page 19 of 21

39	0.00301	0.00299	0.00301	0.00300	0.00001
40	0.00305	0.00300	0.00309	0.00305	0.00004
41	0.00305	0.00304	0.00302	0.00304	0.00001
42	0.00301	0.00301	0.00305	0.00302	0.00002
43	0.00303	0.00288	0.00306	0.00299	0.00008
44	0.00305	0.00302	0.00307	0.00305	0.00002
45	0.00303	0.00308	0.00301	0.00304	0.00003
48	0.00303	0.00303	0.00301	0.00302	0.00001
49	0.00305	0.00304	0.00301	0.00303	0.00002
51	0.00302	0.00301	0.00300	0.00301	0.00001
52	0.00305	0.00301	0.00303	0.00303	0.00002
53	0.00300	0.00303	0.00297	0.00300	0.00002
55	0.00306	0.00303	0.00307	0.00305	0.00002
60	0.00305	0.00285	0.00303	0.00298	0.00009
61	0.00296	0.00297	0.00293	0.00295	0.00002
65	0.00302	0.00298	0.00303	0.00301	0.00002
70	0.00296	0.00299	0.00300	0.00298	0.00002
72	0.00298	0.00294	0.00297	0.00296	0.00002
74	0.00302	0.00301	0.00300	0.00301	0.00001
75	0.00304	0.00295	0.00302	0.00300	0.00004
78	0.00297	0.00299	0.00293	0.00296	0.00002
82	0.00301	0.00305	0.00303	0.00303	0.00002
83	0.00292	0.00291	0.00293	0.00292	0.00001
88	0.00301	0.00303	0.00300	0.00301	0.00001
89	0.00302	0.00301	0.00301	0.00301	0.00000
91	0.00300	0.00304	0.00296	0.00300	0.00003
92	0.00301	0.00294	0.00297	0.00297	0.00003
93	0.00303	0.00304	0.00301	0.00303	0.00001
94	0.00300	0.00300	0.00305	0.00302	0.00002
96	0.00300	0.00298	0.00302	0.00300	0.00002
97	0.00300	0.00305	0.00303	0.00303	0.00002
99	0.00300	0.00301	0.00295	0.00299	0.00003

2.8.3 Fabrication Process

The fabrication process defined in Section 2.7.3 was repeated for the second non-deformed bundle. A series of additional steps was then performed to fully adhere the wire along the entire length of the rod. After attaching the wire to the rod bottom/top, the wire was tacked at eight different axial locations. After curing, inspection was performed on the wire position at the eight tacked locations and at midpoints

	TAMU Wire-Wrapped As-Built Geometry (Non-Deformed Bundle)		
	Document No: TAMU-WW-AS	Rev: 2	Page 20 of 21

between the tacked located. After passing this inspection, the wire was then fully adhered to the rod by applying adhesive to both sides of the wire along its entire length.

3.0 PRESSURE TRANSDUCER FINAL LOCATION


Holes were drilled and tapped into the acrylic hexagonal test section enclosure to accommodate pressure transducer hardware. Table 3.1 lists the final locations of the holes that will accommodate the pressure transducers. Measurements have been performed using a straight-edged ruler with a 0.0625 in accuracy. Holes are located at the midpoint of the width of each face, corresponding to 2.0625 ± 0.0625 in from the external corners of the hexagonal enclosure.

Table 3.1 – Final axial location of all pressure taps

Pressure Tap ID	Final Axial Location (z-coordinate) (in) ^{5,6}	Final Axial Location (pitch number)
PT #0	-2.0000	-0.11
PT #1f	3.0000	0.16
PT #2f	18.7500	1.00
PT #3f	32.8125	1.75
PT #4f	37.5000	2.00
PT #5d	42.1875	2.25
PT #5e	42.1875	2.25
PT #5f	42.1875	2.25
PT #5a	42.1875	2.25
PT #6d	56.2500	3.00
PT #6e	56.2500	3.00
PT #6f	56.2500	3.00
PT #6a	56.2500	3.00
PT #7f	60.9375	3.25
PT #8	67.6250	3.61

⁵ The axial uncertainty of all pressure transducer final locations is ± 0.0625 in.

⁶ The axial position $z = 0.0$ reference is located at the interface between the upper flange of the lower plenum and the lower flange of the test section.

	TAMU Wire-Wrapped As-Built Geometry (Non-Deformed Bundle)		
	Document No: TAMU-WW-AS	Rev: 2	Page 21 of 21

4.0 REFERENCES

- I. TWRP-31-TSPEC-0010 Rev. 1, TAMU Fuel Assembly Flow Visualization Test Specification

APPENDIX B

FACILITY OPERATING PROCEDURES

This appendix includes the filling, starting, stopping, and draining procedures for operating the experimental facility.



TECHNICAL DOCUMENT COVER PAGE

Document No: TAMU-WW-PROC-NDB-PCM	Revision: 1	Page 1 of 11
	Date: 04/18/2016	
Doc Title: TAMU Wire-Wrapped Loop Operation Procedure (Non-Deformed Bundle) – P-Cymene		
Project No: DE-NE0008321		
Project Name: Toward a Longer Life Core: Thermal-Hydraulic CFD Simulations and Experimental		
Document Purpose/Summary: This procedure provides generic instructions to operate the experimental facility. Subsections of this procedure include filling, startup, shutdown, and draining. Total Page Count: 11 pages.		
Continuous Use Procedure		



TEST DATE: _____

TEST NAME: PCM_____



TECHNICAL DOCUMENT COVER PAGE

Document No:	TAMU-WW-PROC-NDB-PCM	Revision: 1	Page 2 of 11
--------------	----------------------	-------------	--------------

Prepared By:	Nolan Goth		04/15/2016
	Printed/Typed Name	Signature	Date
TAMU Reviewed By:	Rodolfo Vaghetto		09/15/2016
	Printed/Typed Name	Signature	Date

REVISION HISTORY LOG

Page: 3 of 11

Document Number: TAMU-WW-PROC-NDB-PCM Revision: 1

Document Title: TAMU Wire-Wrapped Loop Operation Procedure (Non-Deformed Bundle) – P-Cymene

REVISION	DATE	DESCRIPTION
0	04/13/2016	First Final Release
1	04/15/2016	Minor change of steps sequence in Section 3


	TAMU Wire-Wrapped Loop Operation Procedure (Non-Deformed Bundle) – P-cymene		
	Document No: TAMU-WW-PROC-NDB-PCM	Rev: 1	Page 4 of 11

TABLE OF CONTENTS

TABLE OF CONTENTS 4

1.0 PURPOSE 5

2.0 EXPERIMENTAL FACILITY 5


3.0 OPERATING PROCEDURES 5

 3.1 FILL THE TEST SECTION 5

 3.2 START THE FACILITY 8

 3.3 STOP THE FACILITY 10

 3.4 DRAIN THE FACILITY 10

	TAMU Wire-Wrapped Loop Operation Procedure (Non-Deformed Bundle) – P-cymene		
	Document No: TAMU-WW-PROC-NDB-PCM	Rev: 1	Page 5 of 11

1.0 PURPOSE

The purpose of this document is to provide instructions to operate the test loop including:

- Fill the test section
- Start the facility
- Shutdown the facility
- Drain the facility

2.0 EXPERIMENTAL FACILITY

Figure 2 shows the process flow diagram of the Wire-Wrapped Experimental Facility. Figure 2 located at the end of this procedure.

3.0 OPERATING PROCEDURES

Put initials when step is completed

3.1 FILL THE TEST SECTION

1. _____ Open the primary tank snorkel valve.
2. _____ Verify that the drain hose from PTV-08 is connected to a plastic bottle and that the bottle is empty.
3. _____ Check that the waste bottles fluid level is sufficiently low (if not empty the bottles).
4. _____ Open LabView and load file Wire_Wrapped_Data_Acquisition.vi.
5. _____ Verify that the checkboxes marked in red in Figure 1 are switched to “F” (False)

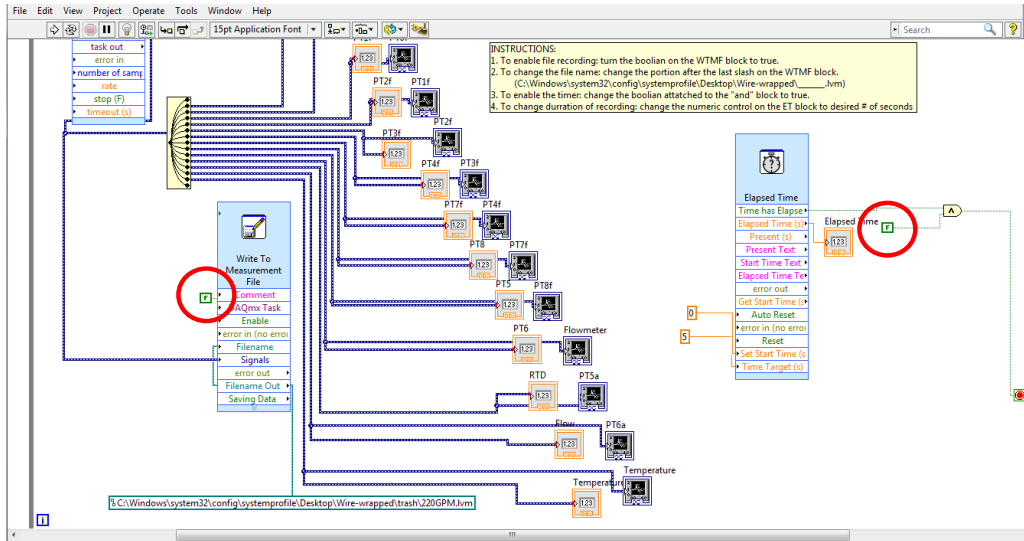




Figure I. LabView Snapshot

6. _____ Power on the DAQ power supply with the front ON/OFF switch
7. _____ Set the constant voltage DC power supply for the pressure transducers to 24 V.
8. _____ Set the constant voltage DC power supply for the flowmeter and thermometer to 18 V.
9. _____ Power on both constant voltage DC power supplies with the front ON/OFF switch
10. _____ Open the following test section valves
PTV-05D
PTV-05E
PTV-05F
PTV-05A
PTV-06D
PTV-06E
PTV-06F
PTV-06A
PTV-08
11. _____ Lock all cam and groove fittings for the green flex hoses
12. _____ Close the primary tank drain valve below the primary tank
SV-01
13. _____ Close the test section drain valve in the lower plenum
PV-05
14. _____ Open the following primary loop valves
PV-01
PV-02
PV-03

	TAMU Wire-Wrapped Loop Operation Procedure (Non-Deformed Bundle) – P-cymene		
	Document No: TAMU-WW-PROC-NDB-PCM	Rev: I	Page 7 of 11

15. _____ Watch for the fluid level in the test section to increase. It should equalize with the fluid level in the snorkel.
16. _____ Confirm that all secondary loop valves are closed
 - SV-01
 - SV-02
 - SV-03
 - SV-04
 - SV-05
 - SV-06
 - SV-07
 - SV-08
 - SV-09
17. _____ Power on the secondary pump VFD at the 240 V B-3 safety switch by moving the lever up
18. _____ **IMPORTANT:** On the secondary pump VFD, make sure that the frequency is reduced to the minimum value. To do this, click on PROG button twice until 0.0 is displayed. Then press the down arrow until the frequency displayed is 3.0.
19. _____ Press the impeller reversal button until the impeller direction indicator LED is red.
20. _____ Press the green button to start the secondary pump (SP-01)
21. _____ Confirm via visual inspection that the secondary pump (SP-01) impeller is rotating in the counterclockwise direction
22. _____ Open the secondary tank outlet valve (SV-06) and the heat exchanger inlet valve (SV-03)
23. _____ While Operator 1 opens slowly the heat exchanger outlet valve (SV-04), Operator 2 increases the frequency of the secondary VFD by pressing the up arrow. This operation should be conducted slowly until the fluid level reaches the elevation of PTV-08. This can be done by continuously checking the fluid level in the test section and the level in the snorkel sight glass. The secondary VFD should read approximately 20.60 Hz.
24. _____ Purge all pressure transducer tubing of air by modulating the following valves.
 - PTV-05D
 - PTV-05E
 - PTV-05F
 - PTV-05A
 - PTV-06D
 - PTV-06E
 - PTV-06F
 - PTV-06A
25. _____ When the fluid level reaches the elevation of PTV-08, Operator 1 shall close the heat exchanger outlet valve (SV-04), and Operator 2 shall shut off the secondary pump (SP-02) by pressing the red button.
26. _____ Check that the fluid draining from PTV-08 is entering the waste bottle
27. _____ Close the primary loop valves to isolate the test section
 - PV-03
 - PV-04

	TAMU Wire-Wrapped Loop Operation Procedure (Non-Deformed Bundle) – P-cymene		
	Document No: TAMU-WW-PROC-NDB-PCM	Rev: 1	Page 8 of 11

28. _____ IMPORTANT: Pressure check. This step verifies that pressure transducers are reading correctly. Confirm that PTV-08 is open. Read the pressure for each pressure transducer PT#0-8 and write the value in the table below. Compare the value with the target and mark as “P” (Pass) if the measured value is within approximately ±0.1 of the target. If not, mark as “F” (Fail) and contact the supervisor before continuing the test.

Table 3-1. Pressure Check #1

Pressure Transducer	Target Pressure (psi) ¹	Measured Pressure (psi)	Difference (psi)	Pass (P) Fail (F)
PT#0	2.14 ±0.1			
PT#1	2.00 ±0.1			
PT#2	1.49 ±0.1			
PT#3	1.05 ±0.1			
PT#4	0.89 ±0.1			
PT#5	0.77 ±0.1			
PT#6	0.34 ±0.1			
PT#7	0.18 ±0.1			
PT#8	0.00 ±0.1			

29. _____ Close PTV-08

3.2 START THE FACILITY

1. _____ Power on the primary pump VFD at the 480 V A-10 safety switch by moving the lever up
2. _____ IMPORTANT: Set frequency in the VFD to zero Hz before turning on the pump
 - a. use the “Shift” button select the digit to change
 - b. use the arrow keys to set the digit to 0
 - c. repeat a) and b) until ALL digits are 0 (the screen MUST display 00.00)
3. _____ Press the green FWD
4. _____ IMPORTANT: To start the pump, always press first the “shift” bottom to select the tenth place to increase the frequency by 1/10 Hz at the time
5. _____ Use the arrow key to increase the frequency up to 3 Hz
6. _____ Increase the frequency of the VFD up to approximately 10 Hz in 1 Hz increments until the flow meter display shows 50 GPM. Refer to steps 2a and 2b
7. _____ Bubbles may be visible in the test section
8. _____ Increase the primary pump VFD to approximately 20 Hz until reaching approximately 110 GPM.

¹ These values are calculated by multiplying the target values for H₂O by 0.86 (specific gravity of p-cymene at room temperature)

9. _____ Maintain the same flow rate for 2 to 5 minutes to complete the degasification
10. _____ Reduce the flow rate to 50 GPM.
11. _____ Check that the fluid level in the primary tank snorkel is at the full line. (if level is low add more fluid)
12. _____ IMPORTANT: Pressure check. Record the pressure from LabView and verify that values are approximately ±0.2 psi from the values listed in the table below.

Table 3-2. Pressure Check #2


Pressure Transducer	Target Pressure (psi)	Measured Pressure (psi)	Difference (psi)	Pass (P) Fail (F)
PT#0	2.92 ±0.2			
PT#1	2.58 ±0.2			
PT#2	2.06 ±0.2			
PT#3	1.81 ±0.2			
PT#4	1.63 ±0.2			
PT#5	1.55 ±0.2			
PT#6	0.86 ±0.2			
PT#7	0.69 ±0.2			
PT#8	0.60 ±0.2			

13. _____ IMPORTANT. Flow meter check. Compare the reading of the flow meter display with the one displayed on LabView and write the values in the table below. Mark the comparison as “P” (Pass) if the values are within 2 GPM.

Table 3-3 Flow Meter Check

Flow Meter Display (GPM)	Flow Meter LabView (GPM)	Pass(P) / Fail(F)

14. _____ Continue adding fluid to maintain the level in the primary tank snorkel at the full line
15. _____ Startup is complete. Adjust pressure transducer valves accordingly based on the planned pressure measurements
16. _____ Proceed to the desired flow rate for measurement by adjusting the VFD. Refer to steps 8a and 8b

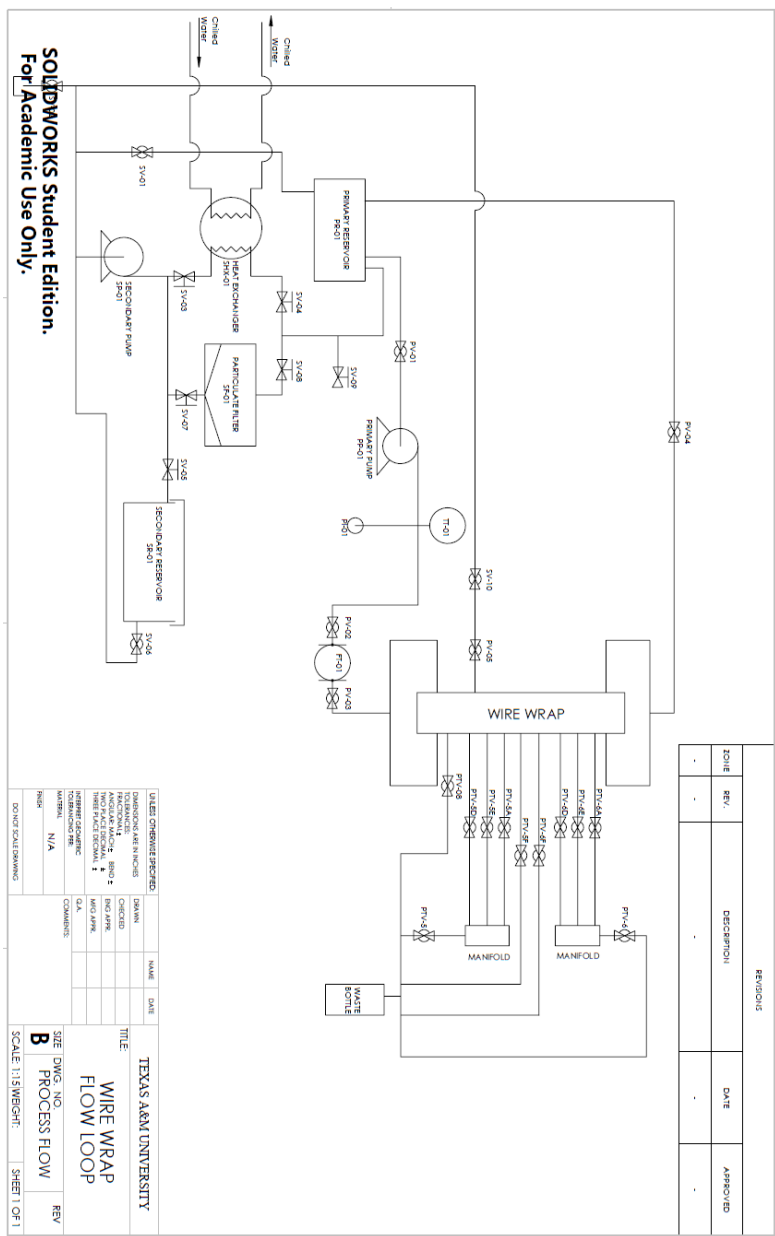
	TAMU Wire-Wrapped Loop Operation Procedure (Non-Deformed Bundle) – P-cymene		
	Document No: TAMU-WW-PROC-NDB-PCM	Rev: 1	Page 10 of 11

3.3 STOP THE FACILITY

1. _____ Decrease the frequency of the primary pump VFD down to 0 Hz in 10 Hz increments.
 - a. Use the “Shift” button select the digit to change
 - b. Use the arrow keys to decrease the frequency
2. _____ Power off the primary pump VFD at the 480 V A-10 safety switch by moving the lever down

3.4 DRAIN THE FACILITY

1. _____ Close primary valves (SV-03) and (SV-04), which are upstream and downstream of the test section.
2. _____ Open the test section drain valve (SV-05)
3. _____ Open the following valves to align the secondary tank (SR-01) to the test section drain
 - SV-10
 - SV-03
 - SV-04
4. _____ Power on the secondary pump VFD at the 240 V B-3 safety switch by moving the lever up
5. _____ IMPORTANT: On the secondary pump VFD, make sure that the frequency is reduced to the minimum value. To do this, click on PROG button twice until 0.0 is displayed. Then press the down arrow until the frequency displayed is 3.0.
6. _____ Press the impeller reversal button until the impeller direction indicator LED is red.
7. _____ Press the green button to start the secondary pump (SP-01)
8. _____ Confirm via visual inspection that the secondary pump (SP-01) impeller is rotating in the counterclockwise direction
9. _____ Increase the secondary pump VFD to 10 Hz to assist draining
10. _____ After the fluid level is below PT#8, open PTV-08 to allow air ingress
11. _____ Continue draining until the fluid level has reached the elevation of PT#0
12. _____ Disconnect one 2” flex hose from the T-junction upstream of the test section
13. _____ Drain contents from the flex hose to the disposal container
14. _____ Disconnect the other end of the flex hose
15. _____ Use a large syringe and flexible tube to remove the remaining fluid from the lower plenum
16. _____ IMPORTANT: Never leave fluid into the test section after completing a test.
17. _____ Close the primary tank snorkel valve.



SOLIDWORKS Student Edition.
 For Academic Use Only.

DATE	BY	REVISION

LISTED COMPONENTS CHECKED DESIGNER: [] APPROVAL: [] THIRD PARTY CHECK: [] INVENTORY DATE: [] UNIT: [] N/A	COMMENTS: CA: [] SCALE: 1:1 SHEET: 1 OF 1
--	---

DATE	BY	REVISION

TITLE: TEXAS A&M UNIVERSITY WIRE WRAP FLOW LOOP SEE DWG. NO. [] PROCESS FLOW	DECISION DATE APPROVED
--	------------------------------

Figure 1. Process flow diagram of the Wire-Wrapped Experimental Facility

APPENDIX C

PROJECT SAFETY ANALYSIS

This appendix includes the project safety analysis performed by the Texas A&M University prior to the construction of the facility room.

Guide to Project Safety Analysis (PSA)

PROJECT IDENTIFICATION SECTION

Project Name:

Toward a Longer-Life Core: Thermal Hydraulic CFD Simulations and Experimental Investigation of Deformed Fuel Assemblies

TEES Project Number (if applicable): Maestro ID M1502013

Project Description (abstract or executive summary):

The purpose of the project will be to conduct isothermal experiments on transparent rod bundles to collect high resolution flow measurements to be used for Computational Fluid Dynamics (CFD) codes validation.

Principal Investigators:

Name: Vaghetto, Rodolfo.
Department/Division: Department of Nuclear Engineering
Office Location: 258, Bizzell Building
Office Phone Number: 979 845-4109
Email: r.vaghetto@tamu.edu

Name: Hassan, Yassin A.
Department/Division: Department of Nuclear Engineering
Office Location: 261, Bizzell Building
Office Phone Number: 979 845-7090
Email: y-hassan@tamu.edu

Name: Anand, N.K.
Department/Division: Department of Mechanical Engineering
Office Location: 312 ADMN
Office Phone Number: 979.845-5633
Email: nkanand@tamu.edu

Researchers:

(List all project personnel: Faculty, PI, Students or Staff)

Saya Lee, Nolan Goth, Mason Childs, Carlos Estrada-Perez
Department/Division: Department of Nuclear Engineering
Office Location: USB
Office Phone Number: N/A
Email: sayalee@tamu.edu (reference)

Location of Project Facilities:

Building No: 3400
Building Name: USB
Room No: 127M

Project Duration (projected dates): 03/15/2015 – 03/14//2017

Guide to Project Safety Analysis (PSA)

REVIEW & AUTHORIZATION SECTION

The attached Project Safety Analysis has been reviewed by the undersigned. Any major modifications of equipment or changes in procedures will require additional review by the Departmental Safety Committee, and/or the Departmental Safety Officer, and the Department Head. In executing this work, you must abide by the Safety Procedures of the Department and University and must inform the Departmental Safety Officer of any changes in personnel or operations outside these procedures.

Ronald G. Vesperto _____ *10/12/2015*
Faculty/PI: _____ Date:

[Signature] _____ *12/10/2015*
Department Head: _____ Date:

[Signature] _____ *12/16/15*
Department Safety Officer: _____ Date:

D. C. Breeding, PhD _____ *2015-12-08*
Director, Engineering Safety: _____ Date:

Guide to Project Safety Analysis (PSA)

C. Optional Informational Copies

Please send a copy of your final approved PSA document to the following TAMU Departments, for their information and use, if/as directed. Any comments or concerns will be conveyed to the PI and to Engineering Safety before initiation date of the proposed project.

TAMU Radiation Safety Officer (RSO) & Laser Safety Officer (LSO) Date:
Mail Stop: 4472 TAMU

(A copy of the draft PSA must be provided to the TAMU RSO & LSO for additional approval(s) where use of radioactive materials, ionizing radiation or nonionizing radiation-producing devices are planned. Approval of the RSO/LSO must be obtained, and proper permits issued before the PSA can receive final approval. Please refer to §. II, Analysis of Potential Hazards, below.)

TAMU Environmental Health & Safety Department (EHSD) Date:
Mail Stop: 4472 TAMU

(A copy of the approved PSA is provided to the EHSD for their information and use, when situations warrant. The EHSD will review and keep on file, and notify Engineering Safety if any additional concerns are noted.)

TAMU Office of Facilities Coordination, MS 1369 Date

(To accompany requests for new space assignments or requests for use of sites at the Riverside Annex Campus or other outdoor sites.)

Other... Date:

Guide to Project Safety Analysis (PSA)

STRATEGY SECTION

Purpose of Project Safety Analysis:

PSA provides the Principal Investigator with the opportunity to review the environmental health, safety and security aspects of the research project to be undertaken, to identify known and potential hazards, to assess risks, and to select and implement necessary protective controls. This will help protect the researchers, graduate students, and staff involved with the project, reduce risk, ensure compliance, and conserve environmental resources, and protect facilities.

Scope:

All Principal Investigators shall file a written report on the safety analysis of each research project prior to the initiation of that exercise. The Project Safety Analysis (PSA) shall identify potential hazards and assess risks by the use of system safety analysis techniques, and shall detail the engineering and administrative controls that will be necessary to reduce risk to acceptable levels for the researchers, graduate students, and staff as well as the occupants of the building and the environment. The PSA will identify the costs, and the source of adequate funding, to implement necessary controls. It will identify necessary personnel training needs. The PSA will identify a plan for ultimate disposal of leftover equipment, materials and wastes, and the decontamination & clean up necessary to render the facility safe to reassign and reoccupy.

Extent of Applicability:

Recognizing that no activity is without some degree of risk, and that certain routine risks are accepted without question by the vast majority of persons (for example: machine shops that do not handle hazardous materials, cars used for personal transportation, etc,) the applicability of this analysis has been limited to those academic research projects that involve hazards not routinely encountered and accepted in the course of everyday living by the vast majority of the general public.

The analysis of a project which involves only hazards of a type and magnitude routinely encountered and accepted by the public will require justification which can be referenced to a recognized source.

Assistance in Conducting PSA

The Office of Engineering Safety is available to work with the Faculty/PI and research staff to identify hazards associated with the project, assess risks, and to identify necessary protective control measures.

Guide to Project Safety Analysis (PSA)

PROCEDURE SECTION

I) Apparatus Used in the Project

A) Equipment Used in the Experiment

{List all equipment; describe it's use, and potential for injury an/or harmful exposure}

The facility consists of a closed loop with a clear vertical test section, piping, a circulation pump, and a storage tank (see attachment). The pump will be turned on to maintain the desired flow conditions at the test section during the duration of the test. Working fluid will be drained and stored in the storage tank at the end of each test. The test facility will be equipped with flow visualization devices, including cameras and light sources (laser). Flow measurements will be recorded as picture frames with a camera connected to a computer. Pressure and temperature measurements will be also conducted and stored in the computer through a Data Acquisition System. The experimental activity will be conducted exclusively in the closed room. Only authorized personnel will have access to the room.

B) Experiments Performed in the Project

{Attach a summary description of the project to be undertaken, research procedures, standard operating procedures (SOP), tasks, and safe work practices (SWP)}

The experimental activity will focus on performing measurements of flow through clear rod bundles. The experimental facility will consist of a clear test section of hexagonal shape containing a rod bundle with 61 vertical rods. Flow will be forced through the test section via circulating pump. No particular operating procedures are required to run the experiments in addition to the actual rules and procedures identified for the laboratory where the experimental facility will be built.

C) Chemicals Used in the Research Project:

{List all chemicals to be used in the project}

Required chemical inventory current and posted? <i>{Attach a copy of the current chemical inventory for this facility}</i>	Y
Material Safety Data Sheets (MSDS)? <i>{Are current MSDS's available for all chemicals?}</i>	Y
All stored chemicals segregated by Hazard Class? <i>{Stored chemicals must be segregated by Hazard Class.}</i>	Y ¹

II) Analysis of Potential Hazards

A) List all Physical Hazards That May Cause:

Electrical Shock:		Electric parts of the facility will be identified and marked. Metal structures will be grounded.
Cuts:		N/A
Burns:	N/A	
Abrasions:		N/A
Slips:		Wet Floor if water is present. Water will be removed immediately if spills occur.
Trips:		Possible Electric Cables running around the facility. Cables will be marked and covered.
Falls:		From the ladder to be used to install instrumentation. Work on ladder will be minimized

¹ Only one type of chemical (P-cymene) will be used
Office of Engineering Safety <http://engineering.tamu.edu/safety/>

Guide to Project Safety Analysis (PSA)

Amputations: N/A
Other... N/A

B) List all Chemical Hazards

*{Identify the name and characteristics of each chemical}
{Use the HazCom Engineering Chemical Inventory form}*

Acids: N/A
Bases: N/A
Oxidizers: N/A
Flammables: P-cymene
Solvents: N/A
Toxic Chemicals: P-cymene
Reactives and Explosives: N/A
Other...

C) Biological Hazards

*** If Biological Hazards are present, OSHA Bloodborne Pathogen requirements and CDC Universal Precautions shall be implemented, and appropriate PPE shall be provided. ***

Microbiologicals: N/A
Bacteriologicals: N/A
Bloodborne Pathogens: N/A
CDC Select Agent: N/A
Other... N/A

D) Secure, Segregated Chemical Storage:

*{Chemical storage areas shall not be accessible to students/passers-by}
{All stored Chemicals and other hazardous materials shall be provided with secure storage and segregated by Hazard Class}*

Locations: 127M – Closed room
Quantities: N/A
Authorized Person(s) Accessing the Chemicals: Y

E) Hazardous Waste Disposal

{All hazardous chemical waste materials must be contained, labeled, tagged, and disposed of in compliance with the TAMU Hazardous Waste Management Program}

Chemical: N/A Disposal method: N/A

F) Monitoring and Detection

Substance: N/A Detection method: N/A

G) List all necessary Personal Protective Equipment (PPE)

{All PPE shall be ANSI/NIOSH/MSHA approved, as appropriate}

No additions to the Laboratory PPE

Long Pants, Long Sleeved Shirts Y
No Shorts, No Skirts Y
Closed-Toed Shoes Y
Aprons/ Lab Coats N
Goggles/Face Shields Y²

² Goggles will be required while operating the loop.

Laser goggles will be required while operating the laser

Guide to Project Safety Analysis (PSA)

Gloves	Y ³
Respirators	Y ⁴
SCBA	N
Other...	

H) Personnel Training Needed for Specific Hazards

{Identify the specific hazard and the individuals affected}

training. All project personnel must complete the Engineering Laboratory Safety Training, Hazard Awareness in Engineering Research, and the TAMU course in Fire Extinguisher usage (call 845-7715). If tools and/or shop equipment is used, personnel must also complete the Engineering Shop & Tool Safety course. All Engineering safety training are available on TrainTraq. Additional, all personnel must complete the TAMU Laser Safety Training course.

Principal Investigator:
Researcher/Lab Technician:
Graduate Student:
Student Workers:
Other...

III) Potential Accidents and Responses *(What if ... ?)*

A) Utility Failure

<u>Utility:</u>	<u>Planned Response (SOP's):</u>
Electricity	Pumps will shut down
Gas	N/A
Air	N/A
Vacuum	N/A
Hot Water	N/A
Cold Water	N/A
Ventilation Hood	Not Required
Room/Lab Ventilation	Required

B) Leaks and Spills

SDS Available:	Y ⁵
Spill Kit Available:	Y
PPE Available:	N/A
Containment Procedures:	Y ⁶
Disposal Procedures:	N/A
Personnel Training:	Y

C) Equipment Failure

{Attach Documentation of All Emergency Shutdown Procedures}

No special Procedures Required

D) Fire Prevention *{Attach the following}*

Laboratory Fire Prevention and procedures apply.

Fire Extinguisher Locations:

Building Emergency Evacuation Plan:

³ Nitrile gloves are required to manage the p-cymene

⁴ Half-face respirators with appropriate cartridges for Aromatic Hydrocarbons should be used while loop is in operation

⁵ Available in the room

⁶ Available in the room

Guide to Project Safety Analysis (PSA)

Evacuation Routes:
Emergency Response Procedure:
Incident Reporting and Notification Procedure:

IV) Equipment Labels

A) Utility Shut-offs labeled:

Electricity	Y
Vacuum	N/A
Gas	N/A
Air	N/A
Hot Water	N/A
Cold Water	N/A
Other...	

B) Identify all necessary Warning Signs:

Equipment:	N/A
Instrumentation:	Laser in Use Sign
Utilities:	N/A
Personal Protective Equipment:	N/A
Reagent Bottles:	N/A
Secondary Containers:	N/A
Refrigerators and Microwaves:	N/A
Chemical Storage:	N/A
*Emergency Contact Information (ECI) <i>{Must be posted on all entry door(s)}</i>	

V) Noise

Will the project/ generate excessive noise?	No
If yes, anticipated dBA is: _____	N/A

Type of hearing protection provided:

VI) List all Personnel Training Needs

Laboratory Safety Training <i>{Mandatory}</i>	
Hazard Communication Training <i>{Mandatory}</i>	
Shop & Tool Safety Training:	Y
Safety Training Needs:	Y ⁷
Standard Operating Procedures (SOP):	Y
Safe Work Practices (SWP) :	Y
Other Project-Specific Training Needs...	

⁷ Laser operation and p-cymene management
Office of Engineering Safety <http://engineering.tamu.edu/safety/>

Guide to Project Safety Analysis (PSA)

VII) Standard Operating Procedures (SOP) for each Planned Procedure

Safe Work Practices (SWP) Identified:	Y
Safe Work Practices Standardized & Documented:	Y
Affected Personnel Trained on SOP's & SWP's:	Y

(Refer to training recordkeeping requirements)

VIII) Ultimate Disposal Plan

{A detailed plan is required for the ultimate disposal of unused equipment, materials, chemicals and wastes following project conclusion; includes the plan for clean up and decontamination of instrumentation, equipment & facilities.}

The instrumentation used during the experimental activity will be uninstalled and moved in other laboratories for other activities. The structure will be de-assembled and can be re-used for other experiments. Non-reusable parts will be wasted using the procedures required for specific materials such as metal and plastic. The facility has no materials that require special treatments, clean up or decontamination.

IX) List & attach all necessary Emergency Planning
Refer to the Emergency Plan of the Laboratory.

Emergency Response Plan
Building Emergency Evacuation Plan
Emergency Contact Information (EC)
{Must be posted on entry door(s)}
Spill Control Plan
Decontamination & Clean Up Plan
Other...

X) Internal Safety Reviews *{self-inspections to be conducted by project personnel}*
The experimental facility will be subject to the standard safety audit and review (if available) of the laboratory.

Procedure for Periodic Internal Safety Audit & Review: N

Schedule for Internal Safety Review: N

List all mechanism(s) to ensure compliance, abatement & accountability: N

Guide to Project Safety Analysis (PSA)

- XI) **Safety Agreements** *{Signatures are required to document the commitment of each participant in maintaining the safe, healthful, and secure project environment}*

Signed By: _____

Location of Files:

During Period of Performance: 102C (USB)
After Project End: Nuclear Engineering Dep.
(current Location: 253 Bizzell Hall West)

Principal Investigator

Researcher/Lab Technician

Graduate Student

Student Worker

Other...

- XII) **Attachment Section** *{List all Attachments to this document, including: }*

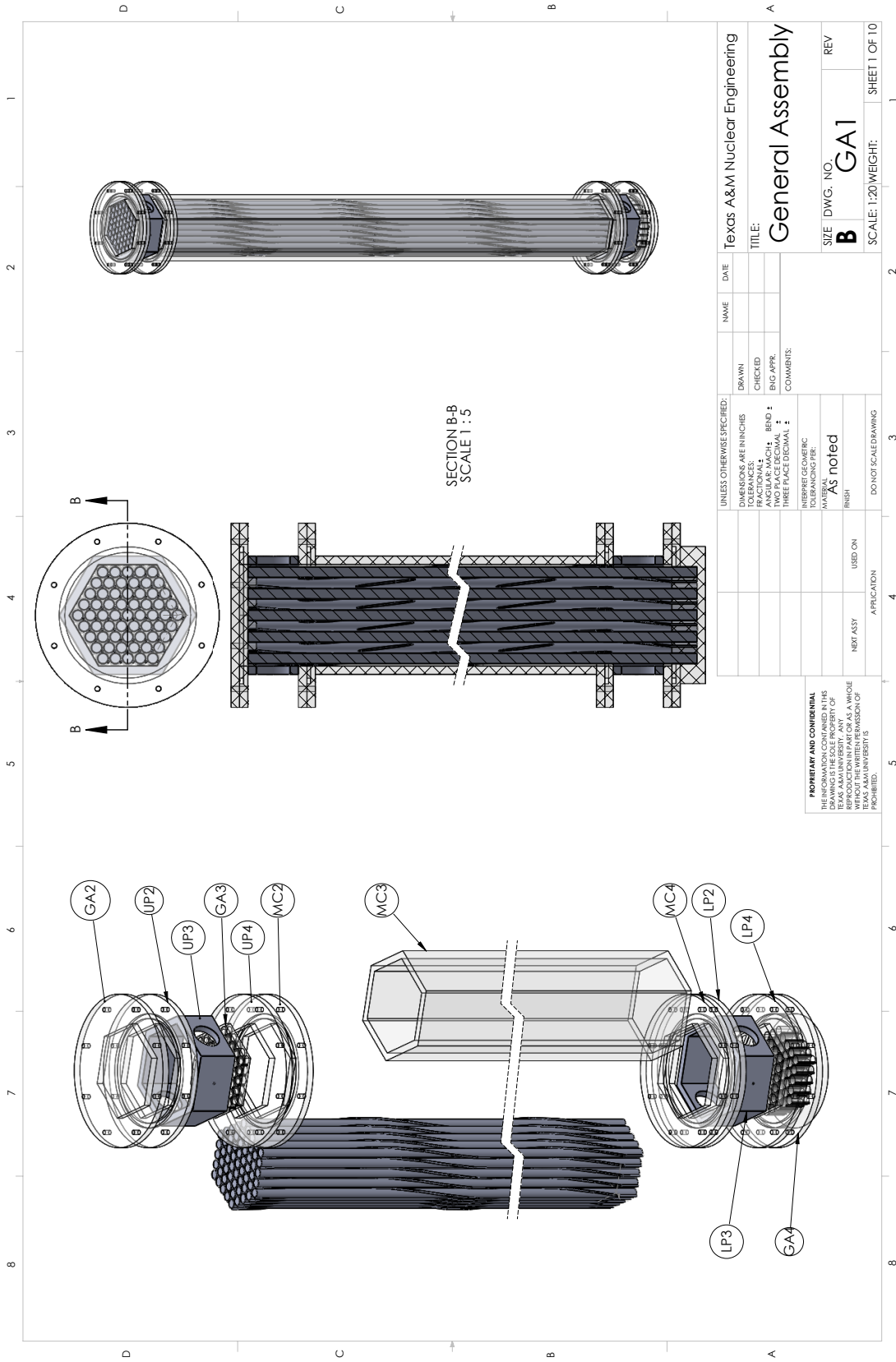
Refer to the Safety documents of the Laboratory.

Hazard Analysis Plan (HAP)
Risk Assessment(s)
Maps
Floor Plan Drawings
Standard Operating Procedures
Training Plans
Chemical Inventory
Supplemental Information
Other...

APPENDIX D

TEST SECTION DRAWINGS

This appendix includes the engineering drawings developed in SolidWorks. These drawings, and their respective 3D CAD part files, were sent to Moore Fabrication, the primary PMMA fabricator.

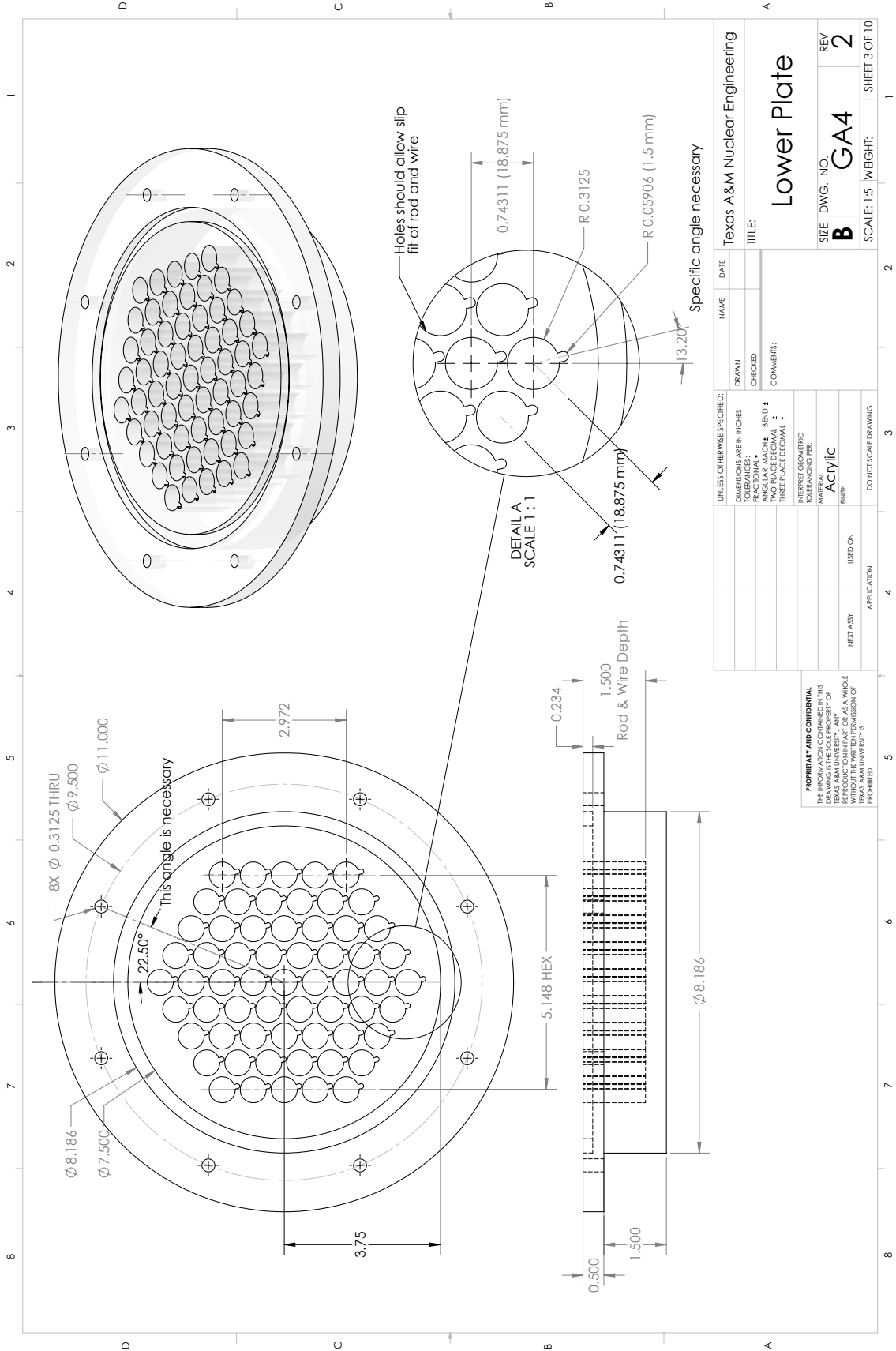


SECTION B-B
SCALE 1:5

UNLESS OTHERWISE SPECIFIED:		DATE	NAME	DATE	NAME	DATE	NAME
DIMENSIONS ARE IN INCHES							
TOLERANCES:							
FRACTIONAL ± .001							
DECIMAL ± .001							
TWO PLACE DECIMAL ± .005							
THREE PLACE DECIMAL ± .001							
INTERPRET GEOMETRIC TOLERANCING PER:							
MATERIALS:							
FINISH:							
NEXT ASST							
USED ON							
APPLICATION							
DO NOT SCALE DRAWING							

TITLE: **General Assembly**
 SIZE DWG. NO. **B GA1** REV
 SCALE: 1:20 WEIGHT: SHEET 1 OF 10

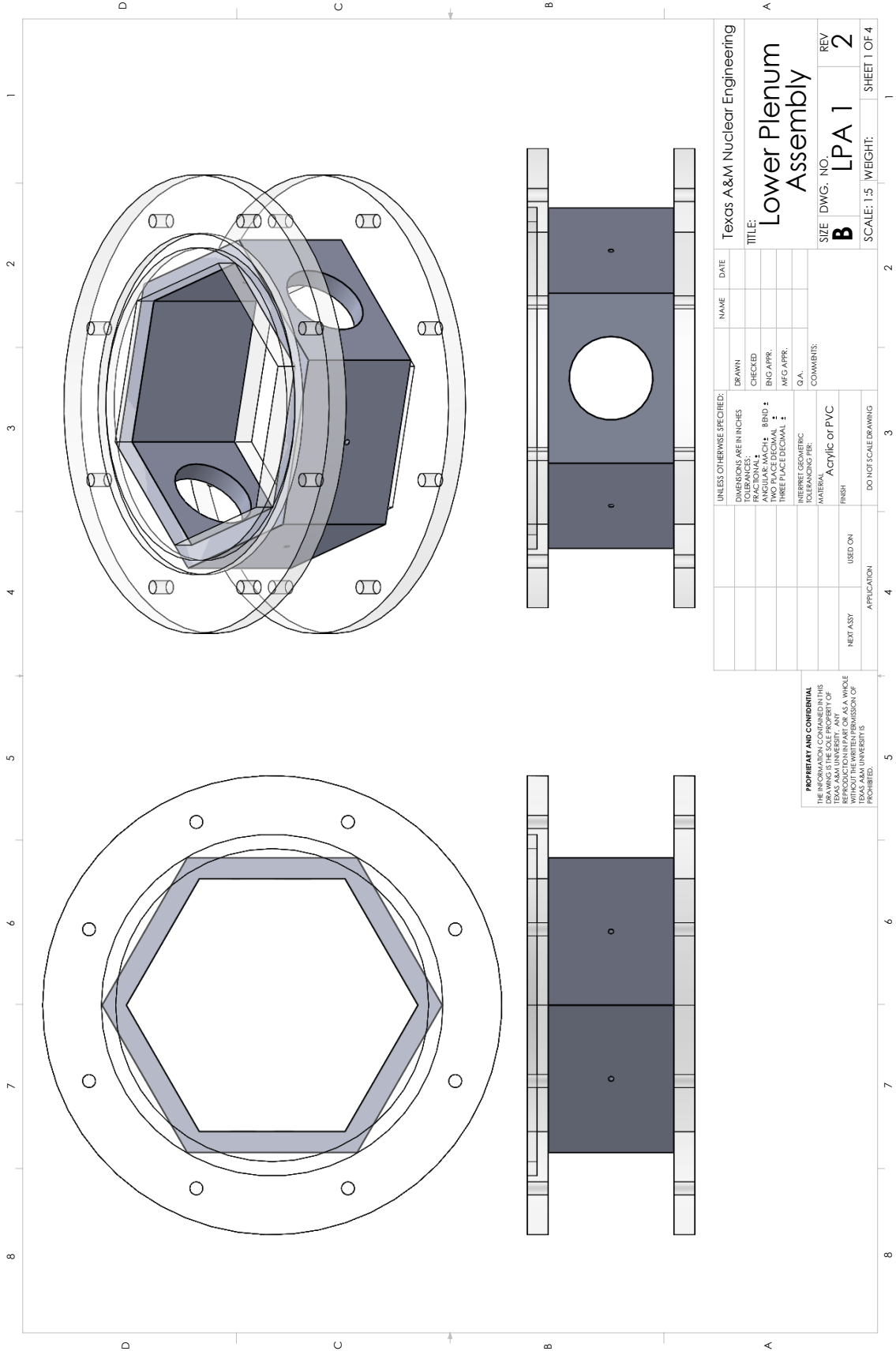
PROPRIETARY AND CONFIDENTIAL
 THIS DRAWING IS THE PROPERTY OF TEXAS A&M UNIVERSITY. ANY REPRODUCTION OR TRANSMISSION OF THIS DRAWING WITHOUT THE WRITTEN PERMISSION OF TEXAS A&M UNIVERSITY IS PROHIBITED.



UNLESS OTHERWISE SPECIFIED:		NAME	DATE
DIMENSIONS ARE IN INCHES		DRAWN	
TOLERANCES:		CHECKED	
FRACTIONS: 1/16, 1/8, 3/16, 1/4		COMMENTS:	
ANGULAR: MACH: 1/4; BIND:			
TWO PLACE DECIMAL:			
THREE PLACE DECIMAL:			
INTERPRET GEOMETRIC TOLERANCING PER:			
MATERIAL:			
FINISH:			
NEXT ASSY:			
USED ON:			
APPLICATION:			
DO NOT SCALE DRAWING			

PROPRIETARY AND CONFIDENTIAL
 THIS DRAWING IS THE PROPERTY OF TEXAS A&M UNIVERSITY. ANY REPRODUCTION OR USE OF THIS DRAWING WITHOUT THE PERMISSION OF TEXAS A&M UNIVERSITY IS PROHIBITED.

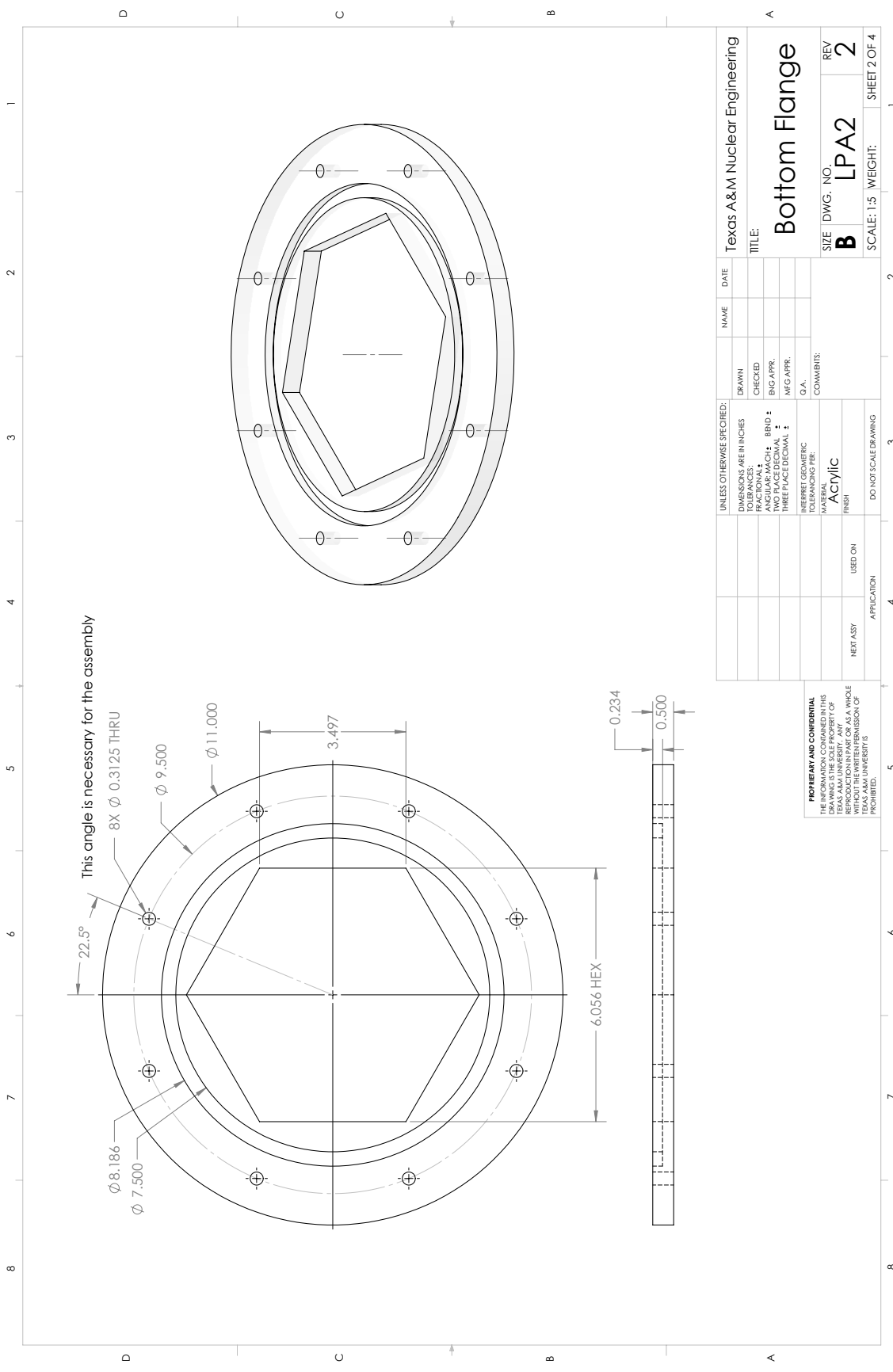
Texas A&M Nuclear Engineering
 TITLE: Lower Plate
 SIZE DWG. NO. GA4 REV 2
 SCALE: 1:5 WEIGHT: SHEET 3 OF 10



Texas A&M Nuclear Engineering
Lower Plenum Assembly
 TITLE: **LPA 1** REV **2**
 SIZE DWG. NO. **B** SCALE: 1:5 WEIGHT: SHEET 1 OF 4

UNLESS OTHERWISE SPECIFIED:	NAME	DATE
DIMENSIONS ARE IN INCHES		
TOLERANCES:	DRAWN	
ANGULAR: MACH: BOND:	CHECKED	
TWO PLACE DECIMAL:	BIG APPR.	
THREE PLACE DECIMAL:	MFG APPR.	
	G.A.	
INTERPRET GEOMETRIC TOLERANCING PER:	COMMENTS:	
MATERIAL: Acrylic or PVC		
FINISH:		
USED ON:		
NEXT ASSY:		
DO NOT SCALE DRAWING		

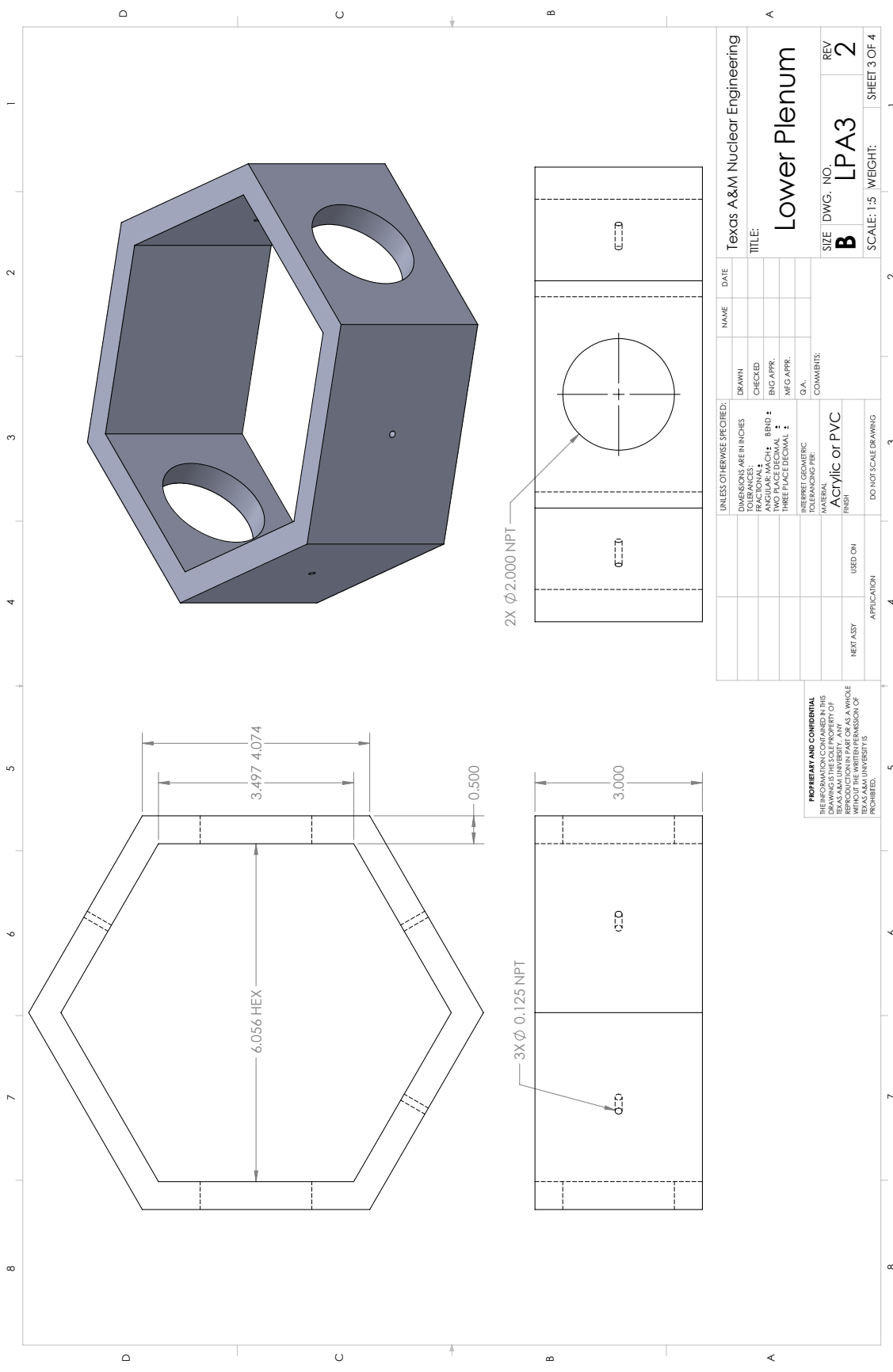
PROPRIETARY AND CONFIDENTIAL
 THIS DRAWING AND THE INFORMATION CONTAINED HEREIN ARE THE SOLE PROPERTY OF TEXAS A&M UNIVERSITY. ANY REPRODUCTION OR TRANSMISSION OF THIS DRAWING OR THE INFORMATION CONTAINED HEREIN WITHOUT THE WRITTEN PERMISSION OF TEXAS A&M UNIVERSITY IS PROHIBITED.



This angle is necessary for the assembly

UNLESS OTHERWISE SPECIFIED: DIMENSIONS ARE IN INCHES TOLERANCES: FRACTIONS DECIMALS ANGULAR MACH: BOND TWO PLACE DECIMAL THREE PLACE DECIMAL G.A. INTERPRET GEOMETRIC TOLERANCING PER: MATERIAL FINISH		NAME	DATE	TEXAS A&M Nuclear Engineering	
DO NOT SCALE DRAWING	APPLICATION	USED ON	COMMENTS:	SCALE: 1:5	WEIGHT:
NEXT ASSY				SIZE DWG. NO.	REV
				B LPA2	2
				TITLE: Bottom Flange	
				SHEET 2 OF 4	

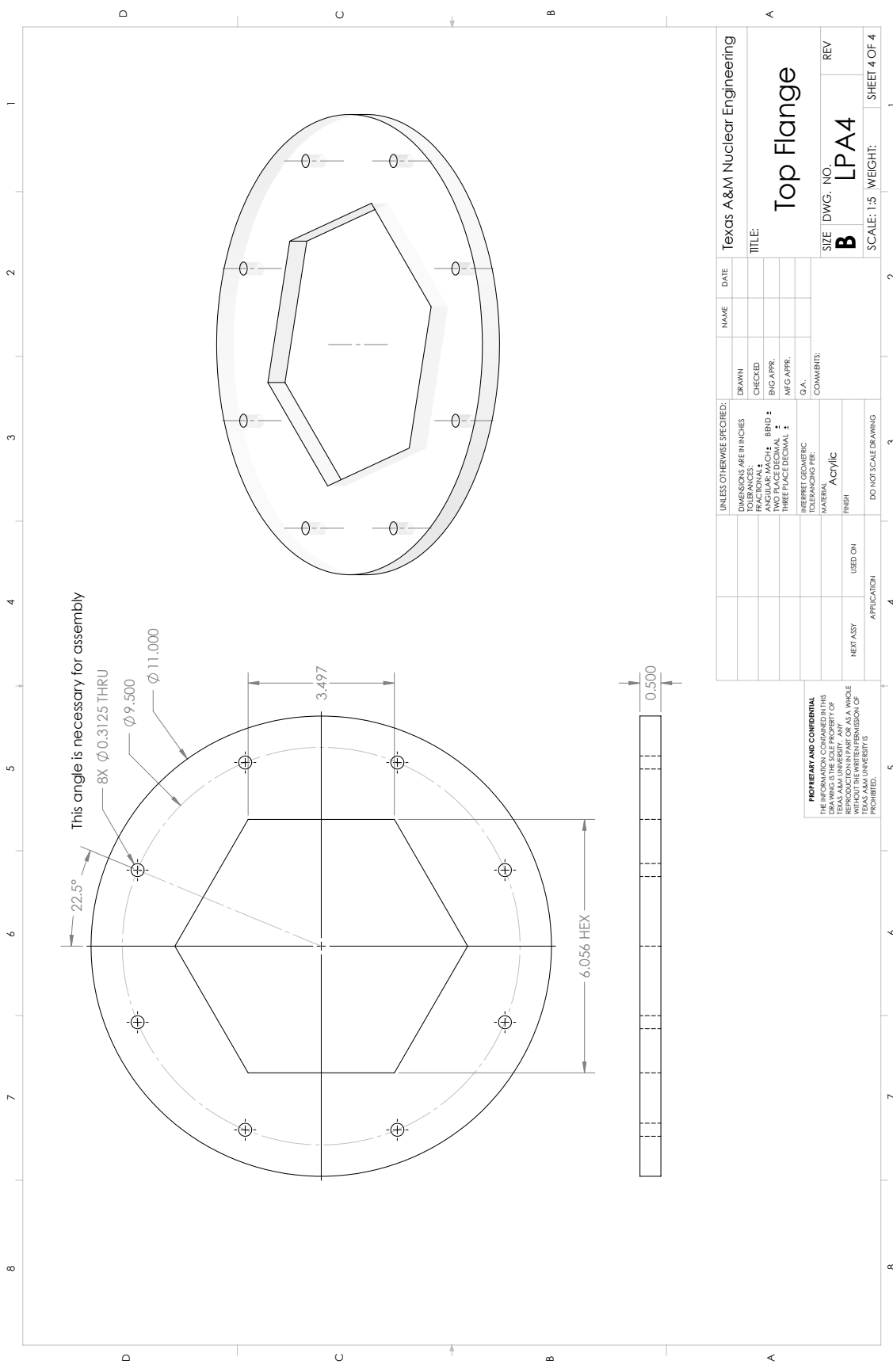
PROPRIETARY AND CONFIDENTIAL
THIS DRAWING CONTAINS
INFORMATION WHICH IS THE
PROPERTY OF
TEXAS A&M UNIVERSITY. ANY
REPRODUCTION OR DISSEMINATION
WITHOUT THE WRITTEN PERMISSION OF
TEXAS A&M UNIVERSITY IS
PROHIBITED.



UNLESS OTHERWISE SPECIFIED:		NAME	DATE
DIMENSIONS ARE IN INCHES			
TOLERANCES:			
FRACTIONS			
DECIMALS			
ANGULAR			
HOLE			
TWO PLACE DECIMAL			
THREE PLACE DECIMAL			
INTERPRET GEOMETRIC TOLERANCING PER:			
MATERIAL			
FINISH			
COMMENTS:			
ACRYLIC or PVC			
NEXT ASSY			
USED ON			
APPLICATION			
DO NOT SCALE DRAWING			

TITLE: Texas A&M Nuclear Engineering
Lower Plenum
 SIZE DWG. NO. REV
B LPA3 2
 SCALE: 1:5 WEIGHT: SHEET 3 OF 4

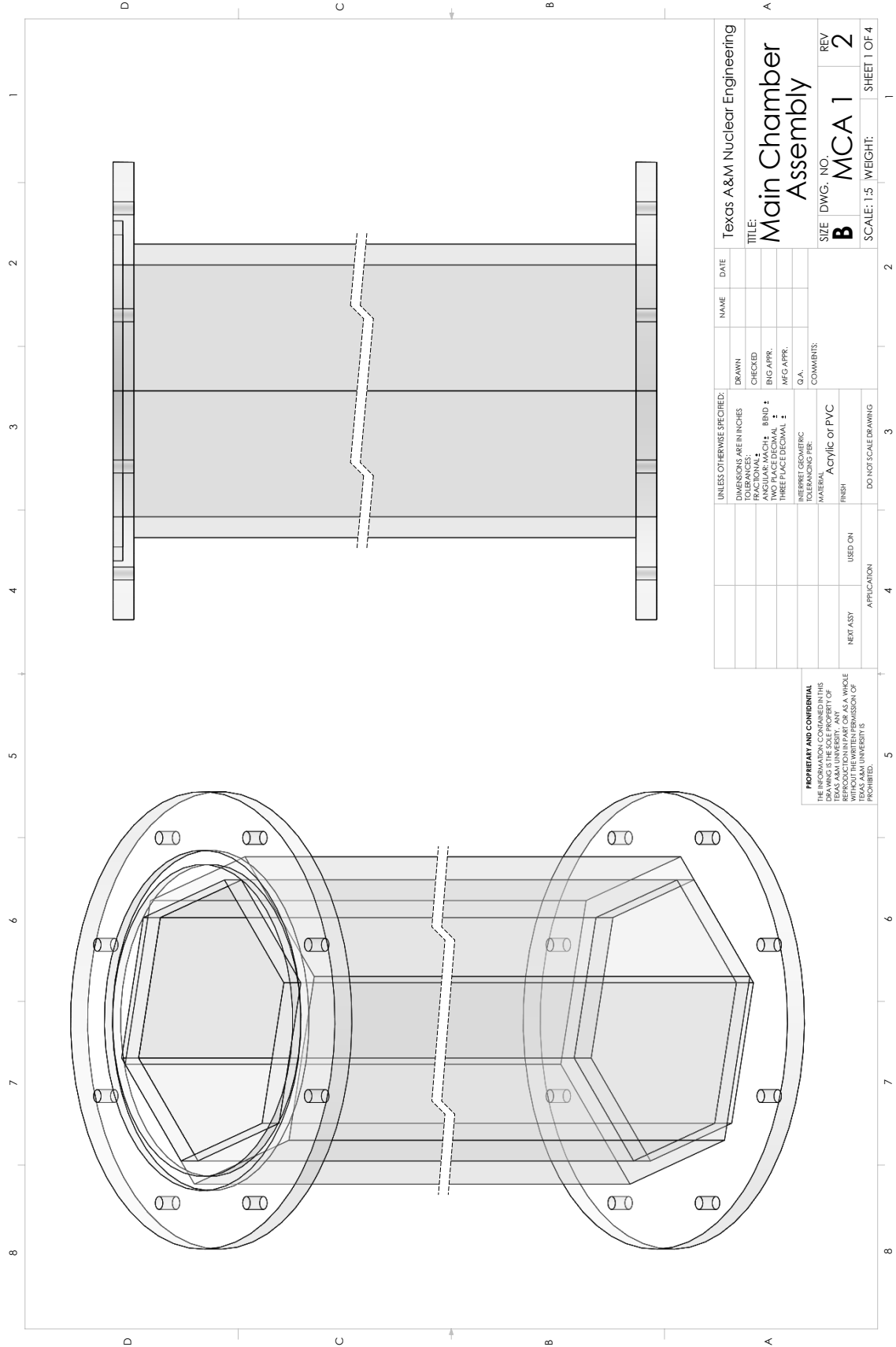
PROPRIETARY AND CONFIDENTIAL
 THIS DRAWING IS THE SOLE PROPERTY OF
 TEXAS A&M UNIVERSITY. ANY REPRODUCTION
 OR TRANSMISSION OF THIS DRAWING OR
 WITHOUT THE WRITTEN PERMISSION OF
 TEXAS A&M UNIVERSITY IS
 PROHIBITED.



This angle is necessary for assembly

UNLESS OTHERWISE SPECIFIED:		DRAWN	NAME	DATE	Texas A&M Nuclear Engineering	
DIMENSIONS ARE IN INCHES		CHECKED			TITLE:	
TOLERANCES:		BIG APPR.			Top Flange	
ANGULAR: MACH: BOND:		MFG APPR.			SIZE	DWG. NO.
TWO PLACE DECIMAL		G.A.			B	LPA4
THREE PLACE DECIMAL		COMMENTS:			SCALE: 1:5	WEIGHT:
TOLERANCING PER:					SHEET 4 OF 4	REV
INTERPRET GEOMETRIC						
TOLERANCING PER:						
MATERIAL:						
Acrylic						
FINISH:						
NEXT ASSY		USED ON	APPLICATION	DO NOT SCALE DRAWING		

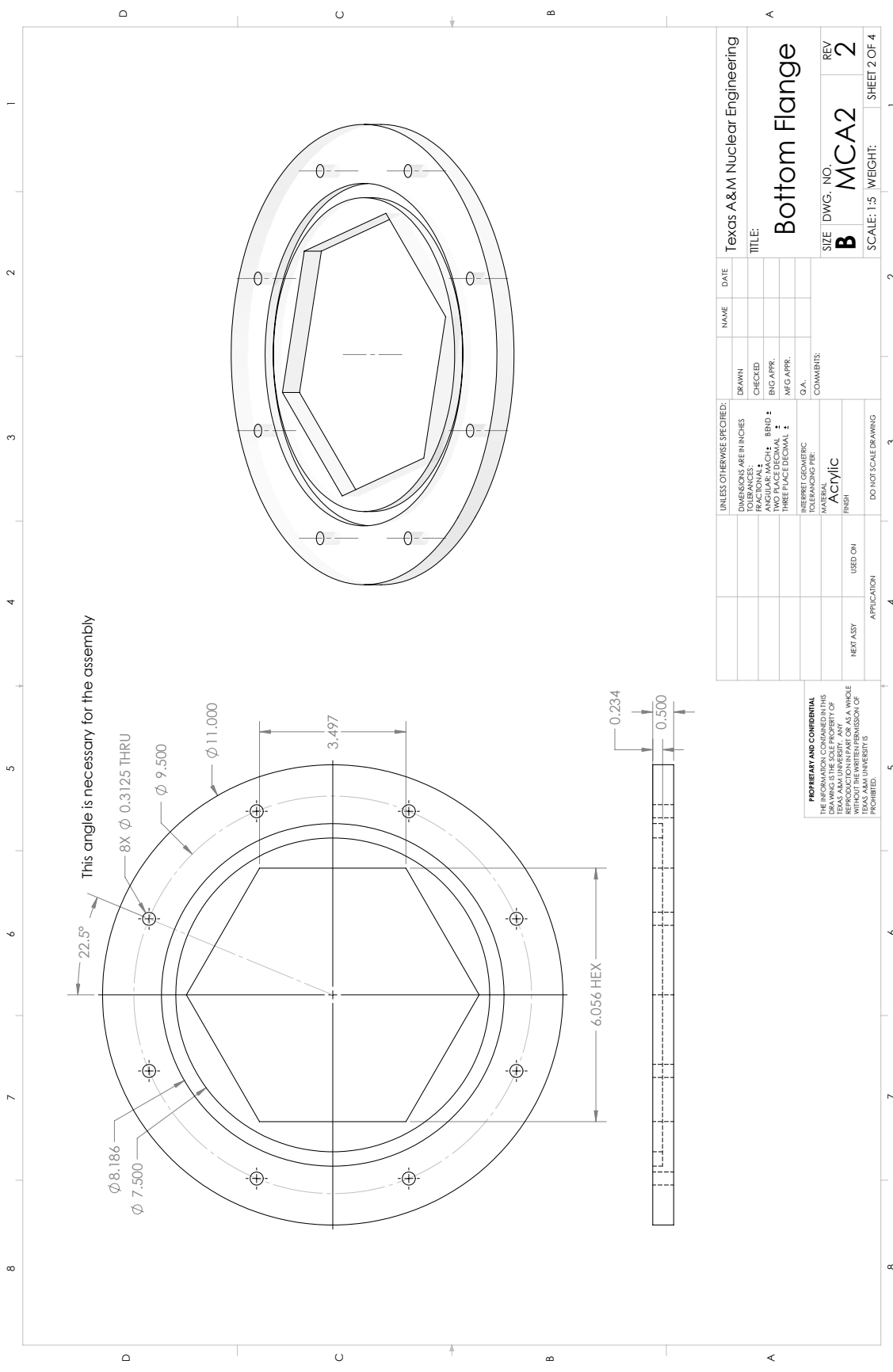
PROPRIETARY AND CONFIDENTIAL
 THIS DRAWING IS THE PROPERTY OF
 TEXAS A&M UNIVERSITY. ANY
 REPRODUCTION OR DISTRIBUTION
 WITHOUT THE WRITTEN PERMISSION OF
 TEXAS A&M UNIVERSITY IS
 PROHIBITED.



Texas A&M Nuclear Engineering
Title: Main Chamber Assembly
Size: DWG. NO. MCA 1 REV 2
Scale: 1:5 WEIGHT: SHEET 1 OF 4

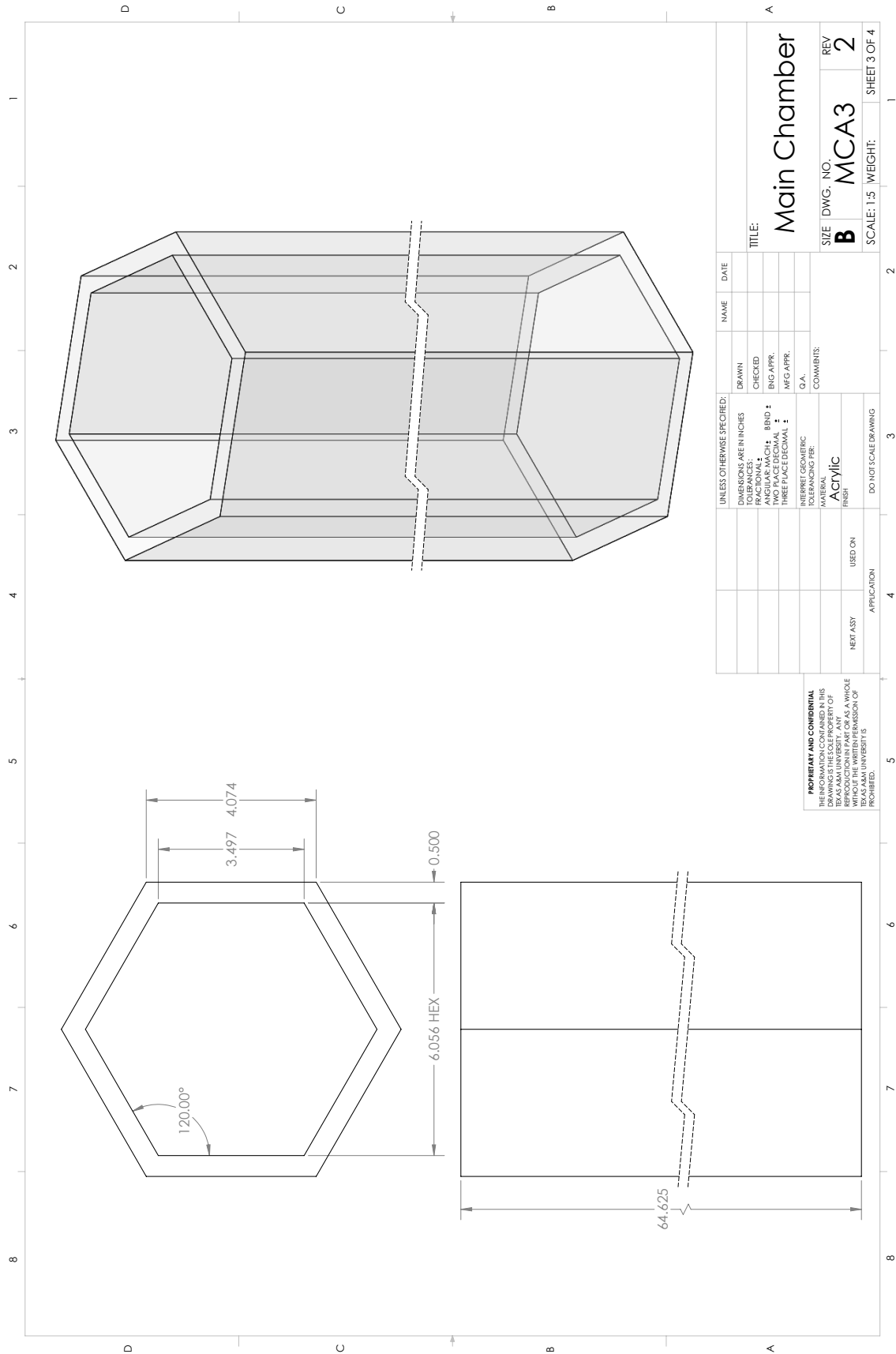
NAME	DATE	UNLESS OTHERWISE SPECIFIED:	DO NOT SCALE DRAWING
DRAWN		DIMENSIONS ARE IN INCHES	
CHECKED		TOLERANCES:	
BIG APPR.		ANGULAR: MACH: BOND:	
MFG APPR.		TWO PLACE DECIMAL:	
G.A.		THREE PLACE DECIMAL:	
COMMENTS:		INTERPRET GEOMETRIC TOLERANCING PER:	
		MATERIAL: Acrylic or PVC	
		FINISH:	
		USED ON:	
		NEXT ASSY:	

PROPRIETARY AND CONFIDENTIAL
 THIS DRAWING AND THE INFORMATION CONTAINED HEREIN ARE THE SOLE PROPERTY OF TEXAS A&M UNIVERSITY. ANY REPRODUCTION OR TRANSMISSION OF THIS DRAWING OR INFORMATION WITHOUT THE WRITTEN PERMISSION OF TEXAS A&M UNIVERSITY IS PROHIBITED.



UNLESS OTHERWISE SPECIFIED: DIMENSIONS ARE IN INCHES TOLERANCES: FRACTIONS DECIMALS ANGULAR MFG APPR. G.A.		NAME	DATE
DRAWN			
CHECKED			
ENG APPR.			
MFG APPR.			
G.A.			
COMMENTS:			
MATERIAL Acrylic			
FINISH			
DO NOT SCALE DRAWING			
APPLICATION	USED ON		
NEXT ASSY			

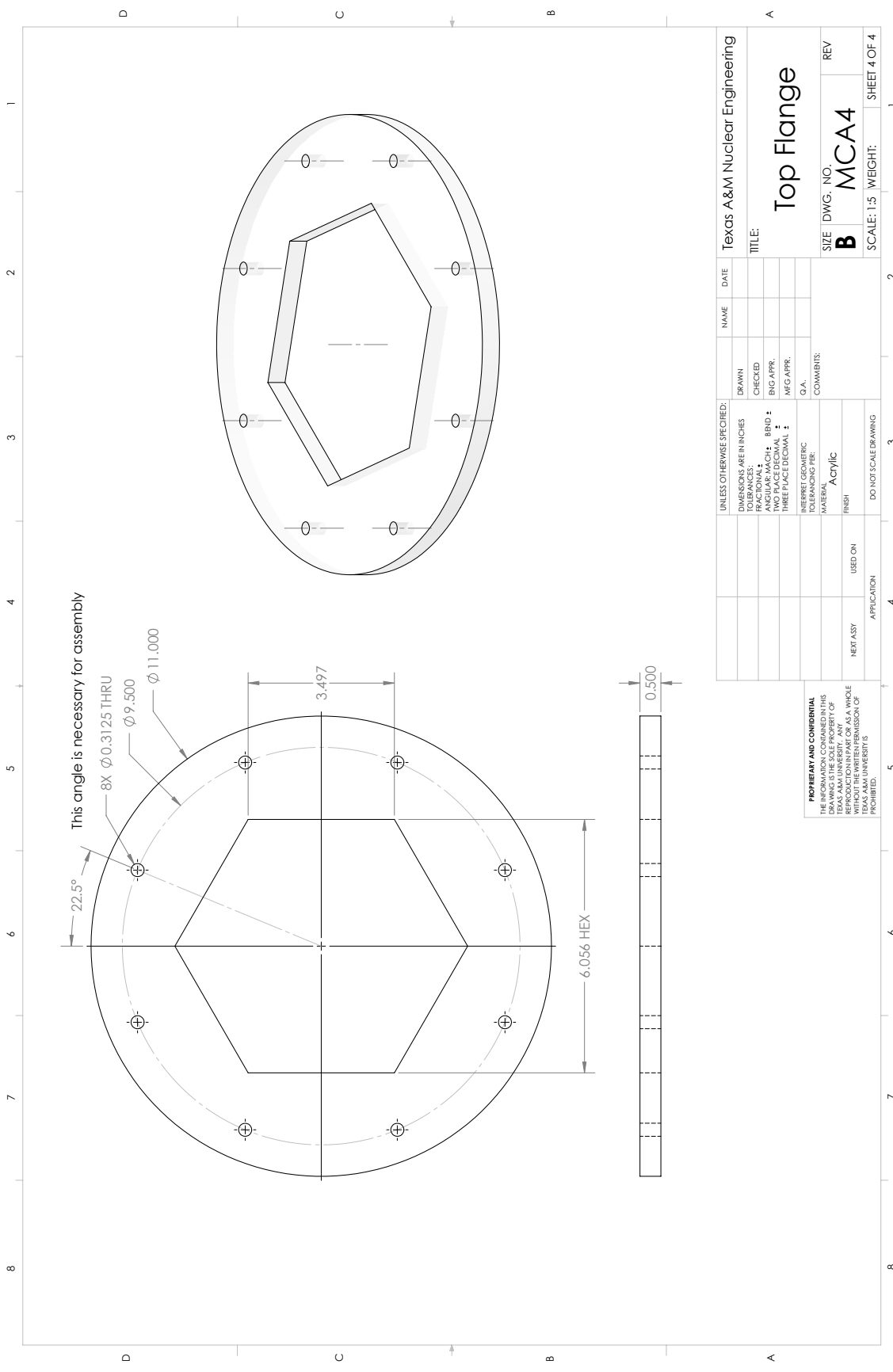
<p>PROPRIETARY AND CONFIDENTIAL THIS DRAWING CONTAINS THE PROPRIETARY AND CONFIDENTIAL INFORMATION OF TEXAS A&M UNIVERSITY. ANY REPRODUCTION OR DISSEMINATION OF THIS DRAWING WITHOUT THE WRITTEN PERMISSION OF TEXAS A&M UNIVERSITY IS PROHIBITED.</p>	
TEXAS A&M Nuclear Engineering	TITLE:
Bottom Flange	
SIZE DWG. NO. B MCA2	REV 2
SCALE: 1:5	WEIGHT:
SHEET 2 OF 4	



UNLESS OTHERWISE SPECIFIED:	DRAWN	CHECKED	NAME	DATE
DIMENSIONS ARE IN INCHES				
TOLERANCES:				
ANGULAR: MACH: BOND:				
TWO PLACE DECIMAL				
THREE PLACE DECIMAL				
MFG APPR:				
G.A.:				
COMMENTS:				
INTERPRET GEOMETRIC TOLERANCING PER:				
MATERIAL:				
FINISH:				
DO NOT SCALE DRAWING				
APPLICATION				
USED ON				
NEXT ASSY				

PROPRIETARY AND CONFIDENTIAL
 THIS DRAWING IS THE SOLE PROPERTY OF
 TEXAS A&M UNIVERSITY. ANY REPRODUCTION
 OR TRANSMISSION OF THIS DRAWING OR
 WITHOUT THE WRITTEN PERMISSION OF
 TEXAS A&M UNIVERSITY IS
 PROHIBITED.

TITLE:		Main Chamber	
SIZE	DWG. NO.	REV	
B	MCA3	2	
SCALE: 1:5		WEIGHT:	
		SHEET 3 OF 4	



This angle is necessary for assembly

8X $\phi 0.3125$ THRU

$\phi 9.500$

$\phi 11.000$

3.497

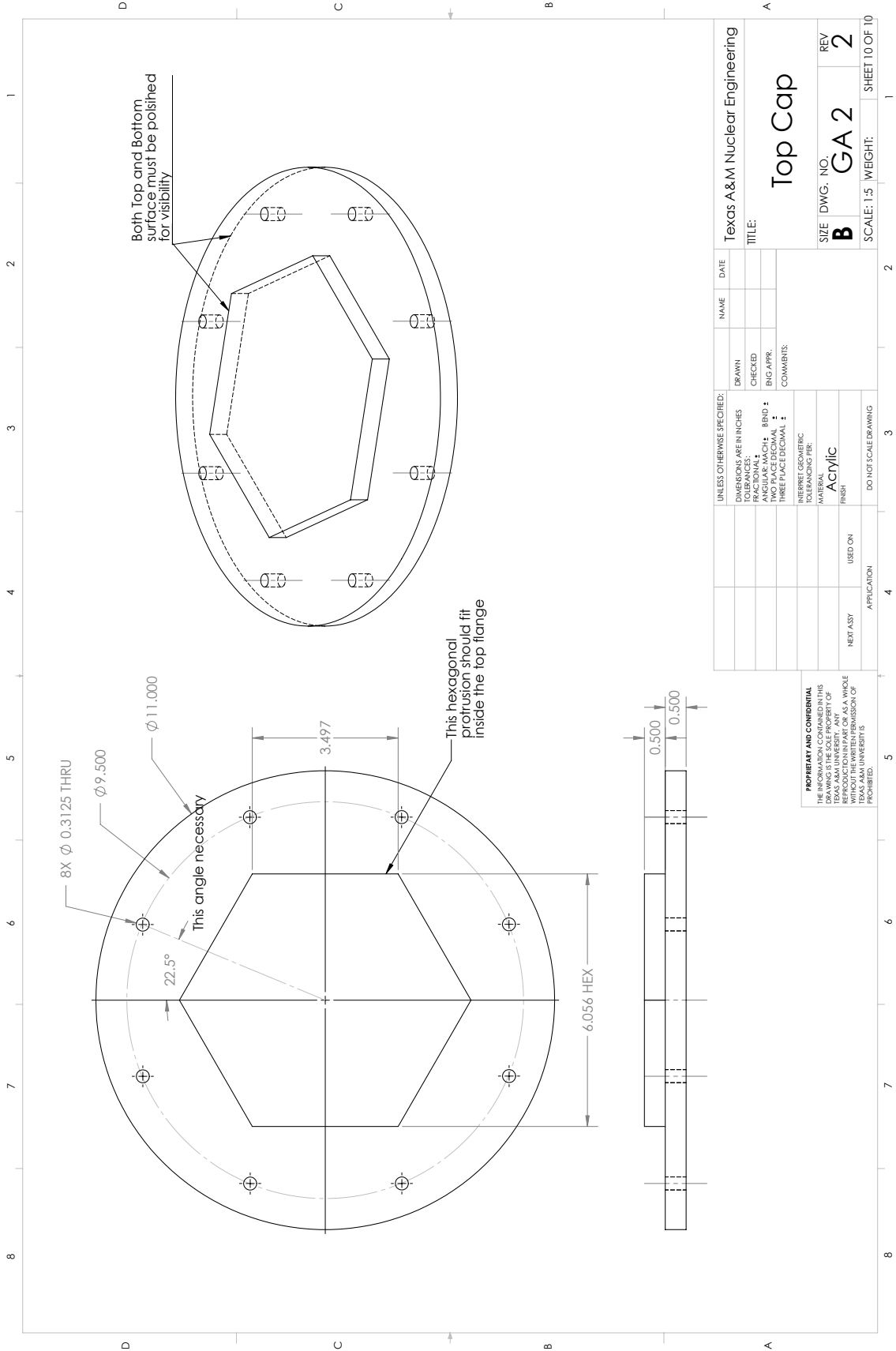
6.056 HEX

0.500

22.5°

UNLESS OTHERWISE SPECIFIED: DIMENSIONS ARE IN INCHES		DRAWN	NAME	DATE	Texas A&M Nuclear Engineering	
TOLERANCES:		CHECKED			TITLE:	
ANGULAR	MACH	BIG APPR.			Top Flange	
TWO PLACE DECIMAL	BIND	MFG APPR.			SIZE DWG. NO.	REV
THREE PLACE DECIMAL		Q.A.			B	MCA4
TOLERANCING PER:		COMMENTS:		SCALE: 1:5 WEIGHT: SHEET 4 OF 4		
INTERPRET GEOMETRIC		MATERIAL		DO NOT SCALE DRAWING		
TOLERANCING PER:		Acrylic		FINISH		
NEXT ASSY		USED ON		APPLICATION		
NEXT ASSY		USED ON		APPLICATION		

PROPRIETARY AND CONFIDENTIAL
THIS DRAWING CONTAINS INFORMATION
THE SOLE PROPERTY OF
TEXAS A&M UNIVERSITY. ANY
REPRODUCTION OR DISSEMINATION
WITHOUT THE WRITTEN PERMISSION OF
TEXAS A&M UNIVERSITY IS
PROHIBITED.



UNLESS OTHERWISE SPECIFIED:		NAME	DATE
DIMENSIONS ARE IN INCHES			
TOLERANCES:		DRAWN	
FRACTIONS: 1/16		CHECKED	
DECIMALS: 0.0005		BIG APPR.	
ANGULAR: MACH: 0.001		COMMENTS:	
TWO PLACE DECIMAL			
THREE PLACE DECIMAL			
INTERPRET GEOMETRIC TOLERANCING PER:			
MATERIAL:			
Acrylic			
FINISH:			
NEXT ASSY		USED ON	
APPLICATION		DO NOT SCALE DRAWING	

Texas A&M Nuclear Engineering

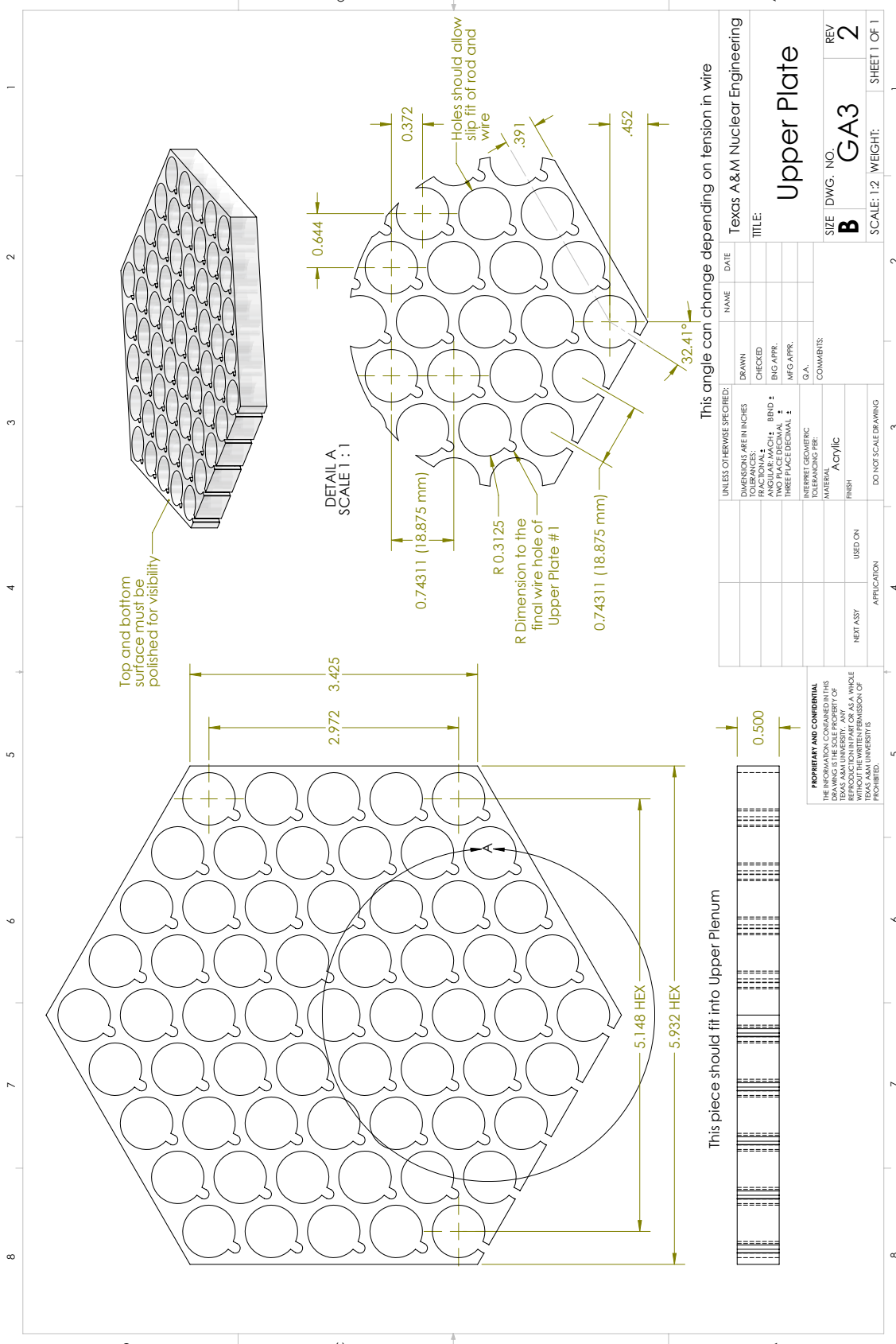
TITLE: **Top Cap**

SIZE DWG. NO. REV

B **GA 2** **2**

SCALE: 1:5 WEIGHT: SHEET 10 OF 10

PROPRIETARY AND CONFIDENTIAL
 THIS WORK IS THE SOLE PROPERTY OF
 TEXAS A&M UNIVERSITY. ANY
 REPRODUCTION OR TRANSMISSION
 WITHOUT THE WRITTEN PERMISSION OF
 TEXAS A&M UNIVERSITY IS
 PROHIBITED.



Top and bottom surface must be polished for visibility

DETAIL A
SCALE 1 : 1

Holes should allow slip fit of rod and wire

This angle can change depending on tension in wire

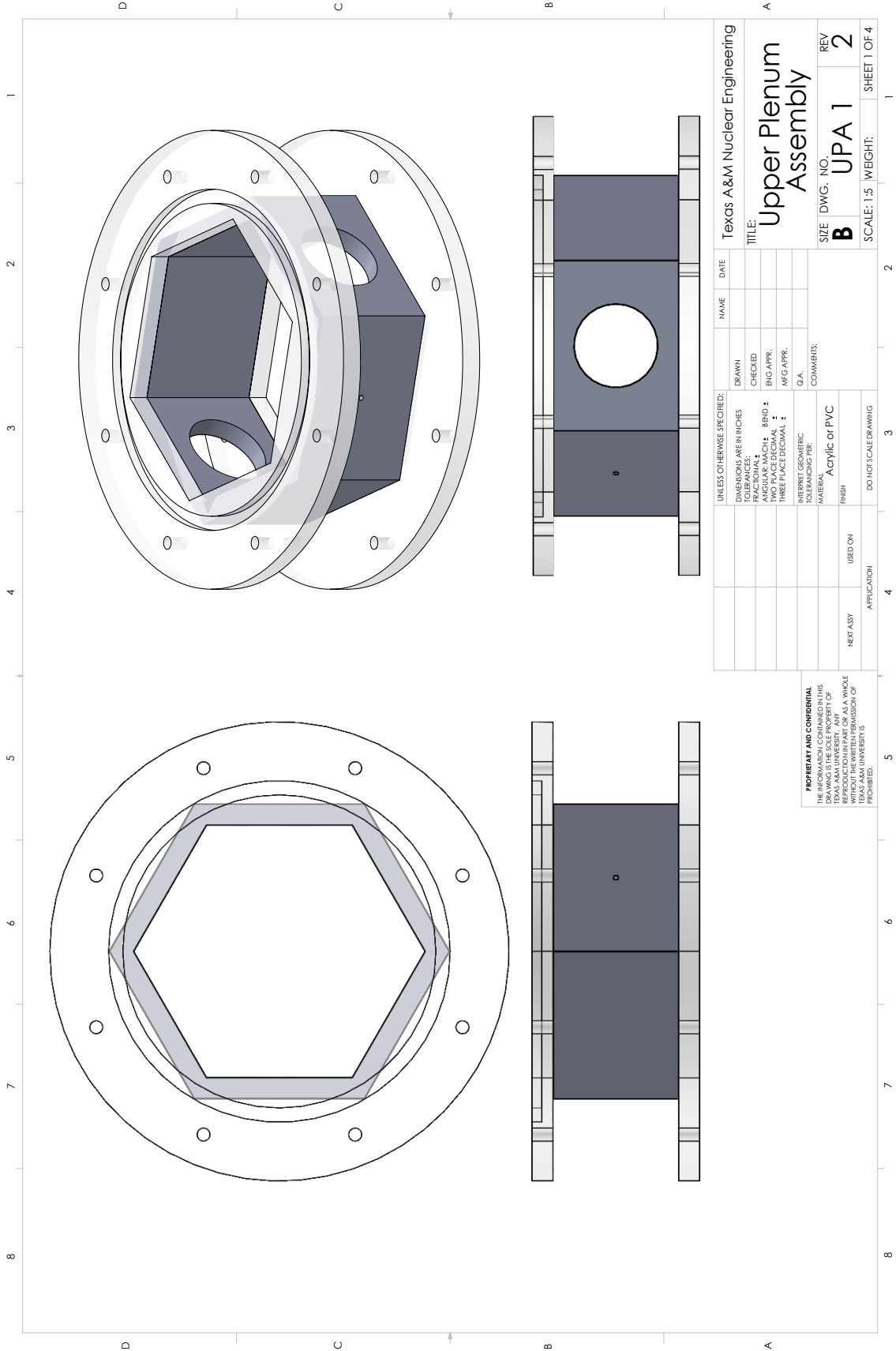
This piece should fit into Upper Plenum

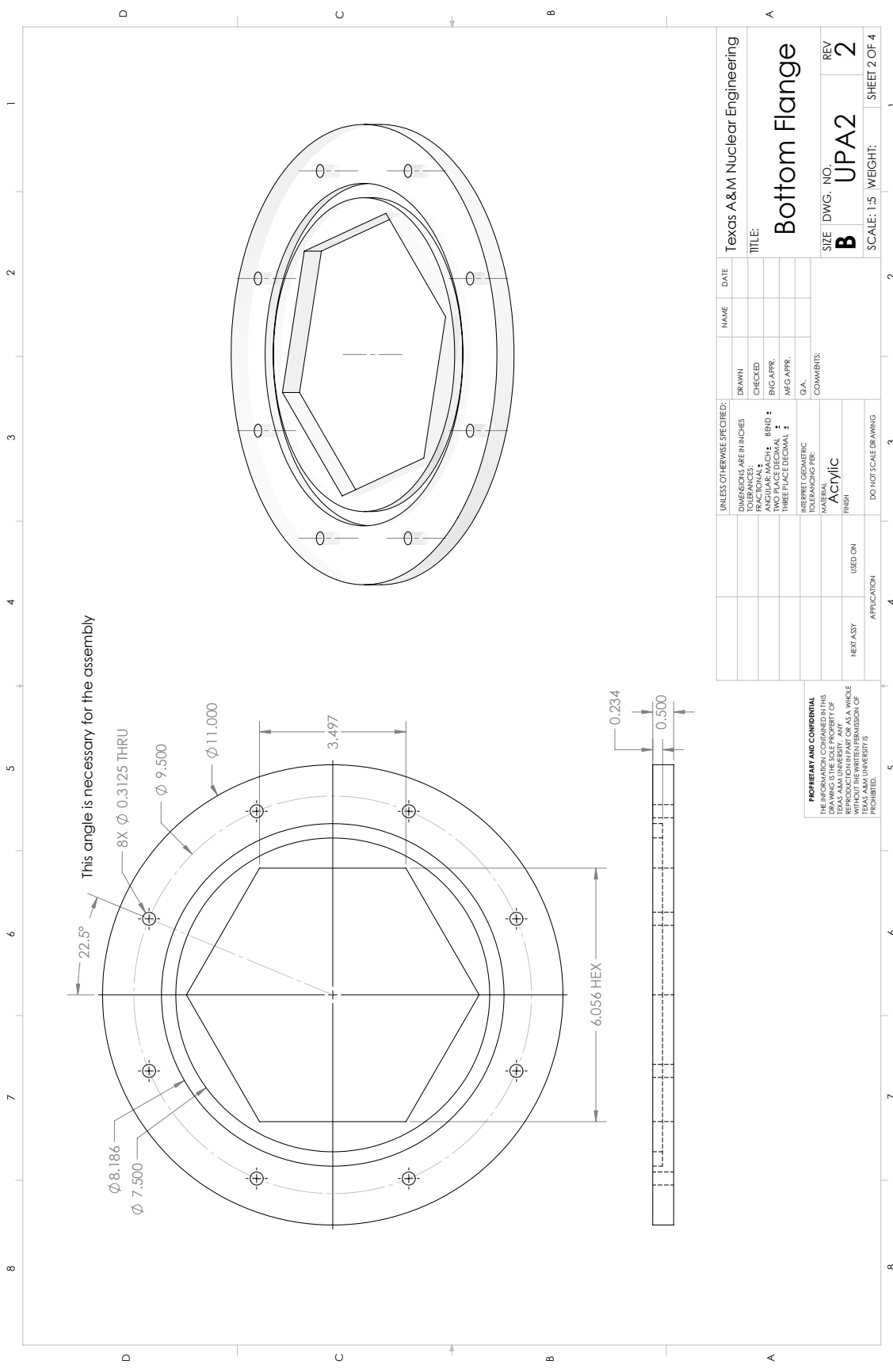


UNLESS OTHERWISE SPECIFIED:		NAME	DATE
DIMENSIONS ARE IN INCHES			
TOLERANCES:			
ANGULAR	MACH: ± .001		
THREE PLACE DECIMAL	BOND: ± .001		
TWO PLACE DECIMAL			
MFG APPR.			
G.A.			
INTERPRET GEOMETRIC TOLERANCING PER:			
MATERIAL		Acrylic	
FINISH			
NEXT ASSY			
USED ON			
APPLICATION			
DO NOT SCALE DRAWING			

Texas A&M Nuclear Engineering
 TITLE: Upper Plate
 SIZE DWG. NO. GA3 REV 2
 SCALE: 12 WEIGHT: SHEET 1 OF 1

PROPRIETARY AND CONFIDENTIAL
 THIS WORK IS THE PROPERTY OF
 TEXAS A&M UNIVERSITY. ANY
 REPRODUCTION OR DISSEMINATION
 WITHOUT THE WRITTEN PERMISSION OF
 TEXAS A&M UNIVERSITY IS
 PROHIBITED.

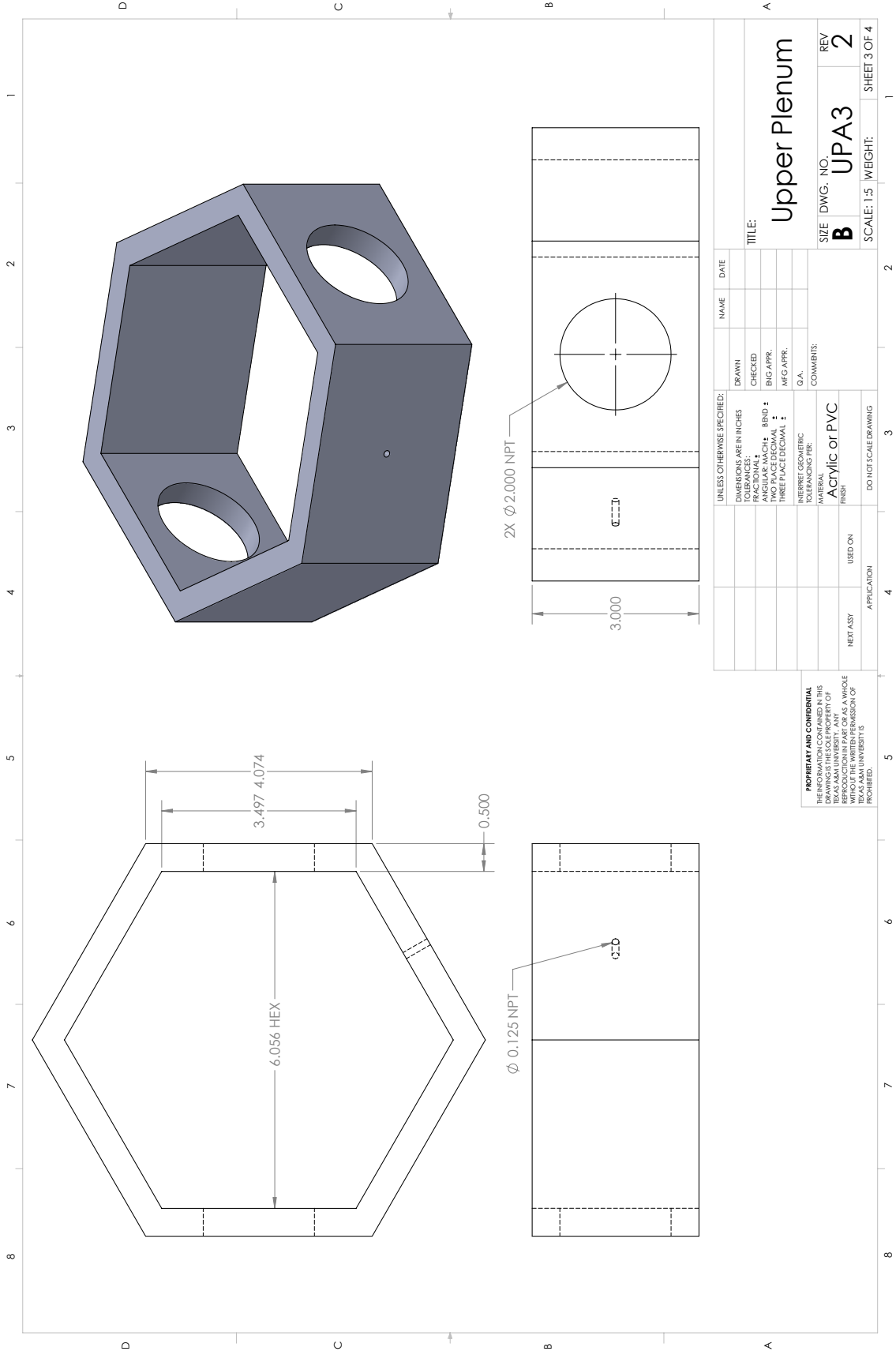




This angle is necessary for the assembly

UNLESS OTHERWISE SPECIFIED: DIMENSIONS ARE IN INCHES TOLERANCES: FRACTIONS DECIMALS ANGULAR MACH: BOND TWO PLACE DECIMAL THREE PLACE DECIMAL G.A.		DRAWN CHECKED ENG. APPR. MFG. APPR. G.A.	NAME DATE	TEXAS A&M Nuclear Engineering	
MATERIAL TOLERANCING PER: ACrylic FINISH		COMMENTS:		TITLE: Bottom Flange	
DO NOT SCALE DRAWING		NEXT ASSY		SIZE DWG. NO. B UPA2	REV 2
APPLICATION		USED ON		SCALE: 1:5 WEIGHT: SHEET 2 OF 4	

PROPRIETARY AND CONFIDENTIAL
THIS DRAWING CONTAINS
INFORMATION WHICH IS THE SOLE PROPERTY OF
TEXAS A&M UNIVERSITY. ANY
REPRODUCTION OR DISSEMINATION OF THIS
DRAWING WITHOUT THE WRITTEN PERMISSION OF
TEXAS A&M UNIVERSITY IS
PROHIBITED.



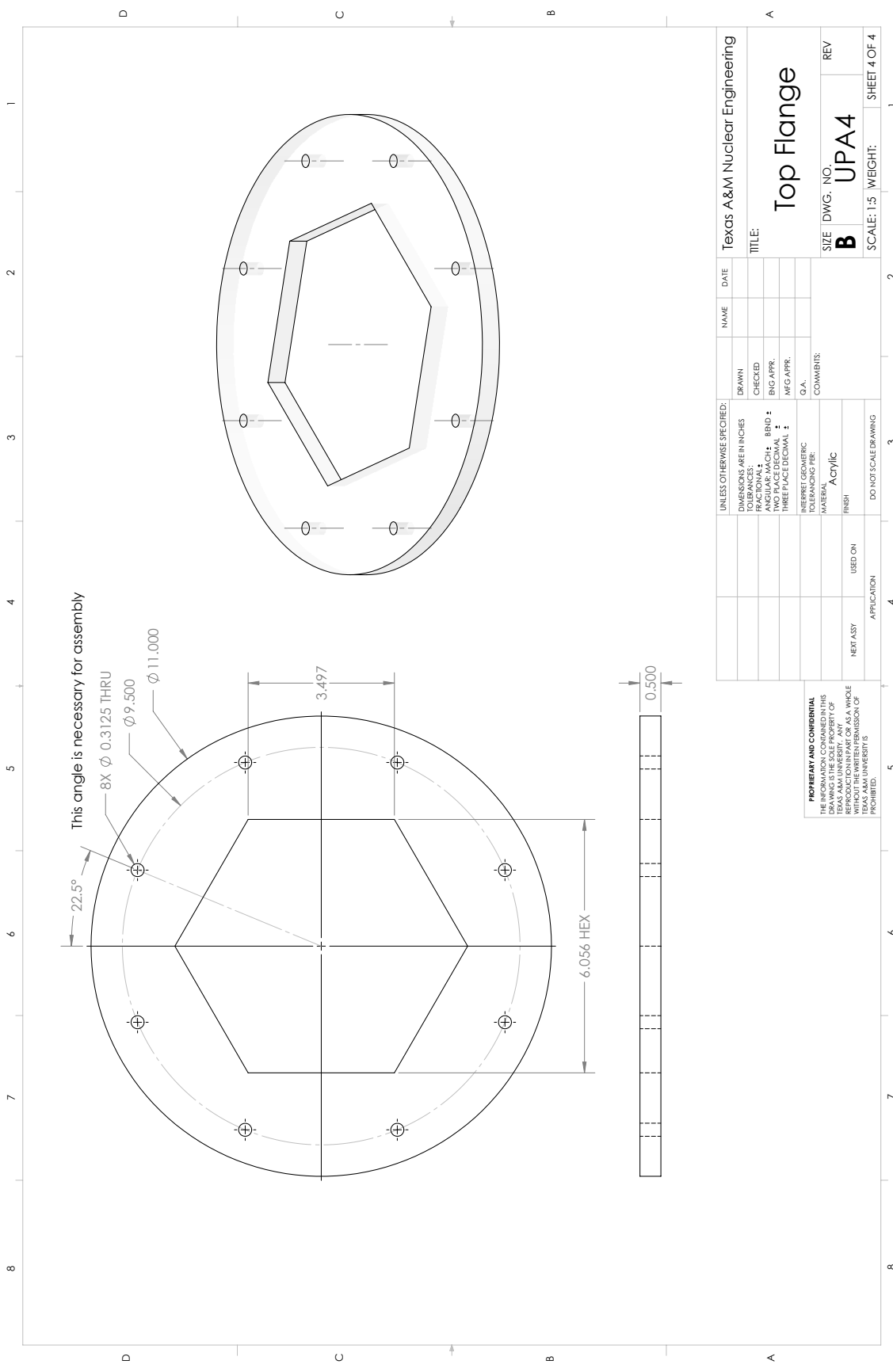
UNLESS OTHERWISE SPECIFIED:		NAME		DATE	
DIMENSIONS ARE IN INCHES	DRAWN				
TOLERANCES:	CHECKED				
ANGULAR: MACH: BOND:	BIG APPR:				
TWO PLACE DECIMAL:	MFG APPR:				
THREE PLACE DECIMAL:	Q.A.				
INTERPRET GEOMETRIC TOLERANCING PER:	COMMENTS:				
MATERIAL:					
FINISH:					
DO NOT SCALE DRAWING					

TITLE: Upper Plenum

SIZE DWG. NO. REV
B UPA3 2

SCALE: 1:5 WEIGHT: SHEET 3 OF 4

PROPRIETARY AND CONFIDENTIAL
 THIS DRAWING IS THE SOLE PROPERTY OF
 TEXAS A&M UNIVERSITY. ANY REPRODUCTION
 OR TRANSMISSION OF THIS DRAWING OR
 WITHOUT THE WRITTEN PERMISSION OF
 TEXAS A&M UNIVERSITY IS
 PROHIBITED.



This angle is necessary for assembly

8X $\phi 0.3125$ THRU

$\phi 9.500$

$\phi 11.000$

3.497

6.056 HEX

0.500

UNLESS OTHERWISE SPECIFIED:		NAME	DATE	Texas A&M Nuclear Engineering	
DIMENSIONS ARE IN INCHES	DRAWN			TITLE:	
TOLERANCES:	CHECKED			Top Flange	
ANGULAR: MACH: BOND:	BIG APPR:			SIZE DWG. NO.	REV
TWO PLACE DECIMAL:	MFG APPR:			B	UPA4
THREE PLACE DECIMAL:	G.A.			SCALE: 1:5	WEIGHT:
TOLERANCING PER:	COMMENTS:			SHEET 4 OF 4	
INTERPRET GEOMETRIC TOLERANCING PER:	MATERIAL:				
	FINISH:				
	ACrylic				
	DO NOT SCALE DRAWING				
	APPLICATION				
	USED ON				
	NEXT ASSY				

PROPRIETARY AND CONFIDENTIAL
 THIS DRAWING IS THE PROPERTY OF
 TEXAS A&M UNIVERSITY. ANY
 REPRODUCTION OR TRANSMISSION OF
 THIS DRAWING WITHOUT THE PERMISSION OF
 TEXAS A&M UNIVERSITY IS
 PROHIBITED.

APPENDIX E

HARDWARE INVENTORY

This appendix includes the set of tables that contain relevant model information for all hardware installed in the experimental facility.




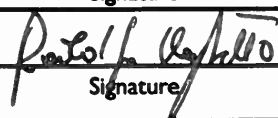
TECHNICAL DOCUMENT COVER PAGE

Document No:	TAMU-WW-INV	Revision: 0	Page 1 of 6
Doc Title: TAMU Wire-Wrapped Hardware Inventory			
Projects No:	DE-NE000832I		
Project Name: Toward a Longer Life Core: Thermal-Hydraulic CFD Simulations and Experimental Investigation of Deformed Fuel Assemblies			
Document Purpose/Summary: This document include the list the hardware used in the test facility. Total Page Count: 6 pages.			



TECHNICAL DOCUMENT COVER PAGE

Document No:	TAMU-WW-INV	Revision: 0	Page 2 of 6
--------------	-------------	-------------	-------------

TAMU Prepared By:	<u>William Headley</u> Printed/Typed Name	<u></u> Signature	<u>04/19/16</u> Date
TAMU Reviewed and Approved By:	<u>Rodolfo Vaghetto</u> Printed/Typed Name	<u></u> Signature	<u>04/19/2016</u> Date


REVISION HISTORY LOG

Page: 3 of 6

Document Number: TAMU-WW-INV Revision: 0

Document Title: TAMU Wire-Wrapped Hardware Inventory

REVISION	DATE	DESCRIPTION
Rev.0	04/19/2016	First release

	TAMU Wire-Wrapped Hardware Inventory		
	Document No: TAMU-WW-INV	Rev: 0	Page 4 of 6

I.0 INVENTORY TABLES

Table I-1. Measurement Devices 5

Table I-2. Pumps 6

Table I-3. Other Hardware 6

Table I-I. Measurement Devices

Instrument Inventory						
Document No. TAMU-WW-INV Rev.0						
Measurement Devices						
Inventory No.	Device Description	Position In Facility	Manufacturer	Model Number	Serial No.	Accuracy
WW-FM-001	Turbine Flow Meter	Primary Loop	Sponsler Inc.	SP-3-MB-PHL-D-4X	3628170601	Display: ±0.01% reading (rate) or ±1 count (total) • Analog output: ±0.025% of fs @20°C • Digital output: ±1 Count
WW-GP-1	15 psi Gauge Pressure Transducer	7F	Omega	MMG015VSP1D0T4AGCEPS	447492	<0.1% F.S
WW-GP-2	15 psi Gauge Pressure Transducer	5F	Omega	MMG015VSP1D0T4AGCEPS	447482	<0.1% F.S
WW-GP-3	15 psi Gauge Pressure Transducer	8A	Omega	PX-309-015G5V	021508-095	<1% F.S for <7.5 psig
WW-GP-4	30 psi Gauge Pressure Transducer	0F	Omega	PX-309-030G5V	070407-011	<4% F.S
WW-GP-5	30 psi Gauge Pressure Transducer	1F	Omega	PX-309-030G5V	070407-077	<4% F.S
WW-GP-7	30 psi Gauge Pressure Transducer	4F	Omega	PX419-030G5V	448166	<0.1% F.S
WW-GP-8	30 psi Gauge Pressure Transducer	6F	Omega	PX419-030G5V	448723	<0.1% F.S
WW-GP-9	30 psi Gauge Pressure Transducer	2F	Omega	PX419-030G5V	461827	<0.1% F.S
WW-GP-10	30 psi Gauge Pressure Transducer	3F	Omega	PX419-030G5V	457001	<0.1% F.S
WW-DP-2	5 in-H2O Differential Pressure Transducer	5	Validyne	P550-4-N-20-S-A	594583	<4.28% F.S
WW-DP-4	10 in-H2O Differential Pressure Transducer	6	Omega	MMDWB10MBV5P2D0T2ACE	456853	<0.1% F.S


	TAMU Wire-Wrapped Hardware Inventory		
	Document No: TAMU-WW-INV	Rev: 0	Page 6 of 6

Table I-2. Pumps


	Instrument Inventory				
	Document No. TAMU-WW-INV Rev.0				
Pumps					
Inventory No.	Device Description	Manufacturer	Model No.	Serial No.	Pump Output
WW-PP-001	Primary Pump	AMT	4251-98	V 08 7598585-0053 M 0012	15 Horsepower
WW-SP-001	Secondary Pump	Chemflo	30708	12J1199	3 Horsepower
WW-SP-002	Chilled Water Pump	Utilitech	PPLSP100-SS	0434281	1 Horsepower

Table I-3. Other Hardware

	Instrument Inventory				
	Document No. TAMU-WW-INV Rev.0				
Generic devices					
Inventory No.	Device Description	Manufacturer	Model No.	Serial No.	
WW-LAP-001	Laptop	DELL	LATITUDE 3550	4L24042	
WW-VFD-001	Primary VFD	FUJI ELECTRIC	FRN020G1S	T45A284A0034PK	
WW-VFD-002	Secondary VFD	WEG	CFW-08	1026972922	
WW-DCP-001	DC Power Supply	KORAD TECHNOLOGY CO.	KA3005D	008250059007	
WW-DCP-002	DC Power Supply	KORAD TECHNOLOGY CO.	KA3005D	008250059005	
WW-HXE-001	HEAT EXCHANGER	XYLEM	BP411-20	1370301	
WW-DAQ-001	Data Acquisition Chassis	National Instruments	SCXI-1000	19A3A93	
WW-DAQ-002	32 Channel Terminal Block	National Instruments	SCXI-1303	1828E98	
WW-DAQ-003	32 Channel +/- 10V Analog input Module	National Instruments	SCXI-1100	1450023	
WW-DAQ-004	32 Channel Thermocouple/Voltage Input Module	National Instruments	SCXI-1102	1A21E55	
WW-DAQ-005	32 Channel Terminal Block	National Instruments	SCXI-1303	1A902C0	
WW-DAQ-006	USB Data Acquisition and Control Module	National Instruments	SCXI-1600	01A837F3	